UCRL-51832

THE STRUCTURE OF STRONG SHOCK WAVES: WITH IMPLICATIONS FOR DEUTERIUM SYNTHESIS IN SUPERNOVAE

Thomas A. Weaver
(Ph. D. Thesis)

May 5, 1975

Prepared for U.S. Energy Research & Development Administration under contract No. W-7405-Eng-48

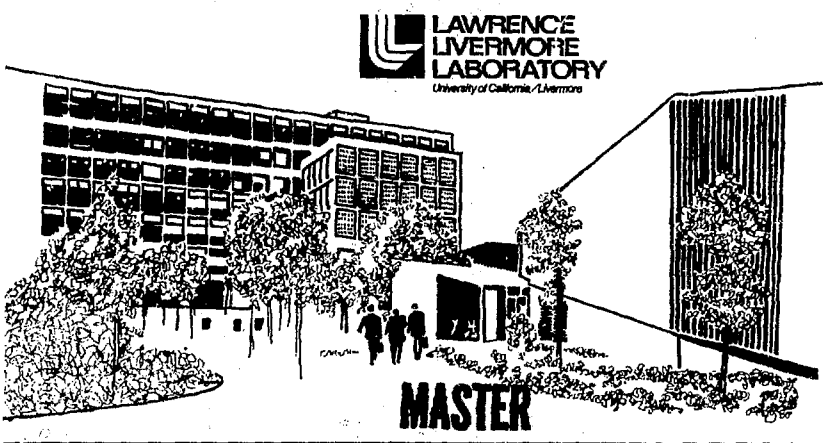

Printed in the United States of America
Available from
National Technical Information Service
U.S. Department of Commerce
5285 Port Royal Road
Springfield, Virginia 22151
Price: Printed Copy $___*; Microfiche $2.25

*Pages	NTIS Selling Price
1-50	$4.00
51-150	$5.45
151-325	$7.60
326-500	$10.60
501-1000	$13.60

LAWRENCE LIVERMORE LABORATORY
University of California / Livermore, California / 94550

UCRL-51832

THE STRUCTURE OF STRONG SHOCK WAVES: WITH IMPLICATIONS FOR DEUTERIUM SYNTHESIS IN SUPERNOVAE

Thomas A. Weaver

(Ph. D. Thesis)

MS. Date: May 5, 1975

THE STRUCTURE OF STRONG SHOCK WAVES:
WITH IMPLICATIONS FOR DEUTERIUM SYNTHESIS IN SUPERNOVAE

ABSTRACT

Thomas A. Weaver

The structure of strong shock waves is calculated over the range of shock energies (1 to 100 MeV/nucleon) and initial number densities (10^{15}-10^{22} cm^{-3}) believed likely to occur in the red-giant-like envelopes of stars undergoing Type II supernovae explosions. These calculations were motivated by the proposal of Colgate (1973, 1974) and Hoyle and Fowler (1973) that the ions in such shocks could be heated to temperatures in excess of 10 MeV by hard ion-ion collisions, resulting in the spallation of helium and the subsequent formation of sufficient deuterium via neutron capture to account for the presently observed abundance, without recourse to its formation in a low density Big Bang.

The general equations governing the structure of such shocks are developed on the basis of a hydrodynamic treatment of a plasma composed of ions, electrons. positrons, and photons, making use of diffusion theory to evaluate the dissipative and transfer terms. The shock models resulting from these equations differ from previous treatments in that the effects of radiation transport on the energy and momentum balance in the shock are taken into account, as well as the relativistic contributions to radiative emission rates due to non-dipole electron-ion bremsstrahlung, electron-electron bremsstrahlung, and radiative Compton scattering. To evaluate such rates, a general theory of relativistic distribution-

averaged reaction rates is developed, featuring an analytic combined-particle distribution function for the case of relativistic Maxwell-Boltzmann distributions. An implicit treatment of inverse Compton scattering is also developed in terms of the creation and diffusion of effective photons that allows a substantial simplification in the treatment of the radiation field.

Several strong shock structure models are formulated and solved on the basis of these equations and physical processes. First, a shock model dominated by radiation pressure and transport is considered, and criteria for its self-consistency deduced. In particular, radiative heat transport is shown to be a sufficient shock dissipation mechanism even for non-equilibrium radiation fields provided that the ratio of radiation to matter pressure in the region of the final shock compression exceeds 4.45. This criterion is found to hold over the entire regime of interest, thus avoiding the necessity of the shock being mediated by hard ion-ion collisions. This fact, combined with the high rates of radiative emission and inverse Compton upscattering of the large reservoir of low energy bremsstrahlung protons, results in peak ion temperatures approximately two orders of magnitude below those possible in a shock mediated by hard ion collisions. Specifically, peak electron temperatures remain below $\sim$ 70 keV for shock energies $\lesssim$ 30-50 MeV/nucleon depending on the initial density, while shocks with energies $\sim$ 1 MeV/nucleon are found to be in nearly complete radiative equilibrium.

For electron temperatures above $\sim$ 70 keV, the $\gamma\gamma \leftrightarrow e^+e^-$ reaction is found to give rise to a sufficient number of pairs to

cause the principal source of shock dissipation to shift from radiative heat transport to ion-lepton Coulomb friction. The properties of such a pair-dominated model are discussed, and it is argued that the peak shock temperatures remain below $\sim$ 200 keV for shock energies below 100 MeV/nucleon.

The stability of radiation-dominated shocks and the lack of self-consistent hot-ion shocks is demonstrated by considering shock models in which both viscosity and helium effects are included. This demonstration leads to the conclusion that peak shock temperatures remain low enough to preclude production of a cosmologically significant amount of deuterium in supernova shock waves.

Finally, the application of these concepts and results to the problems of cosmic-ray composition, neutron star accretion, and proto-galaxy formation is considered.

ACKNOWLEDGEMENTS

First, I would like to thank my advisor, Joseph Silk, and George Chapline and Lowell Wood of the Lawrence Livermore Laboratory for their joint guidance and encouragement of this study. Their insights, suggestions, and interesting ideas have been invaluable, both in the pursuit of this research and in making my graduate study a quite stimulating experience. I would also like to thank Stirling Colgate for his continued encouragement to pursue this work, and Edward Teller for his interest and support. In addition, I am grateful to George Zimmerman, Chris McKee, and Richard Epstein for a number of useful discussions.

The support of the Fannie and John Hertz Foundation throughout the course of my graduate study is gratefully acknowledged, as is the hospitality of the Lawrence Livermore Laboratory.

TABLE OF CONTENTS

I. INTRODUCTION

It is sufficient in most cases of physical and astrophysical interest to treat a shock as a discontinuous transition, since, in general, the final post-shock state is uniquely determined by the pre-shock conditions, independent of the details of the dissipation mechanism involved (Zel'dovich and Raizer 1966). Exceptions can occur, however, if non-equilibrium processes (e.g. nuclear reactions or radiation or neutrino loss) take place within the shock that cannot be relaxed in the final post-shock state, and in these cases a detailed shock structure calculation is necessary.

The structure of strong shocks thus plays an important role in a variety of astrophysical situations, including the proposed production of deuterium and cosmic rays in supernova explosions (Colgate 1974; Colgate and Johnson 1960), the radiation spectrum resulting from the accretion of matter onto a neutron star (Alme and Wilson 1973; Zel'dovich and Shakura 1969), and the formation of protogalaxies in the early universe (Silk 1974).

In this study we shall deal primarily with the question of whether the shocks traversing the extended outer envelopes ($\sim 10^{12}$ - 10^{13} cm in radius) postulated for Type II supernovae (Shklovsky 1968) can reach sufficiently high temperatures to cause deuterium, boron, and other light elements to be produced via nuclear spallation and subsequent neutron capture as Colgate (1973, 1974, 1975) and Hoyle and Fowler (1973) have predicted. They postulate that as the shock formed in the mantle of a star undergoing a supernova explosion moves down the steep density

gradient at the mantle's edge it is accelerated to energies $\sim$ 10 MeV/nucleon in the extended density regime at $\sim 10^{-4}$ g/cm^3, and to $\gtrsim$ 30 MeV/nucleon by the time it reaches a density of $\sim 10^{-7}$ g/cm^3. We will thus examine the structure of those shocks with initial densities ranging from 10^{15}-10^{22} cm^{-3} and initial energies from 1-100 MeV/nucleon to determine if the ion temperatures of $\gtrsim$ 10 MeV needed for deuterium production, or those of $\gtrsim$ 1 MeV required for the production of other light elements, can in fact occur. A brief account of a portion of this calculation was given in Weaver and Chapline (1974).

The magnitude of the shock temperature that will occur is principally determined by the degree of equilibration of the radiation field. If no radiation is present in the shock, the only dissiapation mechanism capable of generating the amount of entropy required by the Hugoniot relations for a strong shock (Zel'dovich and Raizer 1966) is ion viscosity. This results in a shock a few ion-ion mean free paths thick in which "hard" ion-ion collisions transform the kinetic energy of the incoming ions (in the frame of the post-shock material) directly into ion thermal energy. The hot ions then heat the electrons by Coulomb friction, and the electrons in turn lose their energy to radiation in a relatively large post-shock relaxation layer.

On the other hand, for non-relativistic shocks, if the ratio of radiation to matter pressure exceeds 4.45 in the region of final compression, the dissipation due to radiative heat conduction, which typically occurs on the scale of many Compton lengths, is

sufficient to satisfy the Hugoniot relations and prevents the shock from steepening further into the regime where ion viscosity is important. (Belokon' 1959 and Section V.D below.) In such "radiation-dominated" shocks, the photons diffuse ahead creating sufficient pressure to decelerate the electrons (as viewed from the frame in which the shock front is fixed). The ions are then decelerated by a combination of a charge-separation-induced electric field and Coulomb friction with the electrons. The kinetic energy of the ions is thus directly transformed into electron and photon thermal energy. The ions are only weakly heated by Coulomb friction, and by the generally small amount of viscous heating that can still take place over gradients of many Compton lengths. For pre-shock kinetic energies and densities of less than 100 MeV/nucleon and 10^{21} cm^{-3}, the peak temperature of a radiation-dominated shock ranges from less than 10 keV if the radiation field is everywhere in black-body equilibrium to at most 4 MeV at the point where the criterion for radiation-dominance is no longer satisfied. This is in sharp contrast to the up to 50-70 MeV temperatures that would occur in a viscous ion shock. Figure 1.1 illustrates qualitatively these various possible types of shock structure. In addition, as is discussed in Section VI, the presence of electron-positron pairs in the shock front can result in a shock structure in which dissipation occurs principally by ion-pair Coulomb friction.

The essential object of the calculations that follow is to decide which of these structures in fact occurs at a given initial energy and density. Our treatment differs from that of Colgate

(1974) in that we include the effect of photon diffusion on energy and momentum balance in the shock, while Colgate considered only the post-shock radiative equilibration. In addition, we include the effects of electron-electron bremsstrahlung, radiative Compton scattering, electron-positron pair creation, and a more accurate treatment of inverse Compton scattering. As we shall see, these effects substantially increase the rate of radiative equilibration. Further, the suggestions of Colgate (1975) that radiation-dominated shocks may be unstable, or that consistent hot-ion shocks may also exist, are examined in the context of a shock model containing both viscous and radiative effects, and taking into account the presence of helium, and found to be invalid.

In Section II, we derive the hydrodynamic equations governing shock structure in sufficiently general form to treat both viscous and radiation-dominated shocks; and in Section III, discuss and develop the physical processes that determine the parameters in these equations. Section IV describes an approximate treatment of the radiation field in terms of "effective photons" that substantially simplifies the shock equations, while including inverse Compton processes implicitly. The radiation-dominated shock model is formulated and solved in Section V, and is shown to result in shocks whose peak temperatures remain below $\sim$ 100 keV for shock energies $\lesssim$ 40-50 MeV/nucleon, while the effect of pairs is explored in Section VI. Section VII develops shock models containing viscosity, and these are merged with a realistic treatment of the radiation field in Section VIII. The resulting general model

verifies the consistency of the radiation-dominated shock model, while no consistent "hot-ion" shocks are found. The astrophysical implications of these results are discussed in Section IX.

Unless explicitly stated otherwise, cgs-Gaussian units will be used throughout this study. A list of the symbols employed with their definitions and units is given in Appendix E.

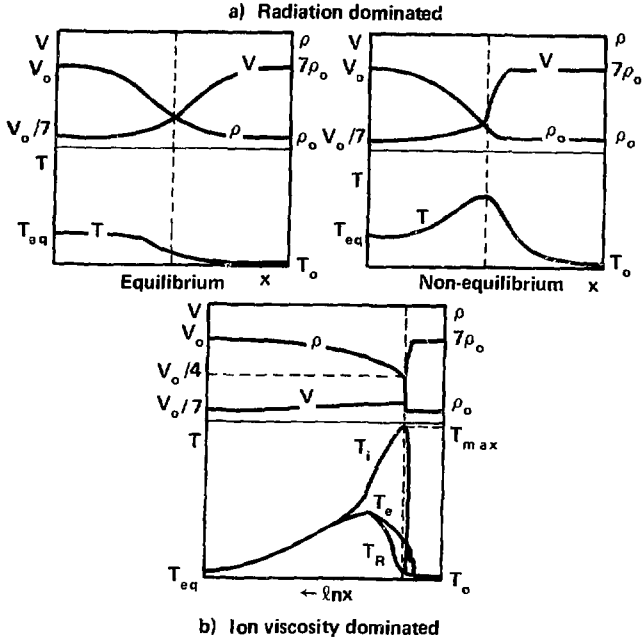

Figure 1.1 - Types of shock structure. These shocks are schematic and are shown in their comoving frame, where the matter moves with velocity v to the left. T_i, T_e, T_R, and T are the ion, electron, radiation, and mean temperatures respectively, while ρ is the matter density and x the spatial coordinate. v_0, ρ_0, and T_0 are the pre-shock values of v, ρ, and T, while T_{eq} is the final post-shock equilibrium temperature.

II. SHOCK STRUCTURE EQUATIONS

A. Basic Hydrodynamic Equations

The general hydrodynamic equations governing the structure of a multispecies shock assumed to be one-dimensional and to have reached a steady state in its comoving frame can be obtained by requiring the conservation of momentum, energy, and particle number for each species, and can be written in the form:

$$\frac{dP^i_{xx}}{dx} = \sum_j p^{ij} \tag{2.1}$$

$$\frac{dE^i_x}{dx} = \sum_j E^{ij} \tag{2.2}$$

$$\frac{d(n^i v^i)}{dx} = Q^i \tag{2.3}$$

where P^i_{xx}, E^i_x, v^i and n^i are the pressure and energy components of the stress-energy tensor, and the macroscopic velocity and number density respectively of the i^{th} particle species or energy group. Here p^{ij} and E^{ij} are the rates of momentum and energy transfer from group or particle j to group or particle i, and Q^i is the rate at which particles of type or energy group i are "created" or "destroyed". All of the above quantities, including the spatial coordinate x, are to be measured in the frame in which the shock is at rest.

If we neglect external electric and magnetic fields, the electrical properties of the shocked plasma are given by the one-dimensional Poisson's equation:

$$\frac{d\mathcal{E}_x}{dx} = 4\pi\rho \tag{2.4}$$

where $\mathcal{E}_x$ is the x component of the electric field and ρ, the charge density.

In their present form equations (2.1) - (2.3) are relativistically correct (cf. Johnson and McKee 1971) and can be most readily evaluated by Lorentz transforming the various stress tensor, transfer, and source terms from the rest frame of each particle species to the shock frame. The resulting relativistic shock equations and shock models will be the subject of a later paper. For the purposes of the present study, however, we shall restrict ourselves to non-relativistic shock velocities and in addition make the following general assumptions:

1) The shocked material is a fully ionized hydrogen plasma and its associated radiation and electron-positron pair fields. (The effect of helium and high-Z components will be discussed in §VIII.B.)
2) The electrons and ions can be characterized macroscopically by temperatures T_e and T_i, velocities v_e and v_i, and densities n_e and n_i (see §IX).

3) Except for the very small differences giving rise to electrical effects, the positrons share the velocity and temperature of the electrons and their number density, n_+, is included in n_e (see §V.D and §VI).

4) The radiation field is allowed to have an arbitrary energy spectrum, but radiation transport in x-space is assumed to be adequately described in terms of the diffusion approximation, (see §III), and to take place in an optically thick region (see §IX).

5) Viscosity, heat conduction, and momentum and energy transfer among the ions and electrons are given by the usual Navier-Stokes relations (e.g., see Landau and Lifshitz 1959, Jaffrin and Probstein 1964, and §IX).

The validity and self-consistency of these assumptions is discussed in the sections noted.

With these assumptions, equations (2.1) - (2.4) can be written in the more explicit form:

$$\frac{d}{dx}\left[n_e kT_e + E_\gamma/3 + m_e n_e v_e^2 - \mu_e \frac{dv_e}{dx}\right] = P'_{ei} + \rho_e \Sigma_x \tag{2.5}$$

$$\frac{d}{dx}\left[n_e v_e (1+\alpha_e) kT_e + \frac{1}{2} m_e n_e v_e^3 + n_e v_e m_e c^2 + \frac{4}{3} E_\gamma v_e \right.$$

$$\left. + S_\gamma - \kappa_e \frac{dT_e}{dx} - v_e \mu_e \frac{dv_e}{dx}\right] = E'_{ei} + j_e \Sigma_x \tag{2.6}$$

$$\frac{d}{dx}\left[n_i kT_i + m_i n_i v_i^2 - \mu_i \frac{dv_i}{dx}\right] = -P'_{ei} + en_i\Sigma_x \tag{2.7}$$

$$\frac{d}{dx}\left[\frac{5}{2}n_i v_i kT_i + \frac{1}{2}m_i n_i v_i^3 - \kappa_i \frac{dT_i}{dx} - v_i\mu_i \frac{dv_i}{dx}\right]$$

$$= -E'_{ei} + ev_i n_i \Sigma_x \tag{2.8}$$

$$\frac{d}{dx}\left[v_e n_\gamma(\epsilon_\gamma)\right] - \frac{d}{dx}\left[D_\gamma(\epsilon_\gamma)\frac{dn_\gamma(\epsilon_\gamma)}{dx}\right]$$

$$= n_e c \int_0^\infty \left[n_\gamma(\epsilon'_\gamma) - n_\gamma(\epsilon_\gamma)\right]\sigma(\epsilon_\gamma \to \epsilon'_\gamma)d\epsilon'_\gamma + Q_\gamma(\epsilon_\gamma) \tag{2.9}$$

$$\frac{d}{dx}\left[n_i v_i\right] = 0 \tag{2.10}$$

$$\frac{d}{dx}\left[n_e v_e\right] = 2Q_\pm \tag{2.11}$$

$$\frac{d\Sigma_x}{dx} = 4\pi[\rho_e + en_i] \tag{2.12}$$

Here m_j, μ_j, κ_j are the mass and coefficients of viscosity and heat conduction respectively for species j; E_γ and S_γ are the energy density and flux of the radiation field in frame of the electrons; P'_{ei} and E'_{ei} are the portions of the total momentum and energy transfer terms not involving the electric field; $n_\gamma(\epsilon_\gamma)$

is the number density of photons in an energy group centered on photon energy ϵ_γ; $\sigma(\epsilon_\gamma \rightarrow \epsilon_\gamma')$ is the cross section for a photon to be Compton scattered from ϵ_γ to ϵ_γ'; $Q_\gamma(\epsilon_\gamma)$ is the rate at which photons are emitted into energy group ϵ_γ; $Q_\pm$ is the production rate for electron-positron pairs; $D_\gamma(\epsilon_\gamma)$ is the diffusion coefficient for photons; ρ_e and j_e are the charge and current density of the electron-positron fluid as viewed from the shock frame; α_e is the ratio of the energy density to pressure of the electrons (assumed $\frac{3}{2}$ for the ions); and as usual c, k, and e are the velocity of light, Boltzmann's constant, and the protonic charge.

Equations (2.5), (2.6), and (2.11) describe momentum, energy, and lepton number conservation for the electrons and positrons, including the effects of radiation energy density, energy transport, and pressure. Radiation momentum transport and all higher transport moments are neglected, due to the assumed non-relativistic bulk velocity and optical thickness of the shocked material. Equations (2.7), (2.8), and (2.10) describe momentum, energy, and particle conservation for the ions, while equation (2.9) describes the diffusion, creation, and scattering of photons. Note that the distribution function $n_\gamma(\epsilon_\gamma)$ is defined in the rest frame of shock and not in the frame comoving with the electrons. Finally, equation (2.12) is Poisson's equation.

The form of the parameters in equations (2.5) - (2.12) depends on the energy and density regime of interest and will be the topic of Section III.

B. Boundary Conditions and Integrated Shock Equations

In order for equations (2.5) - (2.12) to describe a shock, appropriate boundary conditions must be introduced. Specifically, we shall assume that as $x \to -\infty$, $v_e \to v_i \to v_o$, $n_e \to n_i \to n_o$, $T_e \to T_i \to T_o$, $n_\gamma(\varepsilon_\gamma) \to n_{\gamma o}(\varepsilon_\gamma)$, $n_+ \to 0$, $\Sigma_x \to 0$, and the gradients of T_i, T_e, v_i and v_e vanish; and, in addition, that $n_\gamma(\varepsilon_\gamma) \to n_{\gamma 1}(\varepsilon_\gamma)$ as $x \to +\infty$. Here we have associated the subscript "o" with the pre-shock condition of the fluid and the subscript "1" with its post-shock condition thus assuming a fluid flow from $-\infty$ ("upstream") to $+\infty$ ("downstream"). The singular nature of the shock equations at $\pm\infty$ prevents these boundary conditions from being sufficient, and we must also require that the temperature and velocity gradients vanish at $+\infty$, and that $v=v_s$ at some finite point $x=x_s$. The last condition is necessary to fix the location of the shock; and, as we shall see the range of v_s must be restricted to obtain physically realizable shocks.

Utilizing these conditions, we note equations (2.10) and (2.11) imply that net electrical currents vanish. We can then obtain integral momentum and energy conservation equations for the entire plasma by adding (2.5) to (2.7) and (2.6) to (2.8), making use of (2.12), and integrating. Continuity equation (2.10) can also be immediately integrated, while (2.8) can be simplified by subtracting v_i times (2.7). The resulting set of shock structure equations becomes:

$$n_e kT_e + n_i kT_i + \frac{1}{3}E_\gamma - \mu_e \frac{dv_e}{dx} - \mu_i \frac{dv_i}{dx} - \frac{\mathcal{E}_x^2}{8\pi}$$

$$= m_i n_o v_o (v_o - v_i) + m_e (n_o v_o^2 - n_e v_e^2) + P_o \qquad (2.13)$$

$$n_e v_e (1+\alpha_e) kT_e + \frac{5}{2} n_o v_o kT_i + \frac{4}{3} E_\gamma v_e + S_\gamma - \kappa_e \frac{dT_e}{dx}$$

$$-\kappa_i \frac{dT_i}{dx} - v_e \mu_e \frac{dv_e}{dx} - v_i \mu_i \frac{dv_i}{dx} = \frac{1}{2} m_i n_o v_o (v_o^2 - v_i^2)$$

$$+ \frac{1}{2} m_e (n_o v_o^3 - n_e v_e^3) + m_e c^2 (n_o v_o - n_e v_e) + S_o \qquad (2.14)$$

$$n_i k \frac{dT_i}{dx} - \frac{n_o v_o}{v_i^2} kT_i \frac{dv_i}{dx} + m_i n_o v_o \frac{dv_i}{dx} - \frac{d}{dx}\left[\mu_i \frac{dv_i}{dx}\right]$$

$$= - P'_{ei} + e n_i \mathcal{E}_x \qquad (2.15)$$

$$\frac{3}{2} n_o v_o k \frac{dT_i}{dx} + n_i kT_i \frac{dv_i}{dx} - \mu_i \left(\frac{dv_i}{dx}\right)^2 - \frac{d}{dx}\left[\kappa_i \frac{dT_i}{dx}\right]$$

$$= - (E'_{ei} - v_i P'_{ei}) \qquad (2.16)$$

$$n_i v_i = n_o v_o = (n_e - 2n_+)\, v_e \qquad (2.17)$$

$$\frac{d}{dx}\left[n_e v_e\right] = 2Q_\pm \qquad (2.18)$$

$$\frac{d\mathcal{E}_x}{dx} = 4\pi\,(en_i+p_e) \tag{2.19}$$

$$\frac{d}{dx}\left[v_e n_\gamma(\epsilon_\gamma)\right] - \frac{d}{dx}\left[D_\gamma(\epsilon_\gamma)\,\frac{dn_\gamma(\epsilon_\gamma)}{dx}\right]$$

$$= n_e c \int_0^\infty \left[n_\gamma(\epsilon_\gamma')-n_\gamma(\epsilon_\gamma)\right]\sigma(\epsilon_\gamma+\epsilon_\gamma')\,d\epsilon_\gamma' + Q_\gamma(\epsilon_\gamma) \tag{2.20}$$

where P_0 is the pre-shock pressure, and S_0, the energy flux due to the initial internal energy density and pressure.

III. PHYSICAL PROCESSES

A. Radiative Emission Processes

Bremsstrahalung

The photon emission spectrum from a hot plasma due to electron-ion bremsstrahlung is given in the non-relativistic limit by Drummond (1961) as:

$$J_{ei}^{NR}(\varepsilon_\gamma,\theta_e)\, d\varepsilon_\gamma = \frac{16}{3}\left(\frac{2}{m_e\pi\theta_e}\right)^{1/2} Z_i^2\alpha r_o^2 n_e n_i m_e c^2 e^{-\varepsilon_\gamma/2\theta_e}\, K_o\left(\frac{\varepsilon_\gamma}{2\theta_e}\right)\frac{d\varepsilon_\gamma}{\varepsilon_\gamma} \tag{3.1}$$

where K_o is the zeroth order modified Bessel function of the second kind; α is the fine structure constant; r_o, the classical electron radius, $\theta_e = kT_e$, and Z_i is the ionic charge.

It is evident from the form of (3.1) that the number density of photons, $Q(\varepsilon_c,\theta_e)$, emitted per unit time down to some low energy cutoff $\varepsilon_c << \theta_e$, diverges logarithmically. While the total energy emitted in low energy photons is small, they can contribute very substantially to the cooling and effective heat capacity of the electrons via inverse Compton scattering. The treatment of this effect is undertaken in §III.D and §IV, and utilizes the quantity $Q(\varepsilon_c,\theta_e)$ with ε_c taken as the lowest energy from which a photon can be effectively thermalized, which we shall term the "effective photon" emission rate. Non-relativistically, we find from (3.1) that:

$$Q_{ei}^{NR}(\varepsilon_c,\theta_e) = 5.692\times10^{-12} T_e^{-1/2} n_i n_e Z_i^2 g_1(\lambda) E_1(\lambda)\,\mathrm{cm}^{-3}\mathrm{sec}^{-1} \tag{3.2}$$

where $\lambda \equiv \varepsilon_c/\theta_e$, $E_1(x) \equiv \int_x^\infty \frac{e^{-t}}{t} dt$ is the first order exponential integral function, and:

$$g_1(\lambda) \equiv \int_{\lambda/2}^{\infty} e^{-x} K_0(x) \frac{dx}{x} \Big/ E_1(\lambda) \qquad (3.3)$$

g_1 is a slowly varying factor and can be expressed to an accuracy of better than one percent in the numerical form:

$$g_1(\lambda) \approx 1.226 - .475\ \ell n\lambda + .0013\ (\ell n\lambda)^2 \quad 10^{-6} \leq \lambda \leq .8 \qquad (3.4)$$

The $E_1(\lambda)$ function can also be conveniently approximated numerically (Abramowitz and Stegun 1964, p. 231) and in the limit of small λ becomes $E_1(\lambda) \sim -\ell n(\lambda) - .5772$, and thus contains the logarithmic singularity expected from the $1/\varepsilon_\gamma$ term in the emission spectrum.

For plasma temperatures above ~20 keV, electron-electron bremsstrahlung and relativistic corrections to e-i bremsstrahlung must be taken into account. Unfortunately, plasma emission spectra have not been calculated for these processes for most of the range between first order in $\theta_e/m_e c^2$ and the extreme relativistic limit. At present, therefore, we must be content with making approximations to these rates, and then determining the sensitivity of our results to these approximations.

The general effect of relativistic additions to the bremsstrahlung rate is to greatly increase the high energy portion of

the spectrum while more moderately increasing emission in the low energy tail (cf. Quigg 1968]. This results in the temperature dependence of the energy emission rate increasing from $\theta_e^{1/2}$ to $\theta_e \ell n(2\theta_e/m_e c^2)$ (Maxon 1972) as the transition to relativistic temperatures is made, while the mean energy-weighted emitted photon energy increases from $\frac{2}{3}\theta_e$ to $\simeq .85\theta_e$ at $\theta_e = m_e c^2$ to $1.88\theta_e$ in the extreme relativistic limit (e-i case).

This behavior suggests that we take the effective photon emission rate from relativistic corrections to bremsstrahlung to be:

$$Q_{RCB} = \frac{W_{ei}^{RC} + W_{ee}}{\varepsilon_{RC}\theta_e} \qquad \varepsilon_{RC} = \begin{cases} 1 & \text{if } \lambda \leq 1/5 \\ 5\lambda & \text{if } \lambda > 1/5 \end{cases} \tag{3.5}$$

and W_{ee} and W_{ei}^{RC} are energy emission rates for e-e and the relativistic correction to e-i bremsstrahlung. Here the form of the cutoff for large λ was determined by requiring $\varepsilon_{RC} = 3$ for $\lambda = .6$ as is the case non-relativistically. (See §IV.B]. Note that this approximation is conservative in that it ignores photons with energy $<< \theta_e$ produced by relativistic effects.

Maxon (1972) has interpolated between first order and extreme relativistic results. to obtain bremsstrahlung energy emission rates for a plasma of arbitrary temperature. From his results, we obtain:*

$$W_{ei}^{RC} \simeq W_{ei}^{NR} \cdot \begin{cases} \frac{19}{24}\,\tau(1+1.022\tau+.221\tau^2-.239\tau^3) & \tau \leq 1.5 \\ \frac{9}{8}(\frac{\pi}{2})^{1/2}\tau^{1/2}(\ell n 2\tau+.923)-1 & \tau \geq 1.5 \end{cases} \tag{3.6}$$

*Here we have somewhat improved Maxon's interpolation by explicitly introducing the quadrapole correction to e-i bremsstrahlung before interpolating.

$$W_{ee} \simeq W_{ei}^{NR} \frac{n_e}{n_i} \begin{cases} 3\,\tau(1+.128\tau+.898\tau^2-.439\tau^3) & \tau \leq 1.5 \\ \frac{9}{4}\left(\frac{\pi}{2}\right)^{1/2}\tau^{1/2}(\ell n 2\tau + .673) & \tau \geq 1.5 \end{cases} \quad (3.7)$$

where

$$W_{ei}^{NR} = \frac{32}{3} Z_i^2 \alpha r_o^2 n_e n_i m_e c^3 \left(\frac{2\theta_e}{\pi m_e c^2}\right)^{1/2} \quad (3.8)$$

is the non-relativistic e-i bremsstrahlung emission rate, and $\tau \equiv \theta_e/m_e c^2$. The interpolation errors appear to be ~15-20%. Gould (1974), however, has very recently recalculated quantum mechanically the lowest order (i.e. quadrupole) cross sections for e-e bremsstrahlung and found them to average roughly a factor of two lower than the semi-classical cross sections of Fediushin (1952), used by Maxon. The net effect of this correction is to reduce W_{ee} by ~65% for $\theta_e \ll m_e c^2$, which we shall approximate by multiplying (3.7) by the factor $(1 - .642e^{-\theta_e/m_e c^2})$.

Radiative Compton Scattering

The process of radiative Compton scattering

$$e + \gamma \rightarrow e + \gamma + \gamma \quad (3.9)$$

is expected from general quantum electrodynamics arguments to proceed at a rate $\sim\alpha(=1/137)$ below that of ordinary Compton scattering at photon energies $\sim m_e c^2$, and thus be a potentially important source of photons in the extremely hot plasmas characteristic of the strong shocks under consideration. The differential cross-section for this process was calculated by Mandl and Skyrme (1952)

and has recently been numerically integrated by Ram and Wang (1971) to give the total cross section for photon emission for $\epsilon_\gamma > 5$ keV.

In order to average this cross section over a partially relativistic electron distribution, a general theory of relativistic reaction rates has been developed and is given in Appendix A. The most notable results of this theory are exact expressions for total rates involving only a single integral over the cross-section for the usual case of relativistic Maxwell-Boltzmann (RMB) or Bose-Einstein distributions (RBE) (see equations (A11c), (A22b), and (A31)). This results from the fact that in the relativistic as well as the non-relativistic case, an effective combined particle distribution function, F, can be found analytically.

For an RMB electron distribution (eq. (A9)) and RBE (eq. (A18)) photon distribution, the total photon emission rate ($\epsilon_\gamma > 5$ keV), Q_{RC}, is given in Figure 3.1. Here C is the degeneracy parameter for the photon RBE distribution, ranging from 1 for black-body radiation to infinity in the non-degenerate limit. As can be seen, the density-normalized radiative Compton rates (i.e. $\langle\sigma v\rangle_{RC} \equiv Q_{RC}/n_\gamma n_e$) for C = 1 vary from ∿15% below to ∿10% above the non-degenerate rates as θ_e ranges from $\ll m_e c^2$ to $\gg m_e c^2$. (Here n_γ is the number density of photons in the RBE distribution, which we shall associate with the effective photon number density in §IV.) This is due primarily to the relative augmentation of the low energy tail of the black-body distribution and the peak in the total cross-section near $m_e c^2$. Because of this small distribution dependence, and the fact that knowledge of radiative rates is most important far from equilibrium, we shall

adopt the non-degenerate rates for general use in the present work.

The rates given in Figure 3.1 when compared to the effective bremsstrahlung rates given in the last section, indicate that radiative Compton scattering will dominate near-thermal photon production in the θ_e = 50 keV - 5 MeV regime if $n_\gamma \gtrsim n_e$. At higher temperatures, the relatively unexplored processes of multiple bremsstrahlung and multiple radiative Compton scattering may become dominant.

Approach to Equilibrium

Except in the case of the low energy tail of the bremsstrahlung emission spectrum, we shall approximately allow for photon absorption processes by multiplying the emission rates by the factor:

$$f_E = 1 - \frac{n_\gamma}{bT_e^3} \tag{3.10}$$

where b = 20.3 $cm^{-3}/°K^3$ is the radiation equilibrium number density constant, in analogy to the usual relation between emission and absorption for photons of a given energy (Zel'dovich and Raizer 1966). Inverse bremsstrahlung processes will be taken into account explicitly in determining the cutoff energy, ε_c, above which bremsstrahlung photons can be effectively thermalized (see §IV).

B. Electron-Positron Pair Production

Emission Processes

The most important means of electron-positron pair creation at electron and photon temperatures below 1 MeV are the reactions:

$$\gamma + \gamma \rightarrow e^+ + e^- \tag{3.11}$$

$$\gamma + Z \rightarrow Z + e^+ + e^- \tag{3.12}$$

$$\gamma + e^\pm \rightarrow e^\pm + e^+ + e^- \tag{3.13}$$

Like other second-order processes in quantum electrodynamics such as Compton scattering, γ-γ pair production has a cross-section $\sim r_o^2$ in the region where it is energetically allowed. Cross-sections for the third order processes (3.12) and (3.13) are typically a factor of $\frac{1}{137}$ below these levels (for $Z=1$), and so for photon number densities at all comparable to the matter density, γ-γ pair production will dominate.

Jauch and Rohrlich (1955) give the relativistically correct γ-γ pair production cross-section in the form:

$$\sigma = \pi r_o^2 \phi^2 [(2+2\phi^2-\phi^4) \cosh^{-1}(\tfrac{1}{\phi}) - (1+\phi^2)(1-\phi^2)^{1/2}] \tag{3.14}$$

where $\phi = \frac{m_e c^2}{\epsilon_\gamma}$, ϵ_γ is the center of mass energy of one of the photons, and σ is meant in the Lorentz invariant sense of eq. (A24). Using the formalism of Appendix A (see eq. (A31)), this cross-section can be readily averaged over a non-degenerate "RBE" photon distribution, to give the pair production rate, $Q^{\pm}_{\gamma\gamma}$, shown in Figure 3.2. Also plotted is the "non-relativistic" expression for this cross-section, obtained by assuming $kT_\gamma \ll m_e c^2$ and using the non-relativistic limits of (3.14) and (A31) to find:

$$Q_{\gamma\gamma}^{NR} = \frac{n_\gamma^2}{2} \frac{c\pi^2 r_0^2}{4} \left(\frac{m_e c^2}{kT_\gamma}\right)^3 e^{-2m_e c^2/kT_\gamma} \tag{3.15}$$

As is apparent, this attempt to model an intrinsically relativistic process non-relativistically is a reasonable but not complete success, which suggests expressing $Q_{\gamma\gamma}^{\pm}$ in the convenient form:

$$Q_{\gamma\gamma}^{\pm} = 1.042 \left(1. + .728 \left(\frac{kT_\gamma}{m_e c^2}\right)\right)^{7/2} Q_{\gamma\gamma}^{NR} \equiv \frac{n_\gamma^2}{2} \langle \sigma v \rangle_{\gamma\gamma}$$

$$10 \text{ KeV} \lesssim kT_\gamma \lesssim 100 \text{ KeV} \tag{3.16}$$

which is accurate to 2%.

Pair-Photon Relative Equilibrium

A given number density of pairs will be in relative equilibrium with a Bose-Einstein distribution of photons (via $e^+e^- \leftrightarrow \gamma\gamma$) when:

$$2\mu_\gamma = \mu_{e^+} + \mu_{e^-} + 2m_e c^2 \tag{3.17}$$

where μ_j is the chemical potential of species j (cf. Chiu 1968, p. 134). In the case of an RMB distribution, the number density of positrons, n_+, is related to μ_{e^+} by:

$$n_+ = \frac{m^3 c^3}{\pi^2 \hbar^3} e^{(\mu_{e^+} + m_e c^2)/kT} \frac{K_{2(\phi)}}{\phi}$$

$$\equiv n_{+0} e^{(\mu_{e^+} + m_e c^2)/kT} \tag{3.18}$$

and for non-degenerate photons, n_γ, is given by:

$$n_\gamma = \frac{bT^3}{\zeta(3)} e^{\mu_\gamma/kT} \equiv n_{\gamma o} e^{\mu_\gamma/kT} \tag{3.19}$$

where $\Phi = m_e c^2/kT$, $\zeta(3) = 1.2021....$, and K_2 is the second order modified Bessel function of the second kind. Since in full thermodynamic equilibrium $\mu_\gamma = 0$ and $\mu_+ = -m_e c^2$, we identify n_{+o} and $n_{\gamma o}$ with the final equilibrium density of pairs and photons, at temperature T, that would occur if these particles remained non-degenerate. Numerically we find:

$$n_{+o} = 1.77 \times 10^{30} \frac{K_2(\Phi)}{\Phi} \text{ cm}^{-3} \xrightarrow[\Phi>>1]{} 2.22\times10^{30}\, \Phi^{-3/2} \cdot e^{-\Phi} \text{ cm}^{-3} \tag{3.20}$$

and

$$n_{\gamma o} = 16.9\, T^3\, (^\circ K)\ \text{cm}^{-3} = 3.52\times10^{30}\, \Phi^{-3}\ \text{cm}^{-3} \tag{3.21}$$

Returning to (3.17), we find that for the case of non-degenerate distributions, $\mu_{e+} = \mu_{e-}$, and $T_\gamma = T_e$, that the pair-photon ratio is given in relative equilibrium by:

$$\frac{n_+}{n_\gamma} = \frac{n_{+o}}{n_{\gamma o}} \tag{3.22}$$

Thus, for example, a 100 keV plasma would contain .04 positrons per photon. Such a relative equilibrium is expected when the

$\gamma\gamma \leftrightarrow e^+e^-$ reaction succeeds in interchanging pairs and photons much more reapidly than bremsstrahlung and radiative Compton scattering can make new photons.

C. Transport Coefficients

Ion and Electron Viscosity and Heat Conduction

We wish to find the transport coefficients for a plasma containing protons electrons, and photons where the ions and electrons may have different temperatures. To do this, we shall start from a generalized diffusion approximation and then normalize our results to the case of a uniform temperature, radiationless plasma which has been treated more precisely.

From the diffusion approximation, we find the coefficients of viscosity and heat conduction for species j to be:

$$\mu_j = C_\mu \, n_j m_j v_j^{th} \lambda_j \tag{3.23}$$

$$\kappa_j = C_\kappa \alpha_j n_j k v_j^{th} \lambda_j \tag{3.24}$$

where C_μ and C_κ are constants of order unity (usually taken equal to 1/3, (cf. Bond, Watson, and Welch 1965, p. 240, 255)); α_j is the ratio of internal energy density to the pressure and equals 3/2 for a non-relativistic perfect gas; v_j^{th} and λ_j are the mean thermal velocity and "transport mean free path" for species j given non-relativistically by:

$$v_j^{th} = \left(\frac{3\theta_j}{m_j}\right)^{1/2} \tag{3.25}$$

$$\lambda_j = \left[\sum_k \left(\lambda_{jk}(v_j^{th})\right)^{-1}\right]^{-1} \tag{3.26}$$

Here $\lambda_{jk}(w)$ is the transport mean free path for a particle of species j with velocity w in a gas of k-particles, defined by:

$$\frac{\lambda_{jk}(w)}{w} \equiv \frac{-w}{<\Delta w_{11}>} \equiv t_{sjk} \tag{3.27}$$

where $<\Delta w_{11}>$ is the expected initial rate of change of the parallel component of the j-particle's velocity. For interactions between charged particles, t_{sjk}, is given by Spitzer (1962) as:

$$t_{sjk} = \frac{w m_j^2 (v_k^{th})^2}{(1+m_j/m_k)\ 12\pi e^4 n_k Z_j^2 Z_k^2 \ell n\Lambda\ G(\sqrt{1.5}\ w/v_k^{th})} \tag{3.28}$$

$$G(x) = \frac{\text{erf}\ (x) - x \frac{d}{dx}(\text{erf}\ (x))}{2x^2} \tag{3.29}$$

$$\Lambda = \frac{3}{2Z_j Z_k e^3} \left(\frac{\theta_e^3}{\pi n_e}\right)^{1/2} \tag{3.30}$$

where erf(x) is the usual error function; and $\ell n\Lambda$, which indicates the relative importance of small-angle scatters, has been taken >> 1 in deriving (3.28) - (3.29).

For e-i, i-e, and j-j Coulomb interactions, we then find (i→p):

$$\lambda_{ep}(v_e^{th}) = \frac{9}{4} \frac{\theta_e^2}{\pi e^4 n_i \ell n\Lambda} \tag{3.31}$$

$$\lambda_{pe}(v_i^{th}) = \frac{3}{8}\left(\frac{6m_i}{\pi m_e}\right)^{1/2} \frac{\Theta_i^{1/2}\,\Theta_e^{3/2}}{e^4 n_e \ell n\Lambda} \tag{3.32}$$

$$\lambda^c_{jj}(v_j^{th}) = .588\,\frac{\Theta_j^2}{e^4 n_j \ell n\Lambda Z_j^4} \tag{3.33}$$

The transport mean free path due to nuclear forces acting between protons dominates the Coulomb cross-section for $\Theta_i \gtrsim 1$ MeV and is given to a rough approximation by (Colgate 1974):

$$\lambda^N_{pp}(v_i^{th}) \approx \left(\frac{\Theta_i(\text{MeV})}{6}\right)^{1/2} \frac{10^{24}}{n_i}\ \text{cm}$$

$$1 < \Theta_i < 10\ \text{MeV} \tag{3.34}$$

For non-relativistic electrons traveling in a photon gas, we have from Section III.D that for $T_e \simeq T_\gamma$:

$$-\frac{\langle \Delta w_{11} \rangle_{e\gamma}}{w}\ \Bigg|_{w=v_e^{th}} \approx \sigma_T n_\gamma c\,\frac{\Theta_e}{m_e c^2} \tag{3.35}$$

implying:

$$\lambda_{e\gamma}(v_e^{th}) \approx \left(\frac{m_e}{3\Theta_e}\right)^{1/2} \frac{3c}{\sigma_T n_\gamma} \tag{3.36}$$

where σ_T is the Thompson cross-section ($\frac{8}{3}\pi r_o^2$). Using these cross-sections the non-relativistic coefficients of electron and proton viscosity can be written in the form:

$$\mu_i^{NR} = \frac{1.018\, C_\mu m_i^{1/2}\, \Theta_i^{5/2}}{e^4 \ell n\Lambda}\ \left[1 + .026\, \frac{n_e}{n_i}\left(\frac{T_i}{T_e}\right)^{3/2}\right.$$

$$\left. + 6.9\, \frac{10}{\ell n\Lambda}\, (\Theta_i(\text{MeV}))^{3/2}\right]^{-1} \qquad (3.37)$$

$$\mu_e^{NR} = \frac{1.018\, C_\mu m_e^{1/2}\, \Theta_e^{5/2}}{e^4 \ell n\Lambda}\ \left[1 + .821\, \frac{n_i}{n_e}\right.$$

$$\left. + 1.5\, \frac{n_\gamma}{n_e}\, \frac{10}{\ell n\Lambda}\, (\Theta_e(\text{MeV}))^{5/2}\right]^{-1} \qquad (3.38)$$

Setting $T_i = T_e$, $n_i = n_e$, $n_\gamma = 0$, and neglecting the nuclear contribution, we see by comparing the sum of equations (3.37) and (3.38) with Spitzer's (1962) eq. (5-54) for the plasma viscosity coefficient that $C_\mu = .55$, when account is taken of the factor of $\frac{4}{5}$ difference in his definition of μ. We see that for equal velocity gradients and temperatures in the Coulomb regime, the overall effects of viscosity increase as $T^{5/2}$, with ion viscosity dominating electron viscosity by a factor $(\frac{m_i}{m_e})^{1/2}$. For $kT_i \gtrsim 1$ MeV, nuclear and radiation effects limit this increase

Similarly the non-relativistic expressions for ion and electron heat conduction are given by:

$$K_j^{NR} = \frac{3}{2}\frac{k}{m_j}\frac{C_\kappa}{C_\mu}\mu_j^{NR} \tag{3.39}$$

where by comparison of (3.39) with the result of Spitzer (1962) for a hydrogen plasma of uniform temperature we find $C_\kappa = 1.14$. We see that for equal temperatures and temperature gradients in the Coulomb regime that heat conduction also increases as $T^{5/2}$, with electron heat conduction dominating ion heat conduction by a factor $(\frac{m_i}{m_e})^{1/2}$.

While a precise extension of these results to allow for relativistic electron effects has not been made, and is beyond the scope of the present work, the following approximate corrections seem evident. First, the mean electron thermal velocity relativistically becomes:

$$v_e^{th} = [1 - (1 + \frac{\alpha_e \Theta_e}{m_e c^2})^{-2}]^{1/2}c \tag{3.40}$$

Second, the factors of Θ_e in the Coulomb mean free paths are transformed to $\frac{2}{3}\alpha_e \Theta_e$ to allow for the increased electronic specific heat (see Section III.E for values of α_e); and third, σ_T in (3.36) goes to the Klein-Nishina cross-section while the factor $(\frac{m_e}{3\Theta_e})^{1/2}$ is limited to $1/c$. As we shall see, electron temperatures for most cases of interest remain below $\sim$200 keV, so relativistic corrections are unlikely to become crucial, especially in view of the large temperature dependence of the Coulomb cross-sections.

For future convenience, we define: $A_2 = \mu_i \theta_i^{-5/2}$.

Photon Diffusion and Heat Transport

Following the diffusion approximation, we take

$$D_\gamma(\varepsilon_\gamma) = \frac{c}{3} \ell_c \equiv \frac{c}{3} \frac{1}{n_e \sigma_c(\varepsilon_\gamma)} \tag{3.41}$$

Here ℓ_c is the Compton transport length, and non-relativistically (i.e. ε_γ, $\theta_e \ll m_e c^2$) $\sigma_c = \sigma_T$. Relativistically, $\sigma_c \sim \frac{m_e c^2}{\varepsilon_\gamma} \sigma_T$ with more precise numerical results and analytic fits being given by Cooper (1974). The use of the diffusion approximation in the form of (3.41) has been shown to be accurate to $\lesssim$ 5% (cf. Alme and Wilson 1973), provided the directed photon velocity $v_\gamma \equiv \frac{S_\gamma}{E_\gamma}$ is much less than c. For $v_\gamma \sim c$, the diffusion approximation can be modified to give accurate results (errors $\lesssim$5%) by limiting v_γ to $\leq$ c by an appropriate multiplicative expression termed a flux limiter (ibid).

The heat transport by radiation relative to the frame of the electrons is then given by (non-flux limited):

$$S_\gamma(\varepsilon_\gamma) = -\varepsilon_\gamma D_\gamma(\varepsilon_\gamma) \frac{dn_\gamma(\varepsilon_\gamma)}{dx} \tag{3.42}$$

D. Transfer Processes

Ion-Electron Energy and Momentum Coupling

Burgers (1960) has calculated the momentum and energy transfer rates, $\vec{P}_{ei}$ and $\vec{E}_{ei}$, between ions and electrons due to Coulomb forces for arbitrary temperature and velocity differences. Assuming $T_i \ll \frac{m_i}{m_e} T_e$, $\left|v_e - v_i\right| \ll v_e^{th}$, $v_e \ll \frac{m_i}{m_e} v_i$, and neglecting terms of order $(\frac{m_e}{m_i})^{1/2}$, his results can be written in the form (cf. Jaffrin and Probstein 1964):

$$\vec{P}_{ei} = - \frac{A_1 n_e n_i m_i (v_e - v_i)}{\Theta_e^{3/2}} \tag{3.43}$$

$$\vec{E}_{ei} = - \frac{A_1 n_e n_i [3(\Theta_e - \Theta_i) + (v_e - v_i) v_i m_i]}{\Theta_e^{3/2}} \tag{3.44}$$

where:

$$A_1 = \frac{8}{3} \sqrt{\frac{\pi}{2}} e^4 Z_i^2 \frac{m_e^{1/2}}{m_i} \ell n \Lambda$$

$$= 3.21 \times 10^{-27} Z_i^2 \ell n \Lambda \ \text{erg}^{3/2} \ \text{cm}^3 \ \text{sec}^{-1} \tag{3.45}$$

While relativistic calculations of electron-ion coupling do not exist at present, an approximate correction can be given if the electrons are not too relativistic (i.e. $\Theta_e \lesssim m_e c^2$). In this case, the low energy electrons to which the ions are most strongly coupled will remain non-relativistic and the coupling mechanism will be affected only by the relative depopulation of the low energy tail of the electron distribution by the factor:

$$f_{ei} = \sqrt{\frac{\pi}{2}}\left(\frac{\Theta_e}{m_e c^2}\right)^{1/2} \frac{e^{-m_e c^2/\Theta_e}}{K_2(m_e c^2/\Theta_e)} \xrightarrow[NR]{}$$

$$\frac{1}{1 + \frac{15}{8}\frac{\Theta_e}{m_e c^2}} \equiv f_{ei}^{NR} \tag{3.46}$$

where the non-relativistic form is accurate to ∿20% up to $\Theta_e = m_e c^2$. At sufficiently high temperature, however, this depopulation will become severe enough to increase the effective interaction energy and thus reduce this effect. For lack of a better treatment, we will use f_{ei}^{NR} as the correction factor for $\Theta_e < m_e c^2$, and correct by $f_{ei}^{NR}(m_e c^2) = .35$ at higher temperatures.

Compton Scattering

The cross-sections indicated by $\sigma(\varepsilon_\gamma \rightarrow \varepsilon_\gamma')$ in the Compton scattering kernel in equation (2.9) have been evaluated numerically by Stone and Nelson (1966) in a relativistically correct fashion. (See Stone 1971, 1973; Cooper 1971, 1974, for subsequent applications and special cases). For electron temperatures below 100 keV and photon energies below 1 MeV, the effects of Compton scattering in changing the energy of continuum radiation can be accurately and much more conveniently represented using the Fokker-Planck approximation (Cooper 1971) according to which:

$$\frac{\partial n(\varepsilon_\gamma,t)}{\partial t} = \frac{1}{\varepsilon_\gamma^2}\frac{\partial}{\partial \varepsilon_\gamma}\left[\alpha_{FP}(\varepsilon_\gamma,T_e)[n(\varepsilon_\gamma,t)(1+n(\varepsilon_\gamma,t)) + \Theta_e \frac{\partial n(\varepsilon_\gamma,t)}{\partial \varepsilon_\gamma}]\right] \tag{3.47}$$

where $n(\varepsilon_\gamma,t)$ is the dimensionless photon distribution function (normalized by requiring $\int_0^\infty n(\varepsilon_\gamma,t)\varepsilon_\gamma^2 d\varepsilon_\gamma = \frac{(hc)^3}{8\pi} n_\gamma$) as a function of photon energy, ε_γ, and time, and $\alpha_{FP}(\varepsilon_\gamma,T_e)$ is the Fokker-Planck coefficient given approximately by:

$$\alpha_{FP}(\varepsilon_\gamma,T_e) = \frac{\sigma_T n_e \varepsilon_\gamma^4}{m_e c} \frac{1 + f(T_e)/(1 + .02\varepsilon_k)}{1 + .009\varepsilon_k + 4.2\times10^{-6}\varepsilon_k^2} \tag{3.48}$$

where ε_k is ε_γ in keV and $f(T_e) = \frac{5}{2}(\frac{\Theta_e}{m_e c^2}) + \frac{15}{8}(\frac{\Theta_e}{m_e c^2})^2(1-\frac{\Theta_e}{m_e c^2})$.

In this approximation, the expectation of the energy change of a photon per unit time is given by:

$$<(\varepsilon_\gamma' - \varepsilon_\gamma)> = \frac{1}{\varepsilon_\gamma}\frac{1}{2}\left[\theta_e \frac{\partial \alpha_{FP}(\varepsilon_\gamma, T_e)}{\partial \varepsilon_\gamma} - \alpha_{FP}(\varepsilon_\gamma, T_e)\right] \tag{3.49}$$

Non-relativistically this reduces to:

$$<(\varepsilon_\gamma' - \varepsilon_\gamma)> = \sigma_T n_e c \left(\frac{\varepsilon_\gamma}{m_e c^2}\right)(4\theta_e - \varepsilon_\gamma) \tag{3.50}$$

corresponding to a fractional photon energy change of $\frac{4\theta_e - \varepsilon_\gamma}{m_e c^2}$ per Compton collision. Thus non-relativistic Compton scattering *is capable of e-folding the energy of a sub-thermal photon* (i.e. $\varepsilon_\gamma < kT_e$) in $\sim \frac{m_e c^2}{4\theta_e}$ collisions.

To very roughly estimate the quantity $<\Delta w_{11}>_{e\gamma}$ (the expectation value of the initial rate of change of the parallel component of an electron's velocity as it passes through a photon gas at temperature $T_\gamma = T_e$) which is required in equation (3.35), we note using (3.50) that:

$$\left.\frac{<\Delta w_{11}>_{e\gamma}}{w}\right|_{w=v_e^{th}} \approx \left.\frac{\frac{1}{2}\frac{<\Delta w_{11}^2>_{e\gamma}}{2}}{}\right|_{w=v_e^{th}}$$

$$\sim \frac{1}{2}\frac{n_\gamma}{n_e}\left.\frac{<(\varepsilon_\gamma' - \varepsilon_\gamma)>}{\frac{3}{2}\theta_e}\right|_{\varepsilon_\gamma = 3\theta_e} = n_\gamma \sigma_T c \frac{\theta_e}{m_e c^2} \tag{3.51}$$

E. Electron Specific Heat

The electron specific heat coefficient, α_e, defined as the ratio of the electron energy density to electron pressure, is given for a non-degenerate arbitrarily relativistic gas by: (cf. Chiu 1968):

$$\alpha_e = \Phi \left[\frac{3K_3(\Phi) + K_1(\Phi)}{4K_2(\Phi)} - 1 \right] \tag{3.52}$$

where $\Phi = m_e c^2/\Theta_e$ and the K_i are modified Bessel functions of the second kind. A convenient numerical expression for α_e is:

$$\alpha_e = \frac{3}{2}\left(1 + \frac{5}{4\Phi+5}\right) \tag{3.53}$$

which is exact to 1st order in $1/\Phi$, goes to the correct relativistic limit and, in general, is accurate to better than 2%.

It is apparent that α_e goes from $\frac{3}{2} \to 3$ as Θ_e goes from 0 to ∞ with substantial (i.e. $\gtrsim$ 10%) relativistic corrections occuring for $\Theta_e \gtrsim 50$ keV.

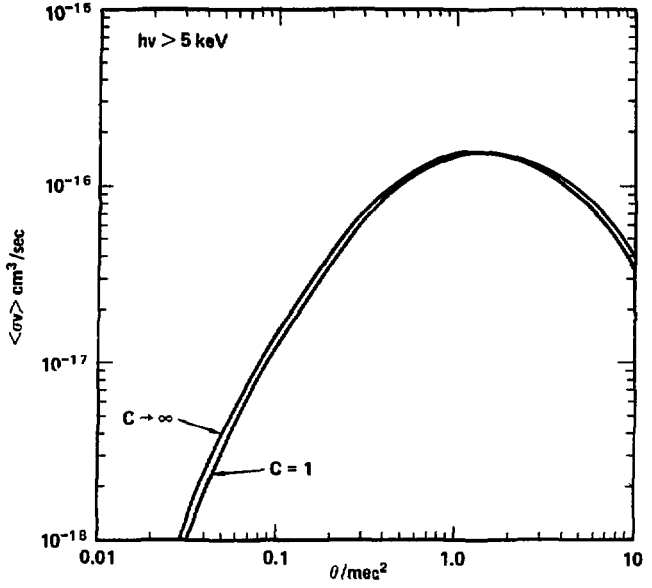

Figure 3.1 - Radiative Compton scattering emission rate. Here $\langle \sigma v \rangle \equiv Q_{RC}/n_e n_\gamma$, $h\nu = \varepsilon_\gamma$, and C is the Bose-Einstein degeneracy parameter of the radiation field.

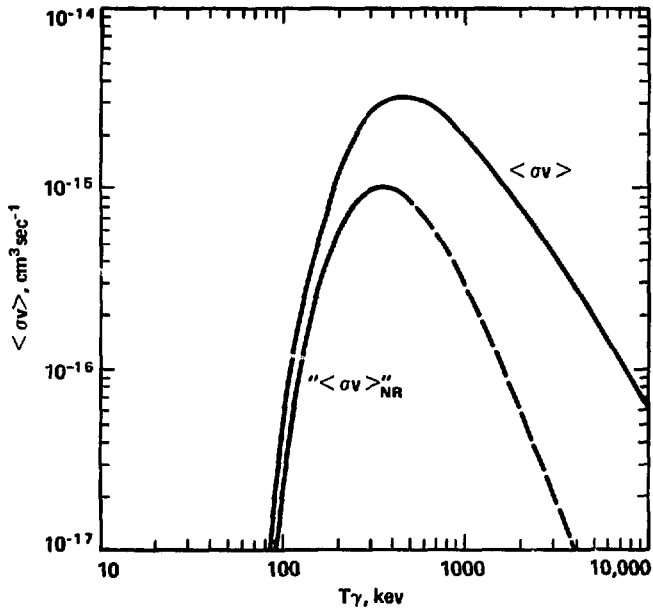

Figure 3.2 - The rate of the $\gamma\gamma \rightarrow e^+e^-$ reaction. Here $\langle\sigma v\rangle \equiv 2Q^{\pm}_{\gamma\gamma}/n^2_{\gamma}$ and "$\langle\sigma v\rangle_{NR}$" is a "non-relativistic" approximation to $\langle\sigma v\rangle$.

IV. THE EFFECTIVE PHOTON APPROXIMATION

A. General Formulation

In their present form, shock structure equations (2.13) - (2.20) are quite cumbersome and do not lend themselves either to numerical solution or analytic interpretation. A key factor in their simplification is to note from § III.D that the time required for a near thermal photon (i.e. $\varepsilon_\gamma \gtrsim .1\theta_e$) to be thermalized to $\sim\theta_e$ is typically quite short in an optically-thick plasma at temperatures above a few keV. For example, a 1 keV photon requires only $\sim \frac{m_e c^2}{4\theta_e} \ell n \left(\frac{\theta_e}{\varepsilon_\gamma}\right) \approx 30$ Compton collisions to be thermalized at $\theta_e = 10$ keV. Since the post-shock velocities ($v_1 = v_0/7$, see § V) under consideration range from c/150 ($E_0 = 1$ MeV) to c/15 ($E_0 = 100$ MeV), such thermalization will occur as the matter is swept through .2 to 2 Compton lengths. As has been shown in the Monte-Carlo Compton scattering calculations described by Chapline and Stevens (1973), such thermalization results in the buildup of a Bose-Einstein distribution of photons, characterized by an "effective" photon <u>number</u> density, n_γ, and an effective temperature $T_\gamma = T_e$.

If ε_c is the lowest energy from which a photon can be thermalized over a "relevant" shock length scale, then from § III.A, we see that the quantity $\ell n\lambda \equiv \ell n(\varepsilon_c/\theta_e)$ provides a rough measure of the importance of subthermal photons in cooling the electrons. Thus, if we find that relevant shocks scales are indeed $\gtrsim$ Compton length as we expect in radiation-dominated shocks, the effect of inverse Compton cooling will be substantial for

$\theta_e \gtrsim$ 5-10 keV.

To make these considerations a logically rigorous basis for simplifying equations (2.13) - (2.20), we shall first explicitly make the following assumptions, and later show that the shock structures that result are self-consistent with them:

1) All but a negligible fraction of the energy in the radiation field can be characterized to sufficient accuracy by a Bose-Einstein distribution with effective photon density n_γ and temperature $T_\gamma \gtrsim T_e$.
2) The creation rate of effective photons, Q_γ^{eff}, can be taken as the integral over the photon emission spectrum down to some cutoff energy ϵ_c, determined by the constraints of inverse bremsstrahlung, screening, and the photon thermalization time with respect to relevant shock time scales, as prescribed in § IV.B.

Using this set of assumptions, which we shall term the effective photon approximation, we can reduce the multigroup treatment of the radiation field implied by equation (2.20) to the following relatively simple equation describing the creation and diffusion of effective photons:

$$\frac{d(n_\gamma v_e)}{dx} - \frac{d}{dx}\left[\frac{c}{3n_e\bar{\sigma}_c}\frac{dn_\gamma}{dx}\right] = Q_\gamma^{eff} \tag{4.1}$$

where

$$Q_\gamma^{eff} = Q_{ei}^{NR} + Q_{RCB} + Q_{RC} \tag{4.2}$$

and $\bar{\sigma}_c \equiv \sigma_c\,(3\theta_e)$ is the mean Compton cross-section. Also we find:

$$E_\gamma = 3P_\gamma = 2.7\, n_\gamma \theta_e \tag{4.3}$$

$$S_\gamma = -\frac{9}{10}\, \frac{c}{n_e \bar{\sigma} c}\, \frac{d}{dx}\,(n_\gamma \theta_e) \tag{4.4}$$

Here we have adopted the black-body specific heat coefficient of 2.7 in (4.3) to achieve consistency with the final equilibrium state. The 10% error this introduces for a non-degenerate Bose-Einstein distribution (where $E_\gamma = 3n_\gamma \theta_e$) will be neglected.

B. Cutoff Energy for Effective Photon Emission

Absorption

Chapline and Stevens (1973) have examined the effect of Compton scattering on bremsstrahlung emission spectra by utilizing the Fokker-Plank approximation (cf. Cooper 1971). They find that low-energy radiation will be absorbed by inverse bremsstrahlung before it can be thermalized for photon energies below

$$\varepsilon_B = .77\ \theta_e^{-5/4}(\text{keV})\left(\frac{n_e}{10^{20}\text{cm}^{-3}}\right)^{1/2}\text{keV} \qquad (4.5)$$

provided $\varepsilon_B << m_e c^2$.

Screening

In a plasma, bremsstrahlung emission occurring at impact parameters larger than the Debye length, $\lambda_D = \left(\frac{\theta_e}{4\pi n_e e^2}\right)^{1/2}$, will be suppressed by Coulomb screening. This effect will be important for a given photon energy, ε_γ, only if

$$\lambda_D \lesssim b_{max} \simeq \frac{\gamma^2\beta}{\varepsilon_\gamma}\hbar c \qquad (4.6)$$

where b_{max} is the normal cutoff impact parameter for that photon energy (cf. Jackson 1962, eq. (15-28)), and $\gamma^2\beta \simeq \frac{v_e^{th}}{c}\left[1-\left(\frac{v_e^{th}}{c}\right)^2\right]^{-1}$ where v_e^{th} is given by eq. (3.40). We find that the photon energy, ε_{sc}, below which screening is important is given approximately by:

$$\varepsilon_{sc} \gtrsim 5.2 \times 10^{-4}\ \alpha_e^{1/2}\left(\frac{n_e}{10^{20}\text{cm}^{-3}}\right)^{1/2}\left(1+\frac{\alpha_e\theta_e}{2m_e c^2}\right)^{1/2}\left(1+\frac{\alpha_e\theta_e}{m_e c^2}\right)\ \text{keV} \qquad (4.7)$$

Thus ε_{sc} is typically $\lesssim 1$ eV, and exceeds ε_B for $\theta_e \gtrsim 160$ keV. It is often the

case, however, that not enough time is available to thermalize a 1 eV photon to $\theta_e > 100$ keV, and thus the dynamical cutoff discussed in the next section usually dominates where screening would otherwise have been important.

Thermalization

Since according to (3.50), a non-relativistic, sub-thermal photon will be e-folded in energy in $\sim \frac{m_e c^2}{4\theta_e}$ Compton collisions, the lowest energy, ε_d, from which a photon can be thermalized in a dynamical time, τ_d, is:

$$\varepsilon_d = 2.7\theta_e \exp\left(-4cn_e\sigma_T\tau_d\theta_e/m_ec^2\right)\left(1 + \frac{\Delta\theta_e(\tau_d)}{\theta_e}\right) \tag{4.8}$$

where $\Delta\theta_e(\tau_d)$ is the mean change of temperature that a photon experiences during τ_d. In the shock models discussed below, τ_d will be taken as the time a photon at mean velocity, v_γ, takes to cross the photon number or electron temperature e-folding distance, whichever is smaller. The mean photon velocity is defined by (see (4.1)):

$$v_\gamma \equiv -\frac{c}{3n_e\bar{\sigma}_c n_\gamma}\frac{dn_\gamma}{dx} + v_e \tag{4.9}$$

(See § V.D for a discussion of shock structure sensitivity to this choice of τ_d.)

Maximum Cutoff Energy

When conditions are such that $\varepsilon_d/\theta_e \sim 1$, we expect the effective photon approximation to become inaccurate. In this case, we can still obtain the proper bremsssrahlung energy loss rate from the electrons by not letting ε_c exceed ε_{max}, the cutoff energy

at which

$$3\theta_e(Q_{ei}^{NR} + Q_{RCB}) = W_{ei}^{NR} + W_{ei}^{RC} + W_{ee} \tag{4.10}$$

where the W's are the bremsstrahlung energy loss rates given in § III.A. From the relations in § III.A, we find:

$$\lambda_{max} \equiv \frac{\epsilon_{max}}{\theta_e} \approx .6 \tag{4.11}$$

The effective photon cutoff energy , ϵ_c, is then taken as the maximum of ϵ_B, ϵ_{sc}, and ϵ_d up to a maximum of .6 θ_e.

V. RADIATION-DOMINATED SHOCK MODEL

A. Assumptions and Basic Equations

The radiation-dominated shock model is based on the general formalism of Section II, with the following additional assumptions and restrictions:

1) The pre-shock internal energy is negligible compared to the shock energy.
2) The effect of electron-positron pairs is not crucial.
3) The ions and electrons move together with velocity v, and thus have the same density n.
4) The effective photon approximation is valid. (Note that this includes the assumption $T_\gamma \approx T_e$.)
5) The principal dissipation mechanism is radiative heat conduction.
6) Except at the leading edge of the shock, radiation pressure dominates matter pressure.

The validity and self-consistency of these assumptions in the context of the shock structures they generate is considered in § V.D below. Using them, the shock structure equations, (2.13) - (2.20), can be recast in the particularly simple form:

$$n_\gamma \theta_\gamma = n_0 v_0 m_H (v_0 - v) \tag{5.1}$$

$$4v n_\gamma \theta_\gamma - \frac{cv}{n_0 v_0 \bar{\sigma}_c} \frac{d(n_\gamma \theta_\gamma)}{dx} = n_0 v_0 m_H (v_0^2 - v^2)/2 \tag{5.2}$$

$$\frac{d(n_\gamma v)}{dx} - \frac{d}{dx}\left[\frac{cv}{3 n_0 v_0 \bar{\sigma}_c} \frac{dn_\gamma}{dx}\right] = Q_\gamma^{eff} \tag{5.3}$$

$$n = \frac{n_o v_o}{v} \tag{5.4}$$

$$\frac{3}{2} n_o v_o \frac{d\theta_i}{dx} = -\frac{n_o v_o}{v}\,\theta_i \frac{dv}{dx} + A_2 \theta_i^{5/2} \left(\frac{dv}{dx}\right)^2 + \left(\frac{v_o n_o}{v}\right)^2 \frac{A_1}{\theta_e^{3/2}} 3(\theta_e - \theta_i) \tag{5.5}$$

where $\theta_\gamma \equiv \frac{3}{10} kT_\gamma = \frac{9}{10}\theta_e$, m_H is the mass of a hydrogen atom, and A_2 and A_1 are defined in § III.C and by equation (3.45) respectively. Note that the plasma momentum conservation equation (5.1), is now algebraic and describes a linear relationship between radiation pressure, $n_\gamma \theta_\gamma$, and v. Equation (5.2) is the plasma energy conservation equation, while (5.3) and (5.4) describe photon and matter particle continuity, and (5.5) is the ion heating equation. Due to its small coefficient, ion heat conduction has been neglected in equation (5.5), with the remaining terms on the right-hand-side describing compressional work, viscous heating, and electron-ion coupling.

For future convenience, we define $E_o \equiv \frac{1}{2} m_H v_o^2$, the initial energy per nucleon in the shock frame.

B. Analytical Solutions

By differentiating equation (5.1) and using it to eliminate θ_γ and n_γ from (5.2), we obtain a decoupled equation for v:

$$\frac{dv}{dx} = -\bar{\sigma}_c n_o v_o \frac{(7v-v_o)(v_o-v)}{2vc} \tag{5.6}$$

Using the boundry condition that the velocity gradient vanishes at $x=+\infty$, we immediately obtain the expected post-shock conditions:

$$v_1 \equiv v(+\infty) = v_o/7 \tag{5.7}$$

$$\theta_1 \equiv \theta_\gamma(+\infty) = \frac{6}{7} n_o \frac{m_H v_o^2}{n_\gamma(+\infty)} \tag{5.8}$$

$$n_1 \equiv n(+\infty) = 7n_o \tag{5.9}$$

Equation (5.6) can then be integrated directly to find x(v):

$$x = \frac{c}{21\bar{\sigma}_c n_o v_o} \left\{ \ell n \left[\frac{(v_o-v)^7}{(7v-v_o)v_o^6} \right] - \ell n\left[\frac{1}{3}\left(\frac{3}{7}\right)^7\right] \right\} \tag{5.10}$$

where we have taken $v = 4v_o/7$ at $x=0$.

Thus the velocity profile of the shock is *independent* of the details of radiative equilibration (see Figure 5.1). Near the upstream limit ($v \to v_o$), and using (5.1) and (5.6), we see that the energy in the radiation field, $3n_\gamma\theta_\gamma$, e-folds in a length $\Delta \equiv c/(3\bar{\sigma}_c n_o v_o)$. In the downstream limit ($v \to v_o/7$), the residual directed momentum in the ions e-folds in a length $\Delta/7$. A characteristic shock is then $\sim\Delta$ or $\sim c\sigma_T/3v_o\bar{\sigma}_c$ pre-shock Thompson lengths.

To calculate the peak ion temperature occurring in the shock and thus the expected amount of nucleosynthesis, it is still necessary first to solve the photon continuity equation (5.3) and then the ion heating equation (5.5), which in general must be done numerically. Some analytic insight can be gained, however, by using (5.6) and (5.1) to change the variable in (5.3) from x to v, yielding:

$$(7v-v_o)^2(v_o-v)^2 \frac{d^2n_\gamma}{dv^2} + 8(7v-v_o)(v_o-v)^2 \frac{dn_\gamma}{dv}$$

$$+ 6(7v-v_o)(v_o-v)n_\gamma = -\frac{12vc}{n_o v_o \bar{\sigma} c} Q_\gamma^{eff} \qquad (5.11)$$

Note that by doing this we have explicitly exhibited the singularities in the photon continuity equation by moving them from $\pm\infty$ to $v = v_o$, $v_o/7$.

Equation (5.11) can now be solved analytically for the case of a near equilibrium radiation field (i.e. $f_E << 1$, where f_E is the radiation equilibrium parameter defined by equation (3.10)). T_γ and n_γ then become:

$$T_\gamma = \left[\frac{10 n_o v_o m_H (v_o-v)}{9kb(1-f_E)}\right]^{1/4} \qquad (5.12)$$

$$n_\gamma = \{10 n_o v_o m_H (v_o - v)/9k\}^{3/4} \{b(1-f_E)\}^{1/4} \qquad (5.13)$$

For small f_E and $v_o < c/2$, θ_γ will always be less than 50 keV, and so only the non-relativistic bremsstrahlung photon source term will be important. Setting the $(1-f_E)^{1/4}$ terms in (5.12) and (5.13) equal to unity and using (5.11) together with (3.10) to solve for f_E yields:

$$f_E(v) = \frac{1}{(n_o v_o)^{1/8}} \left(\frac{m_H}{.9k}\right)^{7/8} \frac{\bar{\sigma}_c b^{1/8}}{64 c J_o} \; v\{v_o - v\}^{7/8}$$

$$\cdot \{7v - v_o\}^2 \; (g_2(\lambda))^{-1} \qquad (5.14)$$

where, using equation (3.2), we have defined a bremsstrahlung emission coefficient $J_o \equiv 5.692 \times 10^{-12}\ {}^{o}K^{1/2}\ cm^3\ sec^{-1}$ and combined Gaunt factor $g_2(\lambda) \equiv g_1(\lambda)\ E_1(\lambda)$. The neglect of derivatives involving $(1-f_E)$ in deriving (5.14) is a good approximation except for $v \lesssim 2v_o/7$ where the shock is very close to equilibrium and all gradients are small.

An approximate criterion for the consistency of our assumption of a near-equilibrium shock can be established by requiring that the maximum value of $f_E(v)$ be $\lesssim 1/2$ (with λ held constant), and can be written in the form:

$$E_o \lesssim .71\ (n_{20}^o)^{1/15} \left(\frac{g_2(\lambda)}{3}\right)^{8/15} \text{MeV} \qquad (5.15)$$

where $n_{20}^{o} = n_o/10^{20}cm^{-3}$, and we have taken $\bar{\sigma}_c = \sigma_T$ since the resulting equilibrium temperatures are $<< m_e c^2$.

To determine λ, we note from equation (4.9) that for an equilibrium shock

$$v_\gamma^{eq} = \frac{-cv}{3n_o v_o \bar{\sigma}_c T_\gamma^3} \quad \frac{dT_\gamma^3}{dv} \quad \frac{dv}{dx} + v = \frac{v_o+v}{8} \tag{5.16}$$

while the photon e-folding length, $\ell_{\Delta\gamma}$, is $\frac{1}{3}\ell_{\Delta t}$, the temperature e-folding length, and using (5.10) we find that for $v \gtrsim \frac{2}{7} v_o$:

$$\ell_{\Delta\gamma}^{eq} \approx \frac{cv}{9\,\bar{\sigma}_c n_o v_o^2} \tag{5.17}$$

implying:

$$\tau_d^{eq} \equiv \ell_{\Delta\gamma}^{eq}/v_\gamma^{eq} = \frac{8\,cv}{9\,\bar{\sigma}_c n_o v_o^2 (v_o+v)} \tag{5.18}$$

and:

$$\varepsilon_d = 3.6\,\theta_e \exp\left(-\frac{32}{9}\left(\frac{\sigma_T}{\bar{\sigma}_c}\right)\frac{\theta_e}{m_e v_o (v_o+v)}\right) \tag{5.19}$$

For $E_o = 1$ MeV, $n_o = 10^{20}$ cm^{-3}, and $\bar{\sigma}_c = \sigma_T$, we have at mid-shock ($v = \frac{4}{7}v_o$) that $\varepsilon_d = .31$ keV ($\theta_e = 1.32$ keV); or for $n_o = 10^{17}$ cm^{-3} that $\varepsilon_d = .51$ keV ($\theta_e = .23$ keV). The corresponding inverse bremsstrahlung cutoffs are .54 keV and .15 keV respectively, while those for screening are 6.4×10^{-4} keV and 2.0×10^{-5} keV.

We thus find $\lambda = .41$ and $.6$ yielding $g_2(\lambda) = 1.65$ and 1.47 respectively. Criterion (5.15) thus becomes $E_0 \lesssim .52$ MeV and $E_0 \lesssim .31$ MeV for $n_0 = 10^{20}$ cm^{-3} and 10^{17} cm^{-3} respectively. Thus shocks with $E_0 \lesssim 1$ MeV will be reasonably close to blackbody equilibrium over this density range.

The temperatures of such shocks will remain $\lesssim T_{eq}$, the final equilibrium temperature, given by:

$$T_{eq} = 1.57 \{n_{20}^o E_0(\text{MeV})\}^{1/4} \text{keV} \tag{5.20}$$

The final equilibrium photon density will be:

$$n_\gamma^{eq} = 1.22 \times 10^{23} (E_0(\text{MeV}) n_{20}^o)^{3/4} \text{ cm}^{-3} \tag{5.21}$$

Evaluation of the terms in the ion heating equation (5.5) shows that for temperatures of a few keV and the velocity gradients given by (5.6) that electron-ion coupling dominates, and thus requires $\theta_i \gtrsim \theta_e$.

C. Numerical Solutions

The photon continuity equation (5.3) can be solved in a stable fasion numerically, by using double-side boundary conditions and an appropriate back substitution algorithm. The details of this method of numerical solution are given in Appendix B. These details are important since several straightforward ways of differencing (5.3) lead to unstable results.

The boundary conditions are taken as $n_\gamma(x_0) = n_\gamma^s$ and $n_\gamma(x_1) = n_\gamma^{eq}$. The points x_0 and x_1 are then moved toward $-\infty$ and $+\infty$ respectively until the solution stops changing significantly. The value of n_γ^s is typically chosen either as $10^{-2}\ n_0$ or bT_s^3 where T_s is defined below, and the resulting shock structure is found to be quite insensitive to this choice provided $n_\gamma^s \ll n_0$.

Once n_γ is known, the analytic equations (5.1) and (5.10) serve to determine v and θ_γ, except at the leading edge of the shock where matter pressure becomes important. In addition, at temperatures below a few keV, Compton scattering becomes less and less effective in maintaining $T_e \simeq T_\gamma$. These points are discussed in more detail below, but in fact the shock structure is reasonably insensitive to where the upstream (i.e. $x \to -\infty$) boundary on n_γ is taken. In view of this, it is convenient to use the following procedure for choosing the upstream boundary point.

The matter-pressure terms are re-inserted into the expression for the radiation temperature (see (2.13)) with the assumption $T_\gamma = T_e = T_i$, yielding:

$$T_\gamma = \frac{n_0 v_0 m_H (v_0 - v)}{(.9kn_\gamma + 2n_0 v_0 k/v)} \tag{5.22}$$

The upstream boundary point is then chosen so that the resulting temperature, T_s, is sufficient to ensure that Compton scattering will result in rapid temperature equilibration of newly created photons. Typically T_s is taken $\sim$ 5 keV and $n_\gamma^s = 10^{-2} n_0$ for $E_0 \gtrsim 10$ MeV. The peak shock temperatures that result are found to agree within $\sim$ 1% with calculations where T_s is chosen such that $n_\gamma^s = bT_s^3 \sim .1\ n_0$. For $E_0 < 10$ MeV, adequate Compton thermalization can occur for $T_s \gtrsim$ 1-2 keV while at lower temperatures the number of near thermal bremsstrahlung photons emitted over a characteristic shock scale is sufficiently great to insure a near equilibrium photon number (although the spectrum will probably be distorted). Such shock calculations are started using the $n_\gamma^s = bT_s^3 \sim .1\ n_0$ condition.

Given the temperature and velocity, the ion heating equation (5.5), can be solved by taking $\theta_i(x_0) = \theta_e(x_0)$ and integrating downstream. The appropriate difference equation is given in Appendix B.

The Bose-Einstein radiation-dominated shock structures that result from the present model are shown in Figures 5.1 and 5.2 for typical values of E_0 and n_0. The abrupt rise of n_γ and corresponding fall in T apparent in some of these shock structures near the downstream boundary (e.g. 5.2(a)), is due to numerically forcing the shock to come to final equilibrium at a point, x_1, not sufficiently far downstream, and is done so the shock can be zoned

and plotted on a reasonable length scale. Test calculations show that this has essentially no effect on the structure of the shock outside the "flared" region. Figure 5.3 plots the peak temperature reached in the shock as a function of E_0 over the range 1-100 MeV/nucleon, and shows explicitly the effect of the various sources of radiation, as well as various characteristic temperatures. In these models $\bar{\sigma}_c = \sigma_T$, which is a reasonable approximation considering the temperatures involved. The effect of decreasing $\bar{\sigma}_c$ is to somewhat lengthen the shock width and thus somewhat increase the degree of radiative equilibration (note that inverse Compton scattering involves σ_T, not $\bar{\sigma}_c$).

Before discussing the details of these results and the implications of the relatively low temperatures involved in these shocks for nucleosynthesis, it is necessary to determine under what conditions our model is valid. This is undertaken in the next section.

D. Self-Consistency of the Radiation-Dominated Shock Solution
Sufficiency of Dissipation by Radiative Heat Conduction

We wish to derive the value of the ratio of the radiation to matter pressure, $\xi \equiv P_\gamma/P_m$, below which radiation heat conduction is insufficient to prevent a shock discontinuity in the absence of viscosity. To this end, we introduce matter thermal energy and pressure terms into the equations of momentum and energy conservation, (5.1) and (5.2), and utilize the variable $\eta = \frac{v}{v_o}$, yielding:

$$P_m + P_\gamma = n_o m_H v_o^2 (1-\eta) \tag{5.23}$$

$$\frac{5}{2}\eta P_m + 4\eta P_\gamma - \frac{c\eta}{n_o v_o \bar{\sigma}_c}\frac{dP_\gamma}{dx} = n_o m_H v_o^2 (1-\eta^2)/2 \tag{5.24}$$

where $P_\gamma = n_\gamma \theta_\gamma$ and $P_m = 2n_o k\bar{T}_m/\eta$, and where $\bar{T}_m$ is the average of the electron and ion temperature. To determine if these equations can have a simultaneous solution, we note from substituting (5.23) into (5.24) that:

$$\frac{c\eta}{n_o v_o \bar{\sigma}_c}\frac{dP_\gamma}{dx} = (\tfrac{7\eta-1}{2})P_\gamma + (\tfrac{4\eta-1}{2})P_m \tag{5.25}$$

and thus $\frac{dP_\gamma}{dx} > 0$ (for $\vec{v}_o$ in the positive x direction) in the range $1 > \eta > \eta_1$. Here η_1 is the postshock value of η (i.e. the η for which $\frac{dP_\gamma}{dx}\Big|_{\eta_1} = 0$ and $\eta < 1$). From (5.25), we see η_1 must satisfy the Hugoniot relation:

$$\xi(\eta_1) = \frac{1-4\eta_1}{7\eta_1 - 1} \tag{5.26}$$

resulting in 4-fold compression across the shock in the absence of radiation ($\xi(\eta_1) = 0$) increasing toward 7-fold compression as $\xi(\eta_1) \to \infty$.

On the other hand, differentiating (5.23) with respect to x yields:

$$\frac{1}{n_o m_H v_o^2} \frac{dP_\gamma}{dx} = \frac{(2\eta-1)+\eta\xi}{\eta(1+\xi)} \left(-\frac{d\eta}{dx}\right) - \frac{2k}{m_H v_o^2 \eta} \frac{d\overline{T}_m}{dx} \qquad (5.27)$$

where for a physically realizable shock we require $\frac{d\eta}{dx} < 0$ (i.e. that the matter velocity decrease monotonically). Thus to be consistent with the requirement derived from (5.25) that $\frac{dP_\gamma}{dx} > 0$, the right hand side of (5.27) must be positive in the range $1 > \eta > \eta_1$. Physically this requirement amounts to the observation that conservation of energy [(5.24) and (5.25)] requires energy transport by radiative diffusion in the -x direction (and thus $\frac{dP_\gamma}{dx} > 0$) while the conservation of momentum (5.23) determines the relation between P_γ and η. As long as $\frac{dP_\gamma}{d\eta} < 0$, the required magnitude of energy flux can be obtained by adjusting $\frac{d\eta}{dx}$, but this is no longer possible in a region where $\frac{dP_\gamma}{d\eta} > 0$, and thus a discontinuous jump in density and velocity will occur across such a region in the absence of other dissipation mechanisms. (See Zel'dovich and Raizer (1966, p. 477) for analogous arguments concerning electron heat conduction.)

To evaluate the right-hand side of (5.27), requires some assumption about $\frac{d\overline{T}_m}{dx}$. If $\frac{d\overline{T}_m}{dx} \leq 0$, then a <u>sufficient</u> condition that no discontinuity exists is:

$$\xi \geq \frac{1-2\eta}{\eta} \quad \text{for } 1 > \eta > \eta_1. \tag{5.28}$$

This condition is most stringent when $\eta \to \eta_1$. Using the Hugoniot relation (5.26) we find that in this case (5.28) becomes:

$$\xi_1 \geq 2 + \sqrt{6} \approx 4.45. \tag{5.29}$$

It is interesting to note that for $\eta > 1/2$, essentially no radiation is required to prevent a discontinuity. However, if the amount of radiation is small, the gradients needed to obtain the necessary energy flux will become very large, and eventually other dissipation mechanisms will become important, even if they are not strictly needed to prevent a discontinuity. This situation will be considered in the next subsection.

It remains to consider the case when $\frac{d\bar{T}_m}{dx} > 0$. The Bose-Einstein model we are considering assumes $T_\gamma \approx T_e$, while we have found $T_i \gtrsim T_e$. The range of validity of this assumption is considered below. Within this range, we take $\bar{T}_m \simeq T_\gamma$, observe that $\frac{d\bar{T}_m}{dx} > 0$ implies $\frac{dT_\gamma}{dx} > 0$, which implies that if $\frac{dP_\gamma}{dx} < 0$, then $\frac{dn_\gamma}{dx} < 0$. However, the character of the photon continuity equation (5.3) and its associated boundary conditions preclude $\frac{dn_\gamma}{dx}$ from being negative as long as Q_γ^{eff} remains positive, which is the physical case of interest. Thus no discontinuities arise in this case.

Thus, within the framework of the present study, equation (5.28) is a generally sufficient criterion for no shock discontinuities to arise and is plotted in Figure 5.3 as T_{crit}. It might be noted that (5.28) and (5.29) are consistent with previous treatments [(Belokon' 1959), Zel'dovich and Raizer (1966, p. 543)] of the occurrence of discontinuities in shocks where the radiation field is assumed in equilibrium.

As has been pointed out by Zel'dovich and Raizer (1966, p. 546) a more intuitive, if less rigorous, approach to these questions is to note that ion-ion collisions can only substantially influence the shock when the ion sound velocity (at $\eta \sim \eta_1$) is above the velocity of the shock front relative to the post-shock material, i.e. when [using (5.23)]:

$$\frac{v_o}{7} \lesssim \left(\frac{5kT_1}{3m_1}\right)^{1/2} \simeq \left(\frac{5}{49(1+\xi)}\right)^{1/2} v_o \qquad (5.30)$$

or

$$\xi < 4; \qquad (5.31)$$

which is in good agreement with the previous results.

Numerical shock models in which both ion viscosity and radiative diffusion are taken into account are discussed in Sections VII and VIII and shown to be consistent with the above analytic results.

Non-Radiative Dissipation Mechanisms

If the velocity or temperature gradients in a radiation-dominated shock steepen to the order of a few electron or ion

mean-free-paths, non-radiative dissipation mechanisms such as ion viscosity and electron heat conduction will become important.

Quantitatively we shall consider that ion viscosity plays a significant role in determining the shock structure when the viscous stress, P_v, becomes greater than $\frac{1}{5}$ the radiation pressure, corresponding to the level at which matter pressure becomes important. This criterion can then be written:

$$P_v = A_2\, \theta_i^{5/2} \left|\frac{dv}{dx}\right| > \frac{1}{5} P_\gamma = \frac{1}{5}\, n_o v_o m_H (v_o - v) \qquad (5.32)$$

Using (5.6), (5.1) and the main Coulomb term in (3.37), this criterion can be re-written as:

$$\theta_i \gtrsim 2.2 \left(\frac{v}{7v - v_o}\right)^{2/5} \left(\frac{\sigma_T}{\bar{\sigma}_c} \frac{\ell n \Lambda}{10}\right)^{2/5} \text{MeV} \qquad (5.33)$$

Taking $\frac{v_o}{v} = 7/4$ as is typical near the peak shock temperature, $\bar{\sigma}_c = \sigma_T$, $\ell n \Lambda = 10$, and $T_\gamma \sim T_i$, we find that viscous effects can only become important when $\theta_\gamma \gtrsim 0.8$ MeV. (Note, however, the limiting effects of nuclear scattering for $\theta_i \gtrsim 1$ MeV.) This criterion is plotted in Figure 5.3 as T_v. The exception to this, of course, is when the radiation to matter pressure ratio falls below 4.45 at this temperature, causing the shock to steepen until viscosity generates the needed dissipation.

Charge Separation

If the ions are stopped exclusively by the action of an electric field, the maximum electric field occurring in the shock

will be given approximately by $\Sigma_{max} \sim E_o/(e\Delta)$ where Δ is the characteristic shock width. Taking $\Delta = c/(3n_o v_o \bar{\sigma}_c)$ and using Poisson's equation, we find the net charge density, ρ, to be:

$$\frac{\rho}{en_o} \sim 4.7 \times 10^{-19} \left(\frac{\bar{\sigma}_c}{\sigma_T}\right)^2 n_{20}^0 E_0^2 \text{ (MeV)} \qquad (5.34)$$

Thus the maximum required charge separation is quite small, and using (5.4) we see that the difference between the ion and electron velocities is also negligibly small. As discussed below, however, the presence of electron-positron pairs can cause substantial differences between these velocities. In addition, if ions with a different charge to mass ratio from hydrogen are present at levels typical of Population I stars, the electric field is not sufficient to ensure that all species remain co-moving. As will be shown in Section VIII, however, viscous forces acting between ions serve to keep the resulting velocity differentials small.

Consistency of the Effective-Photon Approximation

One expects the effective photon approximation to be valid provided $\lambda_d \equiv \varepsilon_d/\theta_e << 1$. Examination of the numerical solutions shows this to be the case for temperatures $\gtrsim$ 1-5 keV, depending on the shock energy. Temperatures < 5 keV are typically found only near the leading edge of the shock and in the final post-shock equilibrium region for shocks of low density and energy. Numerical sensitivity experiments show, however, that the bulk of the shock structure is little effected by conditions in these extreme regions.

The principal error involved in the effective photon approximation arises from the specification of the time available for photon thermalization, τ_d. By taking τ_d as the smallest relevant shock scale, we neglect soft photons which are thermalized only after times longer than τ_d, but still in time to help cool the downstream portion of the shock. The sharp increase in photon density across the shock, however, will tend to dilute this effect. In addition, this error toward lower photon density is consistent with the policy we have used in resolving uncertainties in the evaluation of Q_γ^{eff} (see Section III.A), and results in the temperatures in radiation-dominated shock models being in fact approximate upper limits on the actual shock temperatures.

Since the electrons serve principally as intermediaries in transferring energy between the hot photons that have diffused upstream and newly created subthermal photons, we expect that their temperature will be a good measure of the effective photon temperature and thus $T_e \approx T_\gamma$.

Pair Effects

From the results of Section III.B we note that the number of electron positron pairs will become significant somewhere in the regime θ_e = 60-100 keV. The substantial changes these pairs make in the shock structure is the topic of Section VI. The critical temperature $T_\pm$ derived there for the onset of the changes is plotted in Figure 5.3.

E. Discussion

Comparison of the radiation-dominated shock structures presented in Figures 5.1 and 5.2, and summarized in Figure 5.3, with the results of Section V.D shows that throughout the range of our calculations, radiative heat transport provides sufficient dissipation to mediate the shock transition, and moreover does so over scale lengths sufficiently large that viscosity never becomes an important dissipation mechanism, and serves only to mildly heat the ions. It is evident that while not required to avoid a viscous shock, inverse Compton scattering provides the dominant mechanism for cooling the electrons and thus reducing the peak shock temperatures by more than two orders of magnitude from those that could occur in a hot-ion shock.

The density dependence of the peak shock temperatures is due primarily to the density dependence of the inverse bremsstrahlung cutoff, τ_B defined in equation (4.5). This cutoff has the most effect in determining the effective photon emission rate at low energies where it is not usually dominated by the thermalization cutoff, τ_d, and this behavior is reflected in Figure 5.3. In the shock calcualtions where inverse Compton processes are neglected, the only residual density dependence is due to the factor f_E, defined in (3.10), which allows for inverse processes near radiative equilibrium, and the very small density dependence of the Coulomb logarithm (see eq. (3.28), (3.30), and (3.45)). The treatment of inverse Compton scattering used in the present study is substantially more accurate than the approximate treatment used in Weaver and Chapline (1974), primarily due to the use of the

variable Gaunt factor $g_{ff}(\lambda)$ (see eq. (3.4)) in place of a constant "averaged" one ($g_{ff} = 2.71$). This results in a reduction of the peak shock temperatures by 5-50% from the previous work, for the case where inverse Compton scattering is included.

The ion temperature is determined primarily by viscous heating and electron-ion coupling (see eq. (5.5)). For $\theta_e \gtrsim 25$ keV the e-i coupling is sufficiently strong to keep T_i essentially equal to T_e, while at higher temperatures the $T_e^{-3/2}$ dependence of this coupling together with the $T_i^{5/2}$ dependence of the ion viscosity allows moderate temperature differences to develop. Since radiative heat transport serves to convert the kinetic energy of the ions directly into electron and photon thermal energy, T_i tends to lag T_e in the upstream portion of the shock where the velocity gradients are small and thus viscosity is negligible. The viscous heating that occurs near the center of the shock (x=0) is usually sufficient to make $T_i > T_e$ there, a difference which is then quickly relaxed in the post-shock region (e.g. see Figure 5.1(g)). For $T_e \gtrsim 300$ keV, however, T_i lags T_e so much in the upstream region that the ion temperature never reaches the maximum electron temperature (see Figure 5.1 (h)). The T_i curve in Figure 5.3 summarizes this behavior.

As predicted by the near-equilibrium analytic shock models of Section V.B, the shocks are close to equilibrium near $E_0 = 1$ MeV, particularly in the upper part of the density range, where fewer photons per electron are required for equilibration (see Figure 5.1(a), 5.3, and eq. (5.21)).

Comparison of the $T_{\pm}$ and T_{γ} curves in Figure 5.3 shows that pairs become important for radiation temperatures $\gtrsim$ 60-70 keV and shock energies $\gtrsim$ 30-50 MeV/nucleon. The general effect of this transition is to increase the degree of radiative equilibrium and thus lower the peak shock temperature relative to the radiation-dominated model. At the same time the source of dissipation is expected to shift from radiative heat transport to ion-lepton Coulomb friction. The calculations leading to these conclusions are given in Section VI.

We thus conclude that the ion temperature remains below $\sim$400 keV for shock energies up to 100 MeV/nucleon, and below $\lesssim$ 100-200 keV when the effect of pairs is taken into account. Since spallation thresholds ($Z > 1$) are $\sim$8 MeV/nucleon, the amount of nuclear spallation that will take place in these shocks is quite small, and thus essentially no deuterium will be produced. Indeed the $n\tau$ products characteristic of the temperature peaks of these shocks (where τ is the time duration) are only of the order of 10^{15}-10^{17} cm^{-3} sec, which for $T_i \lesssim$ 100 keV will only suffice to burn whatever deuterium, tritium, and perhaps He^3, that might have been present originally. For $T_i \sim$ 400 keV and $n\tau \sim 10^{17}$ cm^{-3} sec, some lithium, beryllium, and boron burn up will also occur.

Before accepting these conclusions, it is desirable to investigate whether other self-consistent shock structure solutions can be found (especially one corresponding to a high temperature viscous shock), and indeed, whether the self-consistency of the low-temperature radiation-dominated solutions is stable against perturbations. To do this it is necessary to explicitly include

the effects of viscosity in our calculations. This is done in two stages. Section VII treats one-fluid viscous shocks and their alteration by simple radiation field models. Having thus established workable methods of solution (in particular—efficient, stable numerical approaches), the treatment is generalized in Section VIII to a multi-species, multi-temperature model with a realistic radiation field.

Figure 5.1 - Radiation-dominated shock structures for $n_o = 10^{20}$ cm^{-3}. Here V = v - $v_o/7$, EO = E_o, QNO = n_o, TO = T_s, QNGS = n_γ^s, NG = n_γ, and T = T_γ.

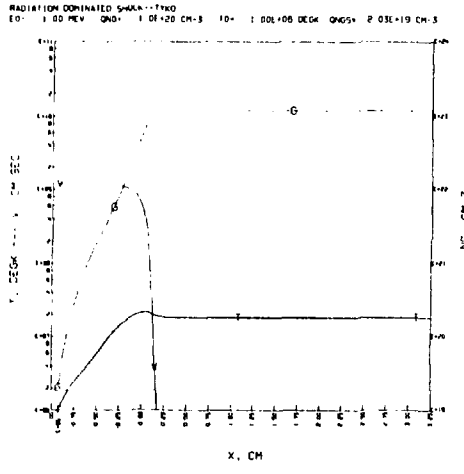

(a) E_0 = 1 MeV

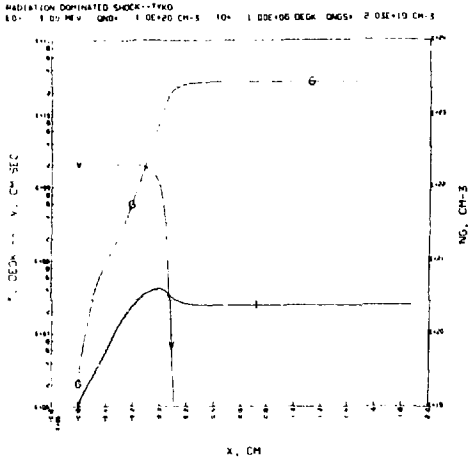

(b) E_0 = 3 MeV

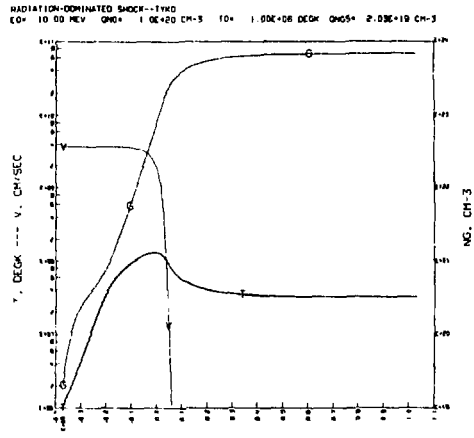

(c) E_0 = 10 MeV

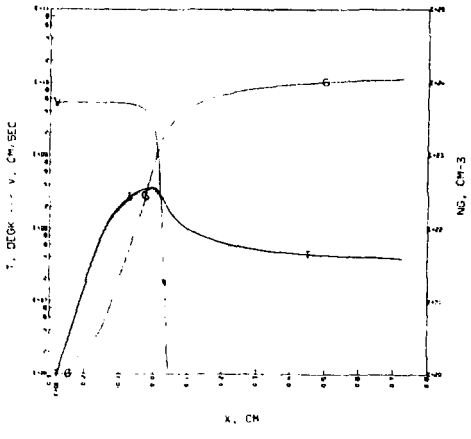

(d) E_0 = 20 MeV

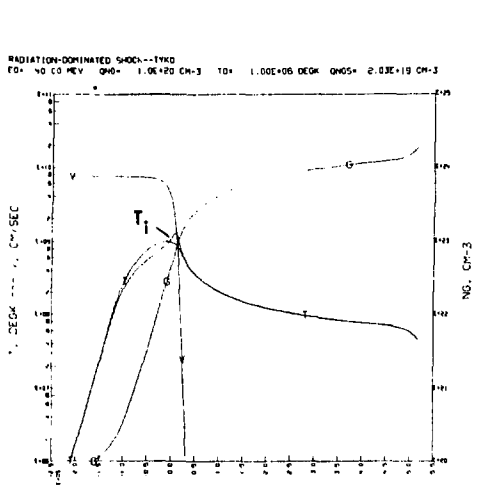

(e) E_0 = 40 MeV

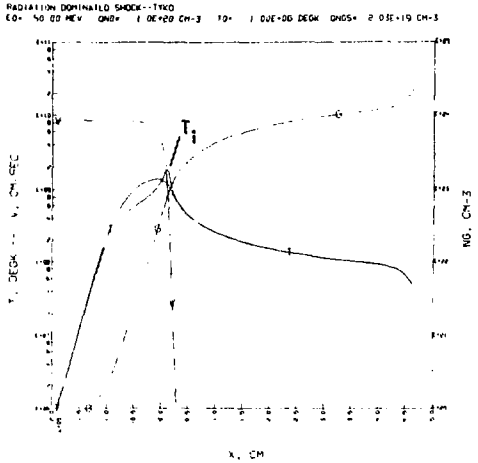

(f) E_0 = 50 MeV

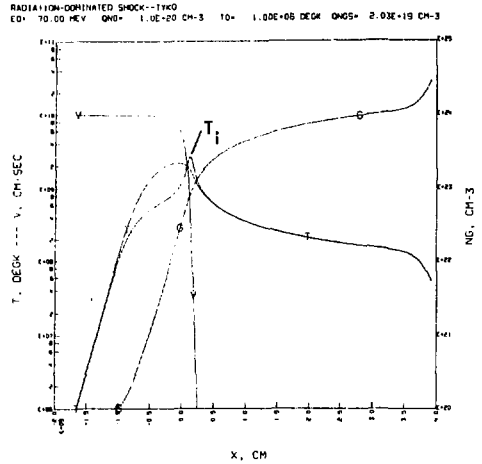

(g) E_0 = 70 MeV

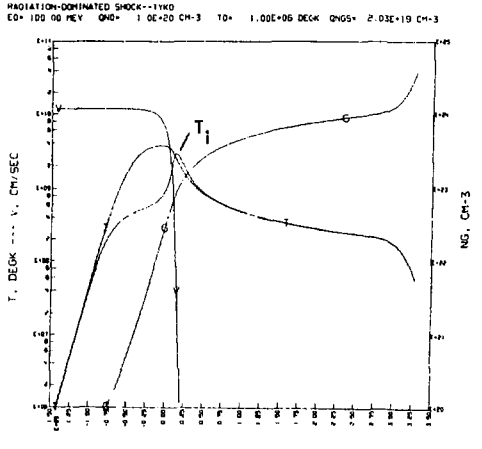

(h) E_0 = 100 MeV

Figure 5.2 - Radition-dominated shock structures for E_o = 30 MeV. (See Figure 5.1 for notation.)

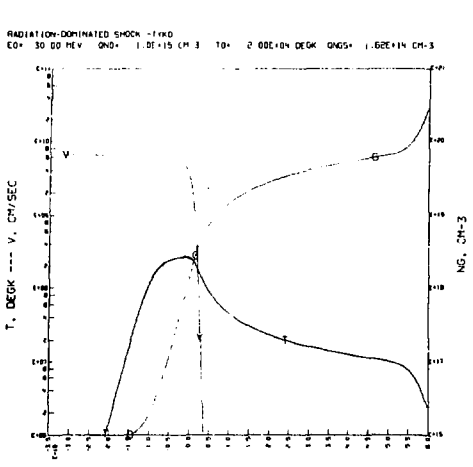

(a) $n_o = 10^{15}$ cm^{-3}

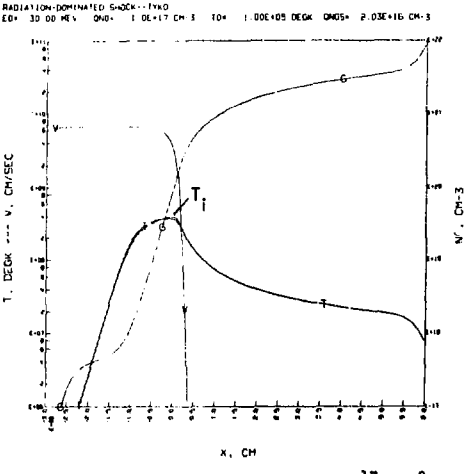

(b) $n_o = 10^{17}$ cm^{-3}

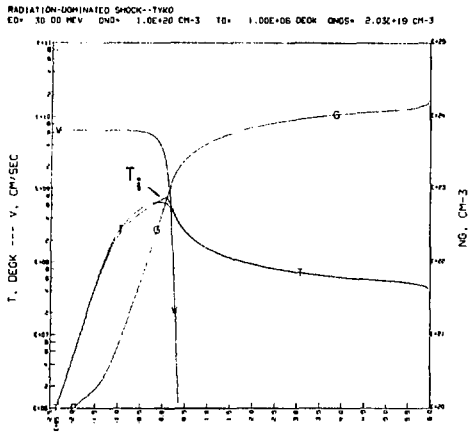

(c) $n_0 = 10^{20}$ cm^{-3}

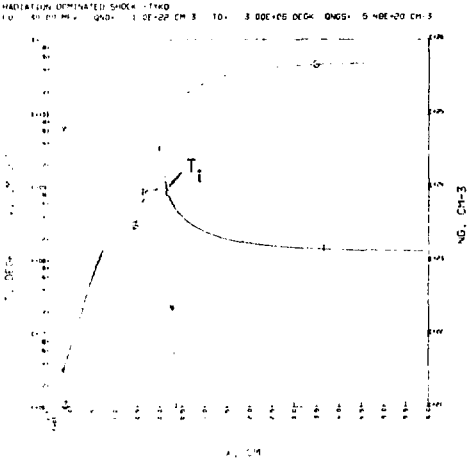

(d) $n_0 = 10^{22}$ cm^{-3}

Figure 5.3 - Peak and characteristic shock temperatures. The curves labeled NRB, RB, and RB+2C show the peak radiation temperature reached in the shock where only non-relativistic bremsstrahlung, relativistic bremsstrahlung, and relativistic bremsstrahlung *and* radiative Compton, respectively, are included in the calculation (and the average thermalizable bremsstrahlung photon energy is conservatively taken as $\frac{2}{3} kT_e$). These curves are plotted for density $n_o = 10^{20}$ cm^{-3}; but except near equilibrium, the density dependence is quite weak. The curves labeled $T_\gamma(10^{15}\text{-}10^{22})$ are the peak radiation temperatures reached in a shock of the indicated density (in cm^{-3}) when all radiation effects including inverse Compton scattering are included, while the curve labeled $T_i(n_o = 10^{22})$ shows the peak ion temperature associated with $T_\gamma(10^{22})$. $T_{i,\,max}$ is the ion temperature that would occur if all the shock energy were transformed into ion thermal energy; T_{crit} is the temperature (near the rear of shock) below which photon diffusion can mediate the shock; T_v is ion temperature above which ion viscosity is important; T_+ is the temperature at which the number density of pairs equals n_o; and T_{eq}^{15} is the final equilibrium temperature at $n_o = 10^{15}$ cm^{-3}.

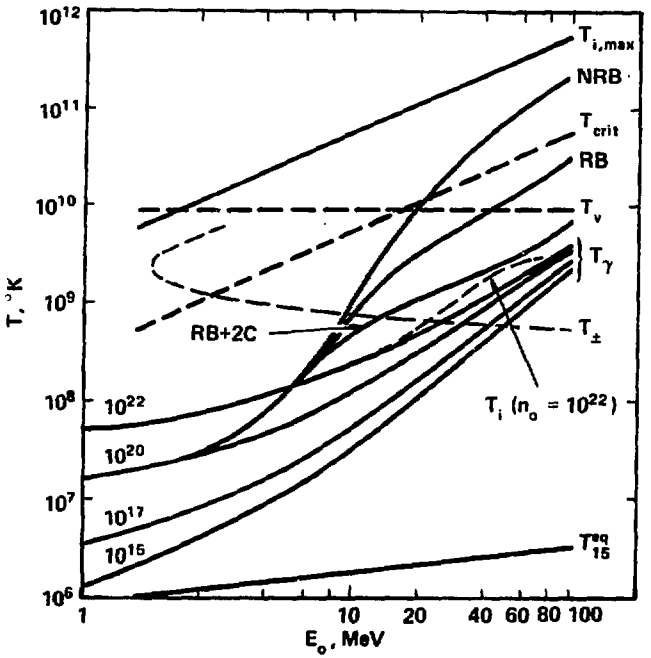
10^{12}
10^{11}
10^{10}
10^{9}
10^{8}
10^{7}
10^{6}
T, °K
$T_{i,max}$
NRB
T_{crit}
RB
T_ν
T_γ
$T_\pm$
RB+2C
T_i ($n_o = 10^{22}$)
10^{22}
10^{20}
10^{17}
10^{15}
T_{15}^{eq}
1
10
20
40
60
80
100
E_o, MeV

VI. EFFECT OF ELECTRON-POSITRON PAIRS ON SHOCK STRUCTURE

The number density of pairs created in a characteristic radiation-dominated shock width, $\left(\frac{c}{3v_o n_o \bar{\sigma}_c}\right)$, by photons moving with velocity

$v_\gamma \sim \frac{v_o}{4}$ is:

$$N_p = \frac{Q^{\pm}_{\gamma\gamma}}{v_\gamma} \cdot \frac{c}{3v_o n_o \bar{\sigma}_c} = 96.0 \left(\frac{n_\gamma}{n_o}\right)^2 \left(\frac{\sigma_T}{\bar{\sigma}_c}\right) \left(1 + .782\phi^{-1}\right)^{7/2} \cdot \phi^3 e^{-2\phi} \frac{n_o}{E_o(\text{MeV})} \qquad (6.1)$$

where we have made use of (3.16); and

$\phi = \frac{m_e c^2}{kT}$. From Section III.B, we have that the number density, $n^{\pm}$, of electron-positron pairs in relative equilibrium with a Bose-Einstein distribution with photon density, n_γ, is:

$$n^{\pm} \approx .50\, \phi^2 K_2(\phi)\, n_\gamma \xrightarrow[\phi>>1]{} .63\, \phi^{3/2} e^{-\phi} n_\gamma \qquad (6.2)$$

and, for example, $n^{\pm} \approx .04\, n_\gamma$ at kT = 100 KeV. Combining (6.1) and (6.2) and assuming $v_\pm \sim v_\gamma$ (see below), we find that γ-γ pair creation will cause the pair density to be in relative equilibrium for:

$$E_o(\text{MeV}) \leq 1.52 \times 10^4 \left(\frac{n_\gamma}{100 n_o}\right) \left(\frac{\sigma_T}{\bar{\sigma}_c}\right) \phi^{3/2} e^{-\phi} (1+0.782/\phi)^{7/2} \qquad (6.3)$$

For θ_e = 50 keV, and $\bar{\sigma}_c = \sigma_T$, we find the pairs will be in relative equilibrium for $E_o \lesssim 23 \frac{n_\gamma}{100 n_o}$ MeV; for θ_e = 75 keV, for $E_o \lesssim 435 \frac{n_\gamma}{100 n_o}$ MeV; and for θ_e = 100 keV, for $E_o \lesssim 1750 \frac{n_\gamma}{100 n_o}$ MeV. Thus for the energies of present interest, (i.e. $E_o \lesssim 100$ MeV), the pairs can be considered to be in relative equilibrium whenever their density is at all significant (i.e. $\gtrsim n_o$).

By combining (5.1) and (6.2) we can derive the condition for $n_\pm \gtrsim n_o$ as

$$E_o \text{ (MeV)} \gtrsim 0.95\, \phi^{-5/2}\, e^{\phi} \qquad (6.4)$$

where ϕ is evaluated at $\frac{v}{v_o} = 4/7$ (i.e. essentially at the peak shock temperature). Since the density of pairs is extremely temperature-dependent for $\theta_e \lesssim 200$ keV, the temperature, $T_\pm$, at which $n_+ = n_o$ (derived from (6.4)), is a good criterion for when pair effects can become important, and is plotted in Figure 5.3.

A principal effect of the pairs is to support a current tending to short out the shock electric field and thus weaken the electron-ion coupling, lengthen the shock scale and allow more time for radiative equilibration. At the same time, however, the presence of pairs increases the opacity as well as the photon production rate, which tends to reduce the scale of the shock, while leaving the degree of equilibrium unchanged. Which effect dominates depends on the pair conductivity, and on the magnitude of the direct ion-lepton coupling via Coulomb friction.

While accurate solution of the resulting shock structure seemingly must be done numerically, and will be the subject of a

later paper, a fairly plausible pair-dominated shock can be sketched out.

Using the facts that the total current t ough the shock must vanish and the fractional charge density must be exceedingly small (i.e. Debye length << shock width), we find that:

$$v_e = v_i \left(1 - \frac{J_\pm}{en_0 v_0}\right) \tag{6.5}$$

where $J_\pm \equiv en_+ (v_e - v_+)$ is the current due to the presence of pairs and v_+ and n_+ are the positron velocity and density. Approximately adopting the classical plasma conductivity given by Spitzer (1962) to a pair gas by multiplying it by a factor $\sqrt{2}\, n_+/n_{e^-}$, we find:

$$\frac{J_\pm}{en_0 v_0} \gtrsim 3.56\times10^{-4}\, \theta_e^{3/2}(\text{keV})\, E_0(\text{MeV})\, \frac{n_+}{n_{e^-}}\, \frac{\bar{\sigma}_c}{\sigma_T}\, \frac{10}{\ell n \Lambda}\, \frac{\Sigma_x}{\Sigma_{max}} \tag{6.6}$$

where Σ_x is the electric field, n_{e^-}, the total e^- density, and Σ_{max} the maximum electric field that can occur in the absence of pairs (see V.D.). We see that for $\theta_e \gtrsim 60$ keV, $E_0 \gtrsim 30$ MeV, $n_+ \gtrsim n_{e^-}$ and $\Sigma \gtrsim \Sigma_{max}$ that $J_\pm/en_0v_0$ is $\gtrsim 1$. Since the velocities in (6.5) cannot be negative, a self-consistent solution of (6.6) will be reached in which $\Sigma_x < \Sigma_{max}$ and $J_\pm/en_0v_0 \gtrsim 1$. Physically, one expects that without the aid of a strong electric field the electrons will be approximately comoving with the radiation field, and most of the shock dissipation will occur via resistive heating of the pairs and Coulomb friction between the ions and leptons. The relative contribution of these effects can be estimated by calculating the ratio of the classical Coulomb stopping distance

ℓ_{ei} (derived from Spitzer 1962) to the distance over which the reduced electric field can stop the ions. This ratio is given by:

$$\frac{\ell_{ei}}{E_0/e\Sigma_x} = 1.26 \times 10^{-4} \; \theta_e^{3/2}(\text{keV}) E_0(\text{MeV}) \left| \frac{v_0}{v_i - v_e} \right| \frac{\bar{\sigma}_c}{\sigma_T} \cdot$$

$$\cdot \frac{10}{\ell n \Lambda} \frac{n_0}{n_e} \frac{\Sigma_x}{\Sigma_{max}} \qquad (6.7)$$

For $J_\pm/en_0v_0 = 1$ appropriate when $\Sigma << \Sigma_{max}$, we find from (6.6) that:

$$\frac{\ell_{ei}}{E_0/e\Sigma_x} = .35 \; \frac{n_{e^-}}{n_+} \left| \frac{v_0}{v_i - v_e} \right| \frac{n_0}{n_e} \qquad (6.8)$$

It thus appears that electron-ion Coulomb friction will provide the dominant dissipation when more than a few pairs per nucleon are present. The scale of the shock, $\Delta_\pm$, is then ℓ_{ei} with $v_0/(v_i - v_e) \sim 1$, i.e.:

$$\Delta_\pm = .7 \; \phi^{-4} \; e^{\phi} \; \frac{10}{\ell n \Lambda} \frac{\bar{\sigma}_c}{\sigma_T} \Delta \qquad (6.9)$$

which holds when $\frac{n_e}{n_0} >> 1$ and $\frac{\theta_e}{m_e c^2} < 1$ and provided the classical e^+e^- conductivity and stopping lengths assumed above are applicable.

Two stream instabilities between the ions and electrons or the electrons and positrons may, however, lead to anomalously small values of ℓ_{ei} and the plasma conductivity. Idealized linear theory (Stringer 1964) predicts the existence of stable counterstreaming for $|v_i - v_e| \lesssim 1.2 \; (\theta_e/m_e)^{1/2}$ when $T_e = T_i$.

For $\theta_e \geq$ 60 keV where pairs become important, we thus require $E_o \geq$ 160 MeV to reach an unstable regime for $|v_i - v_e| = v_o$. Further, McKee (1970) has shown in one-dimensional numerical simulations that the e-i two stream instability leads to heating $\simeq m_e |v_i - v_e|^2$ which is a factor m_i/m_e too small to mediate a collisionless shock. Thus classical two-stream instabilities do not appear to play a crucial role in the shock structures of present interest.

Returning to equation (6.9), we see that due to the rapid rise in pair number with temperature below 200 keV, the absolute size of the shock will be smaller than it would have been without pairs, decreasing to a minimum of $\sim .2\Delta$ at 100 keV and then expanding. When the size of the shock is measured in Compton lengths, however, the shock width with pairs increases monotonically and always remains more than that of a shock from which pairs have been artificially excluded. The pair shock's radiation field will thus be seemingly better equilibrated and reach a lower peak temperature than the pairless shock, although one must solve the problem self-consistently, allowing for the sharp decrease of pair number with temperature. The probable outcome is that the temperature will remain below $\sim$100-200 keV for $E_o <$ 100 MeV/nucleon. Using the criterion of section V.D we see that this is too low a temperature for ion viscosity to become important even over the reduced shock scales. In addition, ion viscosity will be damped by ion-lepton collisions.

We are thus led to the overall picture of a pair-dominated shock

where a relatively cool radiation-pair field stops the incoming electrons fairly abruptly near the front of the shock while the ions are stopped gradually by the pairs, heating and regenerating the radiation-pair field in the process. This scenario is in some respects similar to the equilibrium pair-dominated shocks suggested by Colgate (1969) to occur in the mantles of compact supernovae ($n_0 \sim 10^{28}$ cm^{-3}, $T_{eq} \sim 500$ keV, $E_0 > 16$ MeV) and to be involved in cosmic ray production.

VII. SHOCK MODELS WITH VISCOSITY

A. One Fluid Viscous Shocks Without Radiation

Specializing the shock structure equations (2.13)-(2.20) to the case of a single fluid containing no radiation or pairs, we obtain after some rearrangement:

$$n_0 v_0 kT - \mu v \frac{dv}{dx} = mn_0 v_0 (v_0 - v) \qquad (7.1)$$

$$\alpha n_0 v_0 kT - \kappa \frac{dT}{dx} = \frac{1}{2} mn_0 v_0 (v_0 - v)(v_0 - v + 2\varepsilon_0 v_0) + \alpha_0 P_0 v_0 \qquad (7.2)$$

$$n = n_0 v_0 / v \qquad (7.3)$$

Here P_0 and α_0 are the pre-shock pressure and specific heat coefficient, $\varepsilon_0 = P_0/mn_0 v_0^2$, and the species identifying subscripts have been dropped.

Models of the type represented by (7.1)-(7.3) have been studied by several authors (cf. Zel'dovich and Raizer, 1966). For clarity and continuity, and to develop methods applicable to the more general shock problem, we shall independently derive some of the properties of this model, for the case of constant μ and κ.

It is convenient to first cast equations (7.1)-(7.3) into the dimensionless form:

$$\tau - n\delta \frac{dn}{d\zeta} = n(1-n) + n\varepsilon_0 \qquad (7.4)$$

$$\alpha\tau - \frac{d\tau}{d\zeta} = \frac{1}{2}(1-n)(1-n+2\varepsilon_0) + \alpha_0 \varepsilon_0 \qquad (7.5)$$

$$\frac{n}{n_0} = \frac{1}{\eta} \tag{7.6}$$

where:

$$\eta \equiv \frac{v}{v_0} \qquad \delta \equiv \frac{\mu k}{m\kappa} \qquad \zeta \equiv \frac{\chi n_0 v_0 k}{\kappa} \qquad \tau \equiv \frac{kT}{mv_0^2} \tag{7.7}$$

The Hugoniot relations governing conditions on either side of the shock are obtained as usual by setting the gradients in (7.4) and (7.5) to zero. By construction the pre-shock solution is $n=n_0$, $\eta=1$, $\tau=\varepsilon_0$. For the case of constant α, the post-shock conditions (denoted by the subscript "1") are found directly to be (independent of the constancy of μ and κ):

$$\eta_1 = \frac{1+2(1+\alpha)\varepsilon_0}{2\alpha+1} \rightarrow \begin{cases} \dfrac{1+5\varepsilon_0}{4} & \alpha = \dfrac{3}{2} \\ \dfrac{1+8\varepsilon_0}{7} & \alpha = 3 \end{cases} \tag{7.8}$$

$$\tau_1 = \frac{(1+2(1+\alpha)\varepsilon_0)(2\alpha-\varepsilon_0)}{(2\alpha+1)^2} \rightarrow \begin{cases} \dfrac{(1+5\varepsilon_0)(3-\varepsilon_0)}{16} & \alpha = \dfrac{3}{2} \\ \dfrac{(1+8\varepsilon_0)(6-\varepsilon_0)}{49} & \alpha = 3 \end{cases} \tag{7.9}$$

$$\frac{n_1}{n_0} = \frac{1}{\eta_1} \tag{7.10}$$

For non-constant α, the Hugoniot relations can be solved quadratically and then iterated to find η_1 and τ_1.

For the special case $\delta = 1/(\alpha+1)$ (α constant), equations (7.4)-(7.6) can be solved analytically. (This was first shown by Becker 1922). This is a not unreasonable approximation for

single species gases or single component plasmas. Indeed $\tilde{\delta} \approx .36$ for the latter case, although μ and κ are then highly temperature-dependent. Adding (7.4) to (7.5) and making the above substitution we find:

$$(\alpha+1)\tau + \frac{1}{2}\eta^2 - \frac{1}{\alpha+1}\frac{d}{d\zeta}\left[(\alpha+1)\tau + \frac{1}{2}\eta^2\right] = (\alpha+1)\varepsilon_0 + \frac{1}{2} \qquad (7.11)$$

Making the substitution $h \equiv (\alpha+1)\tau + \frac{1}{2}\eta^2$, we see that (7.11) is a standard first order differential equation having the solution:

$$h = h_0 + D\, e^{(\alpha+1)\zeta} \qquad (7.12)$$

where $h_0 \equiv (\alpha+1)\varepsilon_0 + \frac{1}{2}$ is the upstream value of h, and D is an undetermined constant. Unless D=0 the exponential term in (7.12) will blow up at the downstream limit, while the Hugoniot relations show h_0 to also be the correct downstream value of h. We therefore conclude that $h=h_0$ throughout the shock. Using this result, we find from (7.4) and (7.8) that:

$$-\frac{d\eta}{d\zeta} = \frac{(1-\eta)(\eta-\eta_1)(2\alpha+1)}{2\eta} = \frac{(\alpha+1)}{\eta}\frac{d\tau}{d\zeta} \qquad (7.13)$$

which can be integrated to find ζ:

$$\zeta = \frac{1}{\alpha-(1+\alpha)\varepsilon_0}\, \ell n\left[\frac{(1-\eta)}{(\eta-\eta_1)^{\eta_1}}\right] + \zeta_0 \qquad (7.14)$$

where ζ_0 is a constant fixing the location of the shock. Asymptotically:

$$1-\eta \sim \exp[(\alpha-(1+\alpha)\varepsilon_0)\zeta] \qquad \zeta \to -\infty$$

$$\eta - \eta_1 \sim \exp\left[-\frac{1}{\eta_1}(\alpha-(1+\alpha)\varepsilon_0)\zeta\right] \quad \zeta \to +\infty \tag{7.15}$$

Equation (7.14) is singular for $\varepsilon_0 = \alpha/(1+\alpha)$ which is just the point where v_0 equals the initial adiabatic sound speed, c_s^0, and retracing our steps we find $\frac{d\eta}{d\zeta} = 0$ as expected. In general, the upstream Mach number, M, is given by:

$$M \equiv \frac{v_0}{c_s^0} = \left[\frac{\alpha}{(1+\alpha)\varepsilon_0}\right]^{1/2} \tag{7.16}$$

It is interesting to note that the velocity profile given by (7.14) is identical to that in the radiation-dominated shock model when $\varepsilon_0 = 0$ and $\alpha = 3$ (see(5.10)), although the relation between τ and η is different.

Taking another special case, we can investigate the role of viscosity by setting $\delta = 0$ and seeing if continuous shock solutions can be obtained. Differentiating (7.4) and using (7.5) to eliminate $\frac{d\tau}{d\zeta}$ we find:

$$-\frac{d\eta}{d\zeta} = \frac{2\alpha+1}{2}\frac{(1-\eta)(\eta-\eta_1)}{(1-2\eta+\varepsilon_0)} \tag{7.17}$$

This solution is singular for $\eta_c = \frac{1+\varepsilon_0}{2}$ and we thus expect a shock discontinuity unless $\eta_1 > \eta_c$. This occurs only for weak shocks with:

$$\varepsilon_0 > \frac{2\alpha-1}{2\alpha+3} \quad \text{or} \quad M < \left[\frac{(2\alpha+3)\alpha}{(2\alpha-1)(\alpha+1)}\right]^{1/2} \tag{7.18}$$

For $\alpha = \frac{3}{2}$, this criterion becomes $M < \sqrt{9/5} = 1.34$.

Thus ordinary heat conduction is usually insufficient to mediate a strong shock and some other dissipation mechanism (typically viscosity) is required to prevent a discontinuity. Note, however, that no discontinuity occurs for $\alpha \leq \frac{1}{2}$, a case which might correspond to a highly Fermi-degenerate medium. This fact, together with the large heat conduction coefficient typically associated with such media, might dramatically increase the scale of the shock relative to a viscous mean-free-path estimate. The possible implications of this for carbon-detonation supernovae are being investigated.

In general, the physical content of criterion (7.18) is that in the absence of viscosity, relatively little increase in the energy density near the back ($\eta \sim \eta_1$) of a shock is required to provide pressure balance (scales as $(1-\eta)$ from (7.4)), while the material there is being rapidly compressed ($\sim \frac{1}{\eta}$). For strong shocks, this usually results in a negative temperature gradient and thus the inability to provide the required heat flux toward the front of the shock. Weak or low α thermal conduction shocks are possible because they are not sufficiently compressed to encounter this difficulty. Also, as we have discussed analytically in Section V.D and will treat numerically in the next subsection, strong shocks with sufficiently high radiation pressure may be mediated solely by radiative heat conduction, basically since the radiation field does not take part in the final sharp compression. Note also that the radiation field can transport energy <u>against</u> a temperature gradient if a sharp enough gradient

in photon number exists to compensate.

Returning to the radiationless case at hand, we wish now to solve the basic viscous shock equations, (7.1)-(7.3), numerically in the case of arbitrary δ (but constant μ and κ, and $\alpha = \frac{3}{2}$). This can be done in a stable and convenient fashion by differencing (7.1) and (7.2) in the manner given in Appendix C and solving the resulting equations simultaneously for v^{i+1} and T^{i+1} at point x^{i+1} in terms of the variables at point x^i. The form of the special case solution (7.12) suggests that such an integration will be stable only if carried out in the $-x$ direction, i.e. from the back to the front of the shock, for otherwise the unwanted exponential solution will exponentiate off the noise inevitable in any finite difference scheme. This is indeed observed to be the case.

In order to begin such an integration, one needs an asymptotic solution for the downstream limit for T in terms of v. To obtain such a solution, we make the substitutions $\varepsilon \equiv \eta - \eta_1$ and $\varepsilon_\tau \equiv \tau_1 - \tau$ in equations (7.4) and (7.5). Using the Hugoniot relations (7.8) - (7.10) and neglecting terms higher than first order in ε and ε_τ, we obtain:

$$-\varepsilon_\tau - \frac{\delta}{4}(1+5\varepsilon_0)\frac{d\varepsilon}{d\zeta} = \frac{\varepsilon}{2}(1-3\varepsilon_0) \tag{7.19}$$

$$-\frac{3}{2}\varepsilon_\tau + \frac{d\varepsilon_\tau}{d\zeta} = \frac{\varepsilon}{4}(\varepsilon_0-3) \tag{7.20}$$

The form of these equations and the methods of nonlinear

mechanics (cf. Minorsky 1947) suggest trying exponential solutions in the form:

$$\varepsilon = B\, e^{\lambda\zeta} \qquad \varepsilon_\tau = C\, e^{\lambda\zeta} \tag{7.21}$$

where B,C, and λ are undetermined constants. Making these substitutions and solving for C/B yields:

$$\frac{\varepsilon_\tau}{\varepsilon} = \frac{1}{4}\left[\left[(1-3\varepsilon_0+3\eta_1\delta)^2 - 16\tau_1\delta\right]^{1/2} - 1 - 3(\eta_1\delta-\varepsilon_0)\right] \tag{7.22}$$

The shock integration is then started by choosing $\varepsilon = \varepsilon_s \ll 1$ at $x = 0$ and then finding ε_τ from (7.22). Numerically, we find that using this asymptotic solution leads to the appropriate upstream boundry conditions.

The results of such numerical integrations are shown in Figure 7.1 for the case of strong shocks with various values of δ. Note that the majority of the velocity change takes place over a few viscous lengths ($\lambda_\mu \equiv \frac{\mu}{mn_0v_0}$) near the back of the shock while thermal conduction has preheated the incoming material over a distance $\lambda_\kappa = \frac{1}{\delta}\lambda_\mu$. The analytic solution for the special case $\delta = .4$ agrees precisely with the numerical calculation. It is also clear from Figures 7.1 (a) and (b) that heat conduction does not play an essential role in the formation of a viscous shock.

B. Viscous Shock Models with Specified Radiation Fields

To study the effects of radiation on viscous shocks, we reintroduce the radiation pressure, energy density, and heat transport terms into equations (7.1)-(7.2), yielding:

$$(1+\chi n)n_0 v_0 kT - \mu v \frac{dv}{dx} = mn_0 v_0 (v_0 - v)v + P_0 v \qquad (7.23)$$

$$(\frac{3}{2}+3\chi n)n_0 v_0 kT - \lambda_0 n_0 v kT \frac{d\chi}{dx} - \kappa' \frac{dT}{dx} = \frac{1}{2}mn_0 v_0 (v_0 - v)(v_0 - v + 2\varepsilon_0 v_0) + \alpha_0 P_0 v_0 \qquad (7.24)$$

where:

$$\chi \equiv \frac{9}{10}\frac{n_\gamma}{n_0} \qquad \kappa' \equiv \kappa + \chi n \lambda_0 v_0 n_0 k \qquad \lambda_0 \equiv \frac{c}{v_0 n_0 \sigma_c} \qquad (7.25)$$

and:

$$P_0 = (1 + \chi_0)n_0 kT_0 \qquad \alpha_0 = \frac{3/2 + 3\chi_0}{1 + \chi_0} \qquad (7.26)$$

Here χ_0 is the pre-shock value of χ, and the specific heat coefficient for the matter has been taken as 3/2. In addition, our assumption of constant μ and κ will be retained.

In dimensionless form these equations become:

$$(1+\chi n)\tau - n\delta \frac{dn}{d\zeta} = n(1 - n + \varepsilon_0) \qquad (7.27)$$

$$(\frac{3}{2} + 3\chi n)\tau - An\tau \frac{d\chi}{d\zeta} - (1+\chi nA)\frac{d\tau}{d\zeta} = \frac{1}{2}(1-n)(1-n+2\varepsilon_0) + \alpha_0 \varepsilon_0 \qquad (7.28)$$

where $A \equiv \frac{\lambda_0}{\lambda_\kappa}$. In the present section, we shall assume $\chi(x)$ is a known function.

The main analytic result of this model, the ability of radiation to mediate a strong shock, has already been discussed

in a slightly different form in Section V.D, and we will concentrate here on the methods necessary to obtain specific numerical solutions.

As is obvious from the radiation-dominated shocks shown in Figure 5.1, the photon number gradient, $\frac{d\chi}{d\zeta}$, will not in general vanish at the same downstream region as the velocity and pressure gradients. Instead, an extended radiation relaxation region will typically occur after the shock-proper, in which increasing photon number balances a declining temperature to maintain constant pressure. It is numerically convenient to separate these two regions by choosing an $\chi \equiv \chi_s$ such that $\left.\frac{d\eta}{d\zeta}\right|_{\chi_s} \ll 1$. For the purposes of calculating the structure of the shock-proper, the downstream radiation conditions are taken as $\chi_s \equiv \chi(\chi_s)$ and $\chi_s' \equiv (\frac{d\chi}{d\zeta})_{\chi_s}$; and $(\frac{d\chi}{d\zeta})_{\chi\to-\infty}$ is assumed to become negligible.

Pseudo-Hugoniot relations can then be obtained by first assuming $\frac{d\eta}{d\zeta} \to 0$ in (7.27). Differentiating the result we find immediately that $\frac{d\Pi}{d\zeta}$ also $\to 0$, where $\Pi \equiv (1+\chi\eta)\tau$. We then find the pseudo-downstream conditions (denoted by subscript "1") to be described by the relations:

$$(1+\chi_1\eta_1)\tau_1 = \eta_1(1-\eta_1+\varepsilon_0) \tag{7.29}$$

$$(\frac{3}{2} + 3\chi_1\eta_1)\tau_1 - \eta_1\tau_1\chi_1'\frac{(A-1)}{1+\chi_1\eta_1} = \frac{1}{2}(1-\eta_1)(1-\eta_1+2\varepsilon_0) + \alpha_0\varepsilon_0 \tag{7.30}$$

The second term in (7.30) represents residual dissipation

occuring at the relaxation layer interface and is typically small. Indeed, if this term becomes too large, meaningful solutions of (7.29)-(7.30) for η_1 and τ_1 do not exist, implying that our arbitrary association of shock and radiation field by our choice of x_s was nonphysical. Typically, however, reasonable values of τ_1 and χ_1 are readily found by using (7.29) to eliminate τ_1 from (7.30) and then iterating.

To find pseudo-downstream asymptotic solutions, we proceed as before, except that instead of ϵ_τ we introduce the expansion variable $\epsilon_\pi \equiv \Pi_1 - \Pi$ where $\Pi_1 \equiv (1+\chi_1\eta_1)\tau_1$. We obtain the relation:

$$\left(\frac{\epsilon_\pi}{\epsilon}\right)^2 A\mu_1 + \frac{\epsilon_\pi}{\epsilon}\cdot\left[A\mu_1(1-2\eta_1+\epsilon_0) + A\mu_1\chi_1\tau_1 + \eta_1\delta(\alpha_1-\eta_1 c_\kappa)\right]$$

$$+ \left[(1-2\eta_1+\epsilon_0)A\mu_1\chi_1\tau_1 - \eta_1\delta(1-\eta_1+\epsilon_0-\Pi_1 c_\kappa)\right] = 0 \qquad (7.31)$$

where:

$$\alpha_1 \equiv \frac{3/2 + 3\chi_1\eta_1}{1+\chi_1\eta_1} \qquad \mu_1 \equiv \frac{1+\chi_1\eta_1 A}{A(1+\chi_1\eta_1)} \qquad c_\kappa \equiv \frac{A(1-\mu_1)}{1+\chi_1\eta_1}\chi_1' \qquad (7.32)$$

This relation can be readily solved quadratically with the positive value of the square root term being physical. ϵ_τ is then related to ϵ_π and ϵ by the expression:

$$\epsilon_\tau = \frac{\epsilon_\pi + \tau_1\chi_1\epsilon}{1+\chi_1\eta_1} \qquad (7.33)$$

We can now quantize our earlier specification of x_s by choosing $\eta(x_s) = \eta_1+\epsilon_s$ where $\epsilon_s << 1$ and is typically taken 10^{-3}. We can then find $\tau(x_s)$ by making use of (7.33), and thus have a

starting point for the numerical integration of the shock model equations (7.23)-(7.24).

The difference scheme adopted for equations (7.23)-(7.24) is given in Appendix C. Due the change in character of the shock equations as radiation pressure becomes dominant, most straightforward difference schemes are either intrinsically numerically unstable in one or more limits or require an exceedingly fine x-mesh to be convergent. The method adopted, however, appears to satisfactorily resolve these difficulties.

Figure 7.2 shows the shock structures that result from assuming that the radiation/matter pressure ratio ($\xi \equiv \chi n$) remains constant across the shock, while Figure 7.3 shows the results when χ is taken to be an exponentially increasing function of x given by:

$$\chi(x) = \chi_0 + (\chi_1 - \chi_0)\, e^{3x/\lambda_0} \qquad (7.34)$$

The transition from a viscous to radiation-dominated shock is seen to occur for χ = 3-5 (in the region of the maximum velocity gradient), in agreement with our analytic limits. Specifically, the scale of the velocity gradient undergoes a transition from $\sim\lambda_\mu$ to $\sim\lambda_0 n/3$. In addition, the shocks with exponential radiation fields already exhibit the temperature maximum typical of the non-equilibrium radiation-dominated shocks of Section V.

Figure 7.1 - One-fluid viscous shocks for various values of δ. Here V = v, EO = E_0, QNO = n_0, TO = T_0, EPSP = δ, EPSS = ϵ_s, and XVISC = $2\lambda_\mu$. The curves marked "E" in the δ = .4 case are the special case analytic solutions, and are essentially in coincidence with the numerical solutions marked T and V.

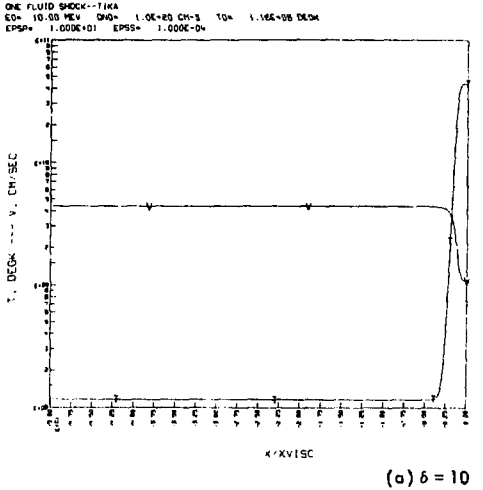

(a) δ = 10

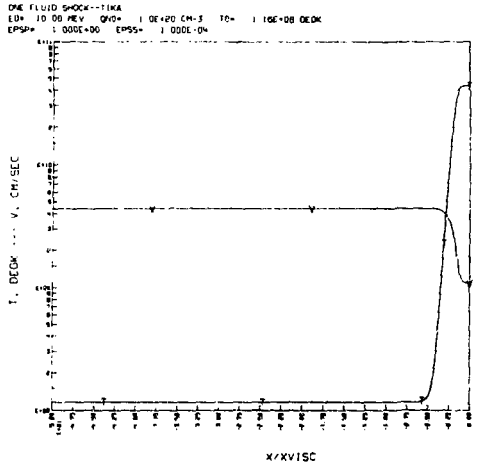

(b) $\delta = 1$

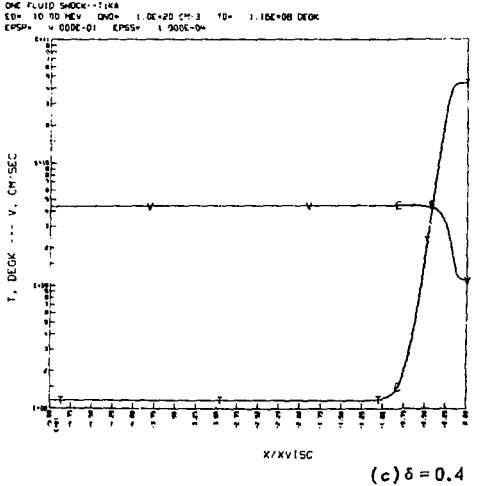

(c) $\delta = 0.4$

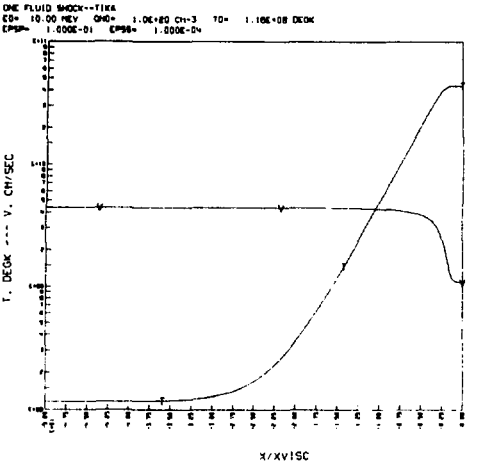

(d) $\delta = 0.1$

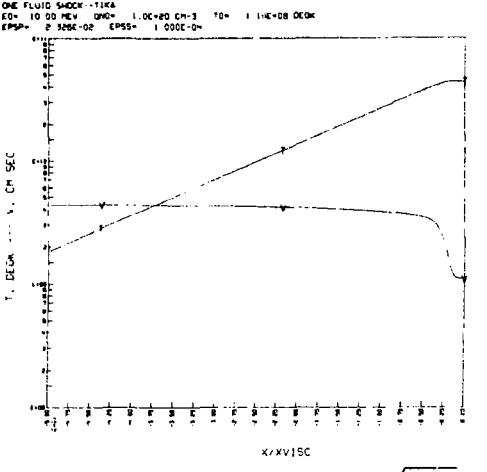

(e) $\delta = \sqrt{m_e/m_i}$

Figure 7.2 - Shocks with constant radiation/matter pressure ratios. Here, and here only, XI = χ_n; ITOT is the total number of zones; and the remaining notation was defined in the caption to Figure 7.1. Note that A $\equiv \lambda_0/\lambda_\kappa$ is equal to the ratio of the radiative diffusion length to the heat conduction length in the upstream region and is $\sim$ 7 times this ratio in the downstream region.

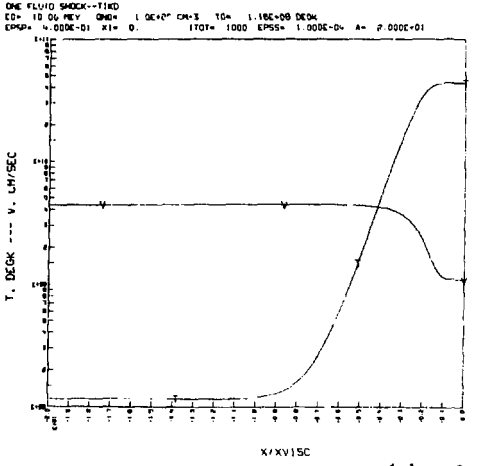

(a) $\xi = 0$

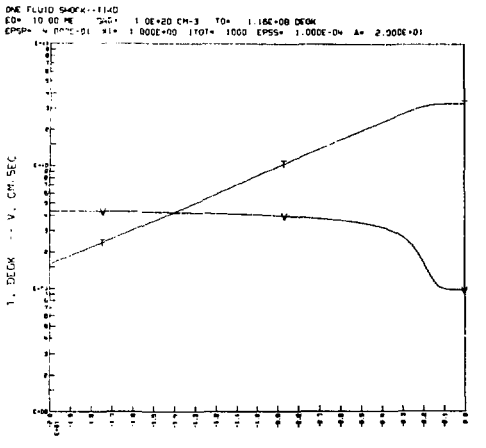
ONE FLUID SHOCK--TIKD
T, DEGK --- V, CM/SEC
X/XVISC

(b) $\xi = 1$

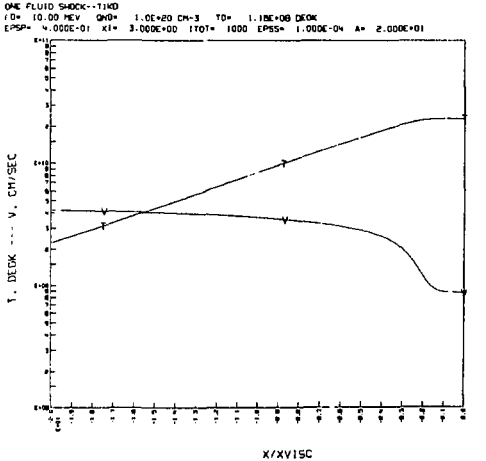
ONE FLUID SHOCK--TIKD
T, DEGK --- V, CM/SEC
X/XVISC

(c) $\xi = 3$

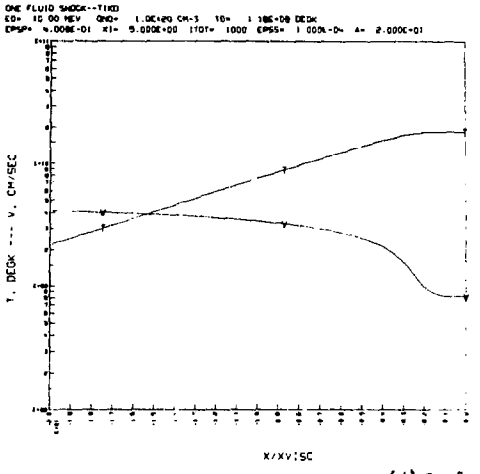
ONE FLUID SHOCK--TIKO
EO= 10.00 MEV QNO= 1.0E+20 CM-3 TO= 1.38E+08 DEGK
EPSP= 4.00BE-01 XI= 5.000E+00 ITOT= 1000 EPSS= 1.000E-04 A= 2.000E+01
T, DEGK --- V, CM/SEC
X/XVISC

(d) $\xi = 5$

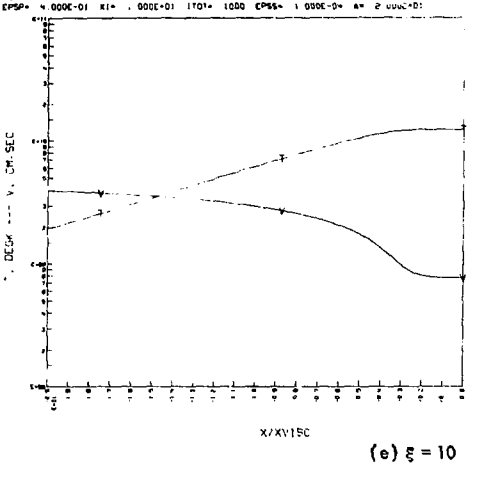
ONE FLUID SHOCK--TIKO
EO= 10.00 MEV QNO= 1.0E+20 CM-3 TO= 1.38E+08 DEGK
EPSP= 4.000E-01 XI= .000E+01 ITOT= 1000 EPSS= 1.000E-04 A= 2.000E+01
T, DEGK --- V, CM/SEC
X/XVISC

(e) $\xi = 10$

Figure 7.3 - Shocks with exponential radiation fields. Here XI = χ_1, and the remaining notation is unchanged. Note that as χ_1 is varied from 0 to 50, a hot viscous shock is transformed into a cool radiation-dominated shock with a characteristic temperature peak.

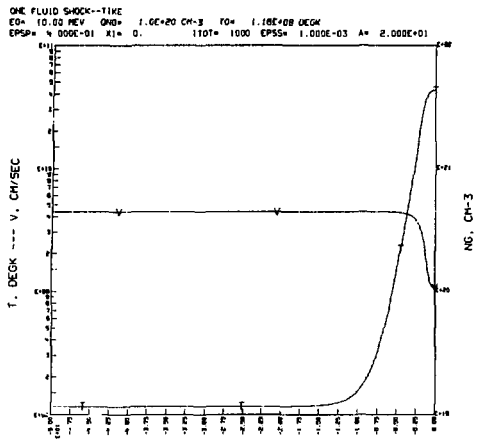

(a) $\chi_1 = 0$

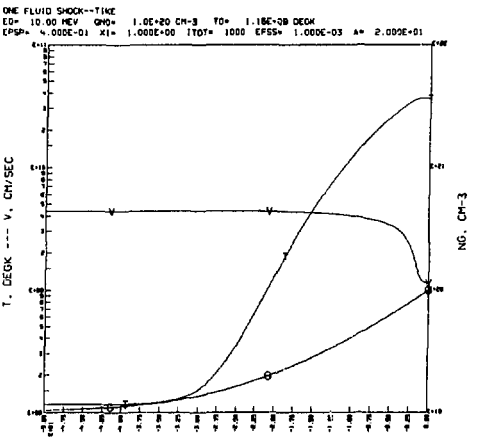

(b) $\chi_1 = 1$

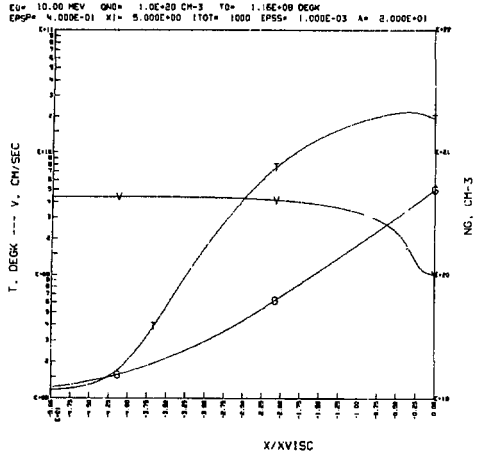
EO= 10.00 MEV QNO= 1.0E+20 CM-3 TO= 1.16E+08 DEGK
EPSP= 4.000E-01 XI= 5.000E+00 ITOT= 1000 EPSS= 1.000E-03 A= 2.000E+01
T, DEGK --- V, CM/SEC
NO, CM-3
X/XVISC

(c) $x_1 = 5$

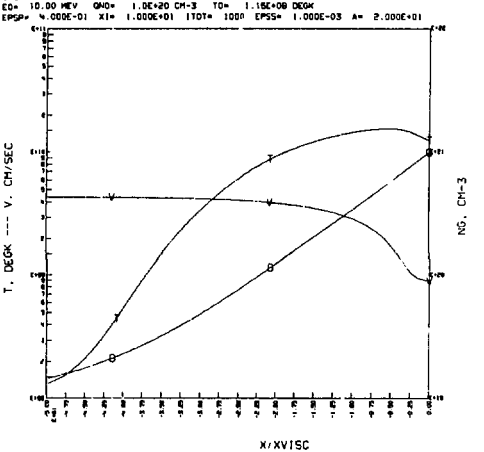
OK, FLUID SHOCK--TIME
EO= 10.00 MEV QNO= 1.0E+20 CM-3 TO= 1.16E+08 DEGK
EPSP= 4.000E-01 XI= 1.000E+01 ITOT= 1000 EPSS= 1.000E-03 A= 2.000E+01
T, DEGK --- V, CM/SEC
NO, CM-3
X/XVISC

(d) $x_1 = 10$

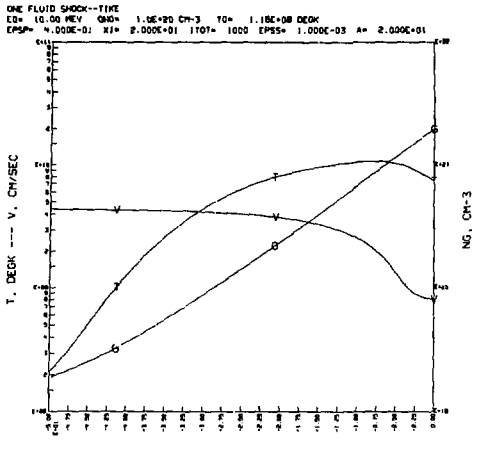

(e) $\chi_1 = 20$

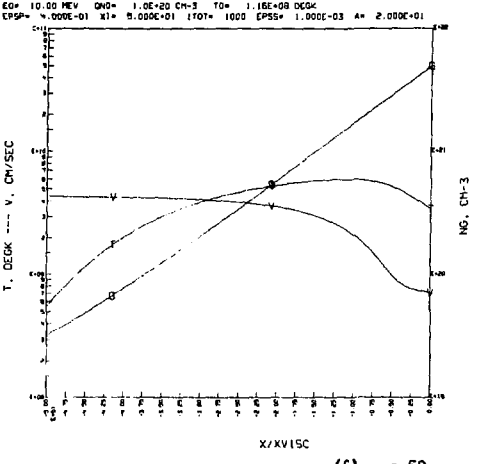

(f) $\chi_1 = 50$

VIII. GENERAL EFFECTIVE PHOTON SHOCK MODEL

A. Formulation of the Model

We are now in a position to consolidate our results into a model containing both explicit viscosity and a realistic treatment of the radiation field based on the effective photon approximation. We shall refer to this as the general effective photon shock model, and base it on the general assumptions of Section II, while in addition assuming essentially comoving ions and electrons, the absence of crucial pair effects, and the validity of the effective-photon approximation.

The shock structure equations (2.13) - (2.20) then take the form:

$$(1 + \tau_R + \chi\eta)\, n_o v_o kT - \mu v \frac{dv}{dx} = mn_o v_o (v_o - v)\, \gamma + P_o v \tag{8.1}$$

$$(\frac{3}{2}\tau_R + \alpha_e + 3\chi\eta)\, n_o v_o kT - \frac{9}{10}\, \lambda_o \nu kT \frac{dn_\gamma}{dx} - \kappa' \frac{dT}{dx} \tag{8.2}$$

$$= \frac{1}{2}\, mn_o v_o (v_o - v)(v_o - v + 2\varepsilon_o v_o) + \alpha_o' v_o$$

$$\frac{d}{dx}(n_\gamma v) - \frac{d}{dx}[\frac{v\lambda_o}{3}\frac{dn_\gamma}{dx}] = Q_\gamma^{eff} \tag{8.3}$$

$$\frac{3}{2} n_o v_o k \frac{dT_i}{dx} = -\frac{n_o v_o}{v}\, kT_i \frac{dv}{dx} + A_2 (kT_i)^{5/2} (\frac{dv}{dx})^2$$

$$+ (\frac{n_o v_o}{v})^2 \frac{A_1}{(kT)^{3/2}}\, 3k(T - T_i) \tag{8.4}$$

$$n = n_e = n_i = \frac{n_o v_o}{v} \tag{8.5}$$

where $\tau_R \equiv \frac{T_i}{T}$, and

$$P_o = (2+\chi_o)n_o kT_o \qquad \alpha_o = \frac{3(1+\chi_o)}{2+\chi_o} \tag{8.6}$$

$$\kappa' = \kappa_e + \chi n \lambda_o v_o n_o k \tag{8.7}$$

As before, we have neglected ionic heat conduction due to its small coefficient, and since as was shown in Section VII.A, it has little effect on the velocity profile and only moderately ($\delta \gtrsim .36$) broadens the temperature profile of a viscous ion shock.

To cast equations (8.1) - (8.2) into dimensionless form, it is convenient to introduce $\zeta' \equiv \frac{x}{\lambda_x}$, where λ_x is an arbitrary constant length. (Note that the heat conduction length, λ_κ, is no longer suitable because of its large ($\sim (kT)^{5/2}$) temperature dependence.) We then obtain:

$$(1 + \tau_R + \chi\eta)\tau - \eta\delta' \frac{d\eta}{d\zeta'} = \eta(1-\eta+\varepsilon_o) \tag{8.8}$$

$$\left(\frac{3}{2}\tau_R + \alpha_e + 3\chi\eta\right)\tau - A'\eta\tau \frac{dx}{d\zeta'} - \delta_\kappa \frac{d\tau}{d\zeta'}$$

$$= \frac{1}{2}(1-\eta)(1-\eta+2\varepsilon_o) + \alpha_o\varepsilon_o \tag{8.9}$$

where

$$\delta' \equiv \frac{\mu}{mn_o v_o \lambda_x} \qquad A' = \frac{\lambda_o}{\lambda_x} \qquad \delta_\kappa = \frac{\kappa'}{n_o v_o k \lambda_x} \tag{8.10}$$

Final Hugoniot relations are then found by setting all gradients to zero and requiring the radiation field to be in equilibrium, yielding:

$$2\tau_f + \chi_q \eta_f \tau_f^4 = \eta_f(1-\eta_f+\varepsilon_o) \tag{8.11}$$

$$(\alpha_{ef}+\tfrac{3}{2})\ \tau_f + 3\eta_f\chi_q\tau_f^4 = \tfrac{1}{2}(1-\eta_f)(1-\eta_f+2\varepsilon_o) + \alpha_o\varepsilon_o \tag{8.12}$$

where $\chi_q \equiv \frac{9}{10}\frac{b}{n_o}(\frac{mv_o^2}{k})^3$ and the subscript "f" denotes a final downstream value. (The subscript "1" will be used below to denote pseudo-downstream variable values.) These relations can be readily quadratically iterated to find τ_f and η_f, and $\chi_f = \chi_q\tau_f^3$.

Pseudo-Hugoniot relations are obtained in the same manner as described in the previous section, with the definition of Π generalized to $\Pi \equiv (1 + \tau_R + \chi\eta)\tau$, yielding:

$$\Pi = \eta(1-\eta + \varepsilon_o) \tag{8.13}$$

$$\alpha\Pi - (1-\mu')A'\eta\tau\frac{d\chi}{d\zeta'} = \frac{1}{2}(1-\eta)(1-\eta + 2\varepsilon_o) + \alpha_o\varepsilon_o \tag{8.14}$$

where:

$$\mu' \equiv \frac{\delta_K}{A'(1+\tau_R + \chi\eta)} \qquad \alpha = \frac{\frac{3}{2}\tau_R + \alpha_e + 3\chi\eta}{1 + \tau_R + \chi\eta} \tag{8.15}$$

By construction, these conditions describe any point, in the radiation relaxation region characterized by $\frac{d\Pi}{d\zeta'}$, $\frac{d\eta}{d\zeta'} \tilde{\approx} 0$, and can be solved iteratively if $\frac{d\chi}{d\zeta'}$, χ, and τ_R are known at that point. Here the relatively small amount of dissipation arising from the slow variation of τ_R in the relaxation layer due to e - i relaxation, and of η due to the change in α during radiative equilibration, has been neglected.

To fix the location of the shock we shall choose a particular point $x = x_s$ near the upstream boundary of this region, by specifying that the true value of η (x_s) differ from the value deduced from pseudo-Hugoniot relations (8.13) - (8.15) by a small amount ε_s. We find T(x) and v(x) by using equations (8.1) - (8.2) to integrate upstream and equations (8.13) - (8.15) to find conditions downstream of x_s. To do this we need to first assume initial values for $\tau_R(x)$ and $\eta_\gamma(x)$. Once values for T(x) and v(x) are found, equations (8.3) and (8.4) are sequentially solved to find new values for $\tau_R(x)$ and $\eta_\gamma(x)$. The whole process is then iterated until it converges.

To begin the upstream integration to find T and v, we still require an asymptotic starting solution. Following the same procedure as before we find ε_π can be obtained by quadratically solving the relation:

$$\left(\frac{\varepsilon_\eta}{\varepsilon}\right)^2 A'\mu_1' + \left(\frac{\varepsilon_\pi}{\varepsilon}\right) \cdot \left[A'\mu_1' (1-2\eta_1 + \varepsilon_0) + A'\mu_1'\chi_1\tau_1 + \eta_1\delta_1' (\alpha_1-\eta_1 c_\kappa')\right] + \left[(1-2\eta_1 + \varepsilon_0) A'\mu_1'\chi_1^{-1}, - \eta_1\delta_1(1-\eta_1 + \varepsilon_0 - \eta_1 c_\kappa')\right] = 0 \qquad (8.16)$$

where:

$$c_\kappa' \equiv \frac{A'(1-\mu_1')\left|\frac{dx}{d\zeta'}\right|}{1+\tau_{R_1} + \chi_1\eta_1}, \qquad \alpha_1 = \frac{\frac{3}{2}\tau_{R_1} + \alpha_{e_1} + 3\chi_1\eta_1}{1+\tau_{R_1} + \chi_1\eta_1} \qquad (8.17)$$

Here τ_1, η_1, and related "1" subscripted quantities have been obtained from the pseudo-Hugoniot relations at point x_s. We then find:

$$\epsilon_\tau = \frac{\epsilon_\pi + \chi_1 \tau_1 \epsilon}{1 + \tau_{R_1} + \chi_1 \eta_1} \qquad (8.17)$$

The photon continuity equation (8.3) and ion temperature equations (8.4) are solved by methods very similar to those used for the photon-dominated model, except that $\frac{dv}{dx}$ is evaluated explicitly from the preceding solution for v(x). The photonic boundary conditions ($n_\gamma = \frac{10}{9} n_0 \chi_f \equiv n_\gamma^{eq}$ as $x \to \infty$ and $n_\gamma = bT_0^3$ or $10^{-2} n_0$ as $x \to -\infty$) are taken at points far enough upstream and downstream as to have negligible effect on the bulk of the shock. The ion heating equation is integrated from upstream to downstream starting from the condition $\tau_R = 1$.

The explicit difference scheme used for equations (8.1) - (8.4) is given in Appendix D. Typically, runs involving $\sim$ 1000 mesh points converge in 10-15 overall iterations.

B. Effect of Non-Hydrogenic Ions

The envelope of a normal population I star contains ∿ 25% by weight of helium and ∿ 2% higher-Z material. Since these ions have different Z/A ratios from hydrogen, a given electric field is not sufficient to keep all species comoving with the electrons. Instead, the electric field will act to keep an "average" ion comoving, while individual ion species develop drift velocities whose magnitude is limited principally by ion-ion collisions.

Quantitatively, we find that to maintain pseudo-charge neutrality:

$$\sum_i n_i Z_i = \sum_i \frac{n_i^o v_o}{v_i} Z_i = \frac{n_e^o v_o}{v_e} \tag{8.19}$$

and assuming the electric field to be the dominant force accelerating the ions, we find:

$$e \frac{n_e^o v_o}{v_e} \Sigma_x = \sum_i m_i n_i^o v_o \frac{dv_i}{dx} \tag{8.20}$$

where n_j^o is the pre-shock density and Z_j, the number of protonic charges in component j. Differentiating (8.19) by time and using it to rewrite (8.20) gives:

$$\Sigma_x = \left[\frac{\sum_i A_i \frac{n_i^o}{n_e^o} \frac{dv_i}{dx}}{\sum_i Z_i \frac{n_i^o v_e}{n_e^o v_i} \frac{dv_i}{dx}} \right] \frac{m_H}{e} v_e \frac{dv_e}{dx} \equiv \left\langle \frac{A}{Z} \right\rangle \frac{m_H}{e} v_e \frac{dv_e}{dx} \tag{8.21}$$

where $A_i \equiv m_i/m_H$.

To use our present model to estimate the magnitude of the ion drift velocities and resultant ion heating, we shall restrict our attention to a hydrogen-helium plasma, and assume that the helium drift velocity, v_{drift}, relative to the protons, is in approximate steady state (i.e. $\frac{dv_e}{dx} \simeq \frac{dv_i}{dx} = \frac{dv_j}{dx}$) and $v_{drift} << v_o$. (This latter assumption is found to be self-consistent over a wide range of parameters). This allows us to approximate the insensitive factor $\langle \frac{A}{Z} \rangle$, as:

$$\langle \frac{A}{Z} \rangle \simeq \frac{\sum_i A_i n_i^o}{\sum_i Z_i n_i^o} \tag{8.22}$$

From Burgers (1960) and Section III.D we find that the force on the α-particles, $F_{\alpha p}$, due to collisions with the protons is given by:

$$F_{\alpha p} = f n_\alpha n_p v_{drift} \tag{8.23}$$

where in cgs units:

$$f \simeq 8.23 \times 10^{-49} \, \ell n \Lambda \, (kT_i)^{-3/2} \tag{8.24}$$

provided $v_{drift} < v_i^{th}$, the ion thermal velocity. Requiring the Coulomb drag force to compensate the differing electric forces on the α's and p's sufficiently to give them roughly equal accelerations, we find:

$$\frac{en_p\Sigma_x - fn_pn_\alpha v_{drift}}{m_p n_p} = \frac{2en_\alpha\Sigma_x + fn_pn_\alpha v_{drift}}{m_\alpha n_\alpha} \qquad (8.25)$$

and solving for v_{drift}, we have:

$$v_{drift} = \frac{e(m_\alpha - 2m_p)\Sigma_x}{f(n_p m_p + m_\alpha n_\alpha)} \simeq \frac{2m_H}{n_p + 2n_\alpha}\,\frac{v}{f}\,\frac{dv}{dx} \qquad (8.26)$$

The rate of ion heating from Coulomb dissipation, $H_{\alpha p}$, is then given by:

$$H_{\alpha p} = F_{\alpha p} \cdot v_{drift} = \frac{n_\alpha n_p}{(n_p + 2n_\alpha)^2}\,\frac{4m_H^2 v^2}{f}\left(\frac{dv}{dx}\right)^2 \qquad (8.27)$$

Inserting $H_{\alpha p}$ on the right-hand-side of the ion heating equation (8.4), and relating $n = \frac{n_o v_o}{v}$ to n_p in such a way as to keep the initial mass density constant (i.e. $n_p = n - 4n_\alpha$), we can approximately include helium effects in our shock model, without extensive modifications. The price we pay for this convenience is to slightly (for small $\chi_{He} \equiv \frac{n_\alpha^o}{n_p^o}$) underestimate the electron-ion density ratio. The resulting apparent over-estimate of photon creation rates, is almost exactly compensated for by the fact that per-particle bremsstrahlung rates are $(Z_\alpha/Z_p)^2 = 4$ times larger for alpha particles than for protons, which we do not include in our calculation of radiative emission.

For $E_o > 1$ MeV, the final equilibrium temperature is high enough to keep the high-Z atoms sufficiently stripped so that

bound-bound and free-bound emission processes do not become important, (see (5.20) and Clayton 1968, p. 224).

C. Results and Discussion

The shock structures that result from this model are shown in Figures 8.1 - 8.3 for various values of n_0 and E_0. The calculations involved were started "hot" with essentially no radiation in the region of the shock. As can be seen, they have in all cases* relaxed to radiation-dominated shocks very similar (typically within 3-5%) to those calculated in Section V, and the discussion of the salient features of these shocks given in § V.E still applies in detail.

Figure 8.4 explores the effects of the presence of helium for a 40 MeV/nucleon shock, and is seen to result in only modest ion heating even for a 50% mass fraction ($x_{He} = .25$). For lower energies, electron-ion coupling and ion-ion Coulomb friction are sufficiently strong that there is virtually no effect. At higher energies pairs become important, and as we have seen, all species will be decelerated principally via ion-lepton Coulomb friction.

To search for stable "hot-ion" shocks of the type predicted by Colgate (1975), runs were made in which radiation emission was reduced by a factor of 100, resulting as expected, in hot viscous shocks. When these had converged, the radiation emission rate was returned to normal and the structure allowed to relax. This always resulted in reaching the same radiation-dominated shock structures obtained above. An example of this process is shown in Figure 8.5. Note, in particular, that when the radiative rates

*Specifically, runs were made for $n_0 = 10^{15}$, 10^{17}, 10^{20}, and 10^{22} cm^{-3} and $E_0 = 1$, 10, 30, 50, 100 MeV.

are returned to their full values, radiation diffuses forward and changes the shock structure in such a way as to allow increased diffusion. The ensuing radiation diffusion wave engulfs the hot-ion shock, broadening and cooling it into a radiation-dominated shock. Figure 8.6 shows some of the typical intermediate hot-ion shocks. Note that even with emission reduced by a factor of 100, the residual amount of radiation is still sufficient to keep $T_e << T_i$ near the center of the shock. In most cases, reducing radiation emission by a factor of 10 is not sufficient to cause a hot-ion shock.

Figure 8.1 - Strong shock structures including viscous effects for $n_0 = 10^{20}$ cm^{-3}. Note the close similarity of these shocks to the radiation-dominated model shocks of Figure 5.1. Here V = v; XIO = χ_0, the upstream value of χ; Y is the helium mass fraction; J is the iteration number; and the remaining notation is common to the previous figures.

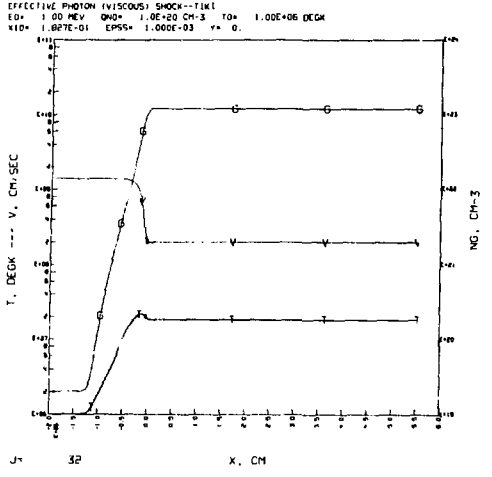

(a) E_0 = 1 MeV

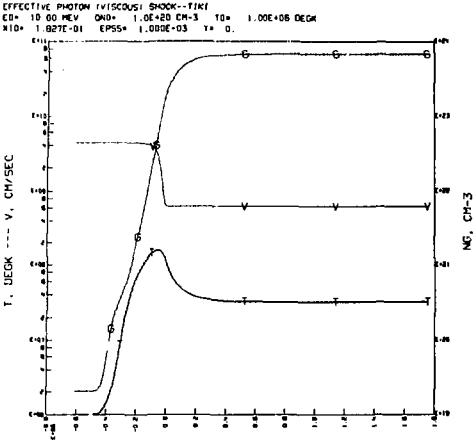

(b) E_0 = 10 MeV

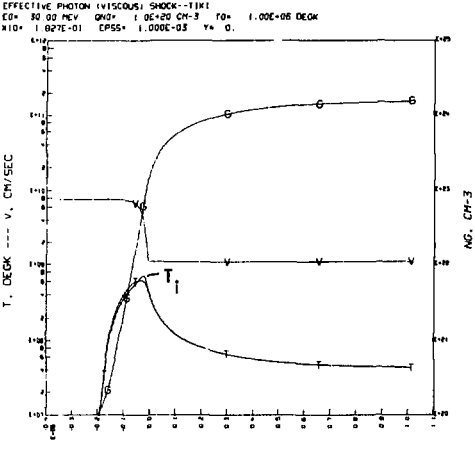

(c) E_0 = 30 MeV

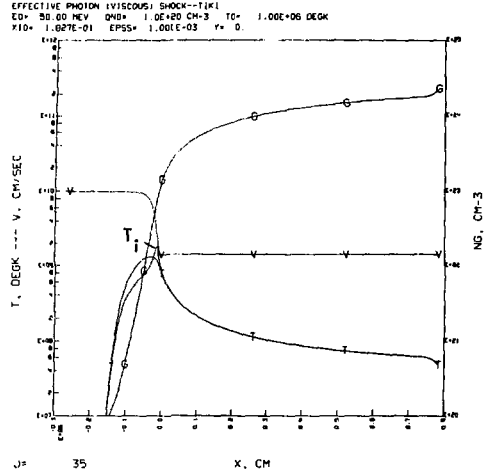

(d) E_0 = 50 MeV

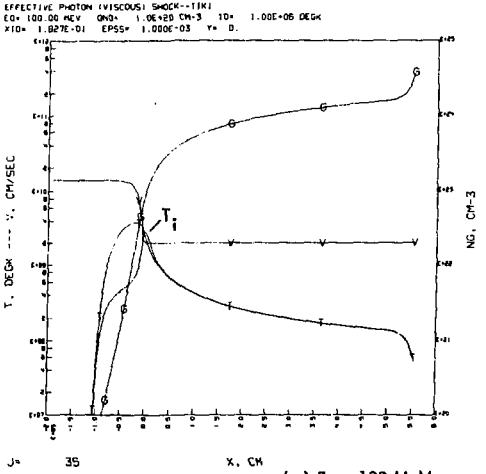

(e) E_0 = 100 MeV

Figure 8.2 - Strong shock structures including viscous effects for $n_o = 10^{17}$ cm^{-3}.

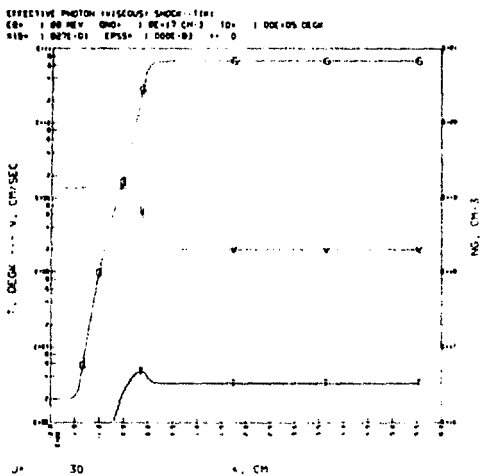

(a) E_0 = 1 MeV

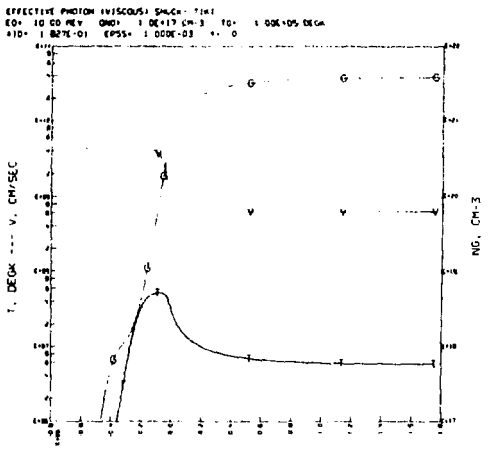

(b) E_0 = 10 MeV

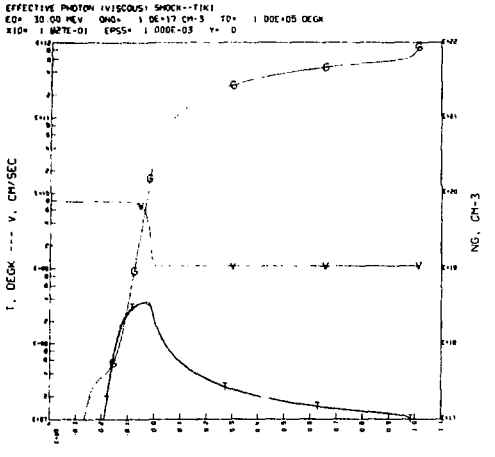

(c) E_0 = 30 MeV

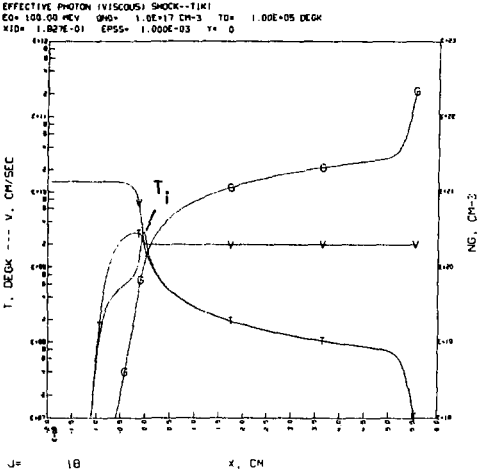

(d) E_0 = 100 MeV

Figure 8.3 - Strong shock structures near the onset of electron-positron pair-dominance (See Figure 5.3).

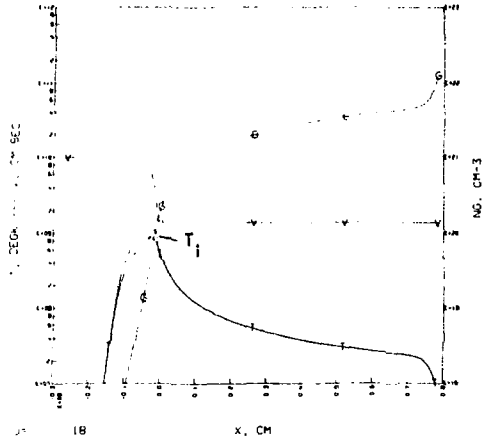

(a) $n_0 = 10^{17}$ cm^{-3}

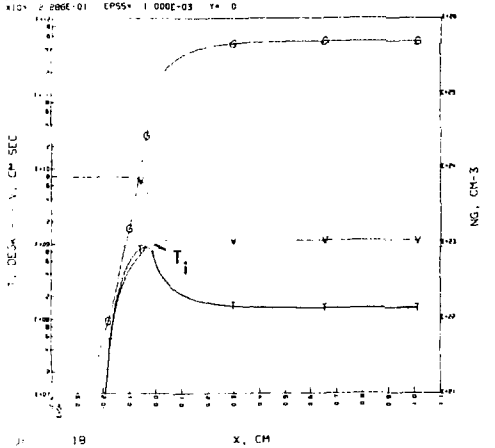

(b) $n_0 = 10^{22}$ cm^{-3}

Figure 8.4 - Effects of the presence of helium (E_0 = 40 MeV; $n_0 = 10^{20}$ cm^{-3}). Note that except for a moderate increase in ion temperature near x = 0 , the shock structure is only very slightly effected.

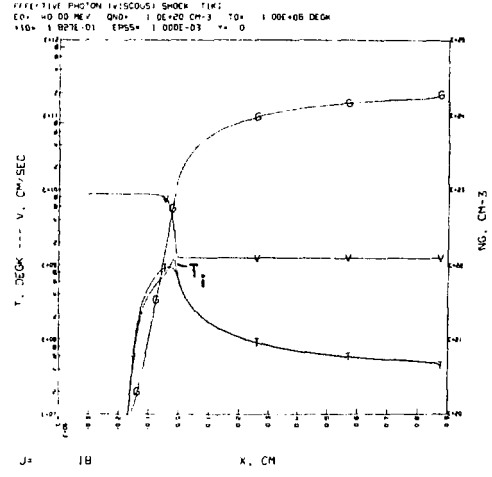

(a) Y = 0

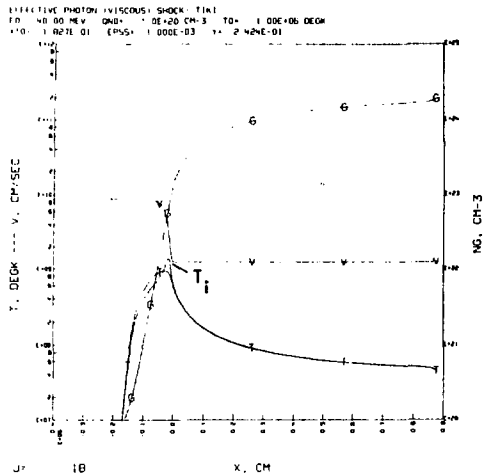
EFFECTIVE PHOTON (VISCOUS) SHOCK: TIKI
T, DEGK --- V, CM/SEC
NG, CM-3
X, CM
T_i

(b) Y = .24

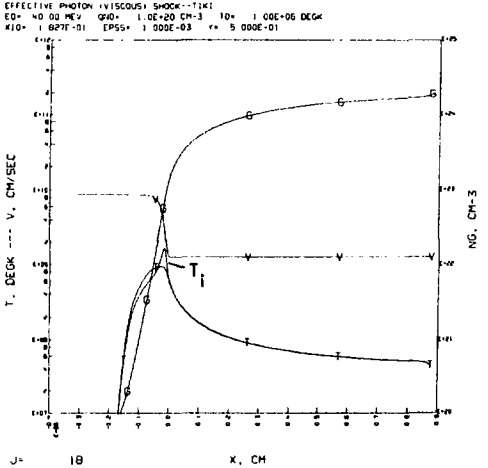
EFFECTIVE PHOTON (VISCOUS) SHOCK--TIKI
T, DEGK --- V, CM/SEC
NG, CM-3
X, CM
T_i

(c) Y = 0.5

Figure 8.5 - Relaxation of a hot-ion shock to a radiation-dominated shock. (E_0 = 30 MeV, $n_0 = 10^{20}$ cm^{-3}, and Y = .25). frame labeled J = 1 shows the initial shock configuration. In frames 2-11, the radiative rates are reduced by a factor of 100, and the initial structure is seen to relax to a hot-ion shock. In frames 12-25, the radiative rates are restored to normal, and the hot-ion shock is rapidly transformed into a radiation-dominated shock idential to that of Figure 8.2(c) (including axis labels) except for a very slightly higher ion temperature at x = 0 due to the presence of helium.

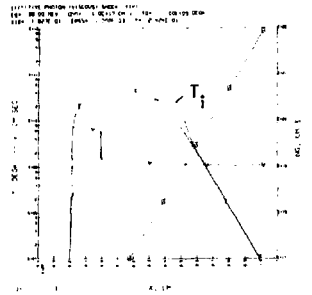
T_i

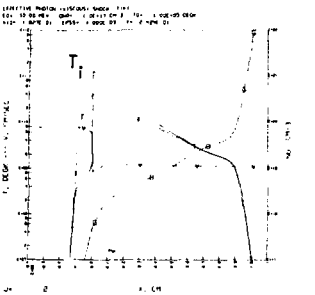
T_i

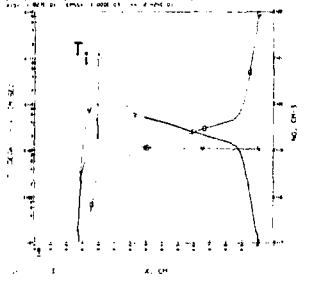
T_i

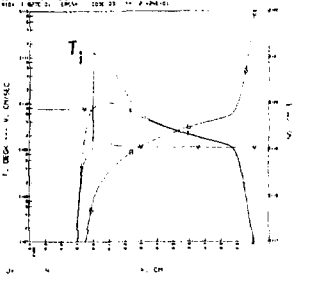
T_i

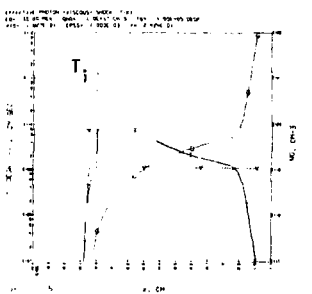
T_i

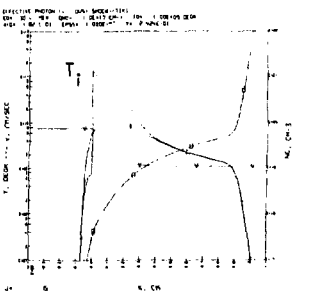
T_i

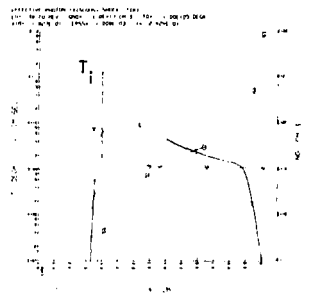
T_i

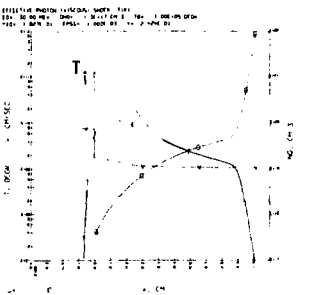
T_i

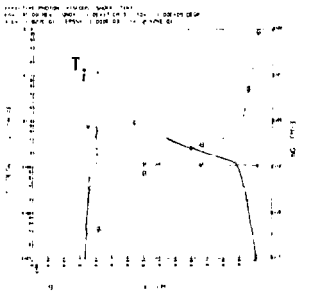
T_i

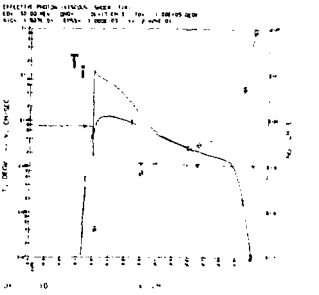
T_i

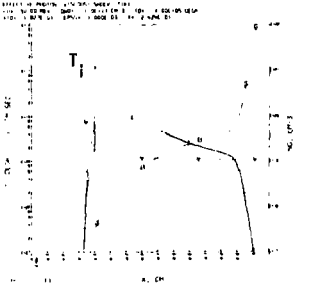
T_i

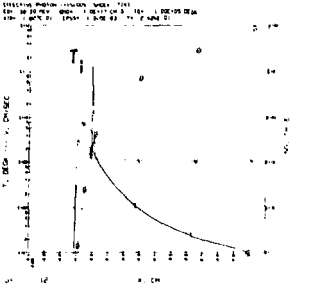
T_i

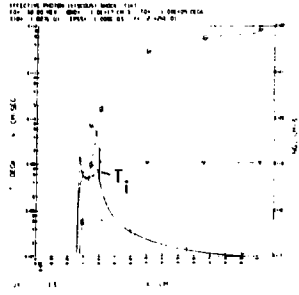
T_i

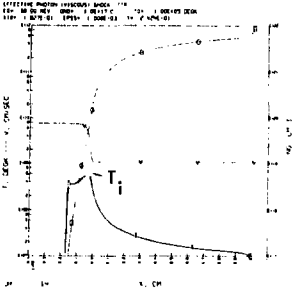
T_i

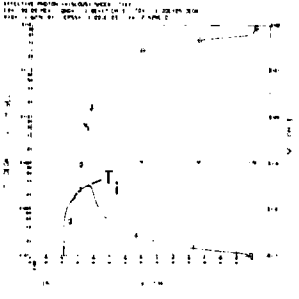
T_i

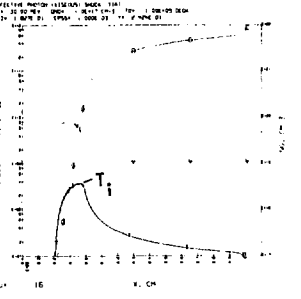
T_i

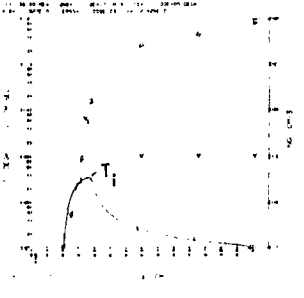
T_i

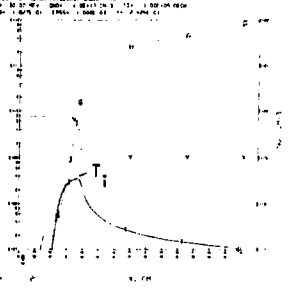
T_i

Figure 8.6 - Typical hot-ion shocks (radiative rates reduced 100-fold).

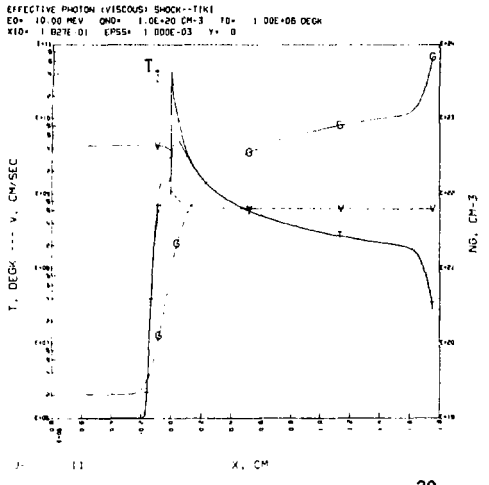

(a) $E_0 = 10$, $n_0 = 10^{20}$

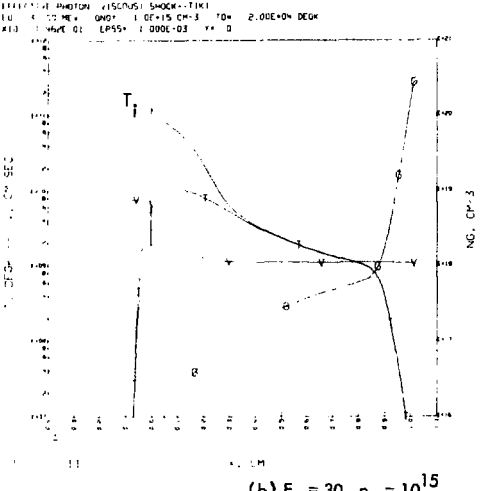

(b) $E_0 = 30$, $n_0 = 10^{15}$

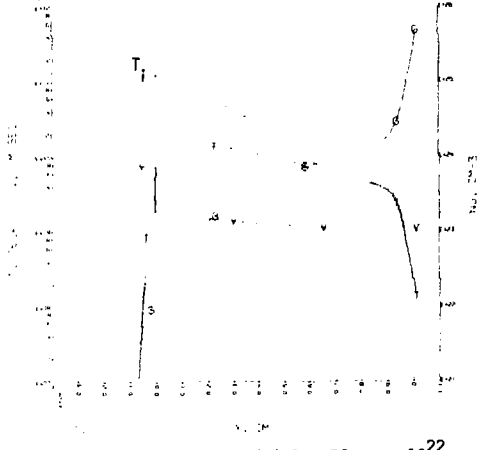

(c) $E_0 = 30$, $n_0 = 10^{22}$

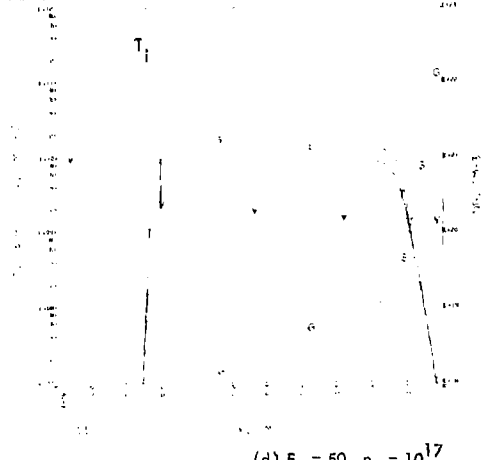

(d) $E_0 = 50$, $n_0 = 10^{17}$

IX. DISCUSSION AND ASTROPHYSICAL IMPLICATIONS

A. Prospects for Deuterium Production in Supernovae

In the previous sections, we have shown under fairly general assumptions that strong shocks in the density regime 10^{15} -10^{22} cm^{-3} and energy regime 1 to $\sim$ 40 MeV/nucleon will be non-equilibrium radiation-dominated and reach peak temperatures below $\sim$ 70 keV, while low temperature ($\lesssim$ 200 keV) pair-dominated shocks are likely to prevail in the $\sim$ 40-100 MeV/nucleon energy range. As we discussed in Section V.E, the limited nucleosynthesis that can occur in such shocks will tend to burn up rather than produce deuterium and other light elements. We conclude that if light elements are produced in supernovae, it will be under circumstances and physical conditions other than those we have assumed. With this in mind, it is useful to review both our general assumptions and the context in which the shocks have been set.

Energy and Density Regime

The density regime was chosen to be that typical of the envelope of a red giant star, but there seems no basic physical reason why our models can't be extended upward in density until the onset of Fermi degeneracy, the breakdown of the assumption that the inverse bremsstrahlung cutoff be $<< m_e c^2$, or the onset of sufficiently relativistic electron temperatures that the physical parameters calculated in Section III become qualitatively suspect (i.e. $\Theta_e >> m_e c^2$). Above $n_0 = 10^{22}$ cm^{-3}, however,

the final post-shock equilibrium temperature is $\gtrsim$ 10 keV for E_o > 3 MeV, so any deuterium produced is likely to be burned up before the post-shock region can be sufficiently cooled by expansion over typical red giant length scales (e.g. for a 10^{12} cm radius and a .1c expansion velocity, we have $n\tau = 2\times10^{25}$ cm^{-3} sec while $\langle\sigma v\rangle_{DD}$ (10 keV) = 1.2×10^{-18} cm^{+3} sec^{-1} and $\langle\sigma v\rangle_{PD}$ (10 keV) = 1.6×10^{-23} cm^3 sec^{-1} (Fowler, Caughlan and Zimmerman 1974)).

Again, while no basic physical approximation breaks down at $n_o = 10^{15}$ cm^{-3}, initial length scales of $\gtrsim 3\times10^{10}$ cm are required at that density to even approach the assumption of reasonable optical thickness (e.g. see Figures 5.2(a)), and distance scales $\sim 10^{14}$ cm are required for such a region to contain a solar mass. Such large red giants are observed to be far from average, and indeed far less than .1 solar mass of such low density material is believed to be contained in a more typical red giant (Iben 1973).

For energies below 1 MeV/nucleon, little nuclear spallation will occur even in a hot-ion shock, while shock energies > 100 MeV/nucleon must of energetic necessity occur only in a small mass fraction of a supernova. Physically, very low energy shocks are likely to be in radiative equilibrium (in part due to bound-bound and bound-free processes) and to eventually become viscosity-dominated when the equilibrium radiation pressure can no longer satisfy criterion (5.29). At energies above 100 MeV/nucleon, higher radiative transfer moments

(e.g. radiative momentum transport) become important since v_0 is no longer << c, and in addition relativistic kinematics must be employed (Johnson and McKee 1971).

Optical Thickness

The assumption of optical thickness for shocks giving rise to a cosmologically significant amount of deuterium can be shown to be reasonable by noting that the radius, R, beyond which a shell 30 Thompson lengths, ℓ_T, wide and containing .01 $M_\odot$, where $M_\odot$ is the solar mass, is given by:

$$R = \left(\frac{\sigma_T M_\odot}{12000\ \pi m}\right)^{1/2} = 1.5 \times 10^{14}\ \text{cm} \qquad (9.1)$$

Since: 1) 30 ℓ_T is a greater distance than radiation can diffuse in a shock passage time for $E_\upsilon \gtrsim 1$ MeV; 2) R is considerably larger than the radius of typical red giants and thus presumably pre-supernova stars; and 3) for a galactic Type II supernova rate of .03 year^{-1}, a galactic age and mass of 10^{10} years and 10^{11} $M_\odot$, and a current D/H ratio of 1.4×10^{-5} (Reeves 1974), a mean supernova event must produce 5×10^{-3} $M_\odot$ of deuterium and thus involve the processing of $\gtrsim$ .01 $M_\odot$ (even for Y = .5) of material to $T_f \gtrsim 10$ MeV; we conclude that significant optically-thin deuterium production is unlikely in supernovae. Such production is not ruled out, however, in supermassive stars of the type discussed by Hoyle and Fowler(1973), although no evidence of the existence of such objects has been found.

Assumption of Steady State

Similar arguments can be made to qualitatively justify the assumption that the density regime through which the shock propagates is sufficiently wide that the shock has reached a near steady state condition. This follows since 30 ℓ_T, equivalent to $\sim$ 90 v_0/c characteristic radiation-dominated shock lengths, is a more than adequate distance to recreate all the radiation in the shock and thus probably to relax any significant structural transients.

Sensitivity to Radiative Rates

As noted in Section VIII.C, a 10 to 100-fold reduction in radiative rates is required to produce a hot-ion shock. Numerical sensitivity experiments suggest, however, that the present treatment of the radiative rates is accurate to within a factor of two, with most of the uncertainty arising from the specification of the dynamical cutoff, τ_d, due to inverse Compton scattering, in Section IV. Note that the most conservative reasonable assumption was made there.

A multigroup treatment of the radiation field in the form indicated by (2.20) is probably required for more accurate results, and is being undertaken in connection with the neutron star accretion problem (See § IX. B). It is evident, however, that the present level of accuracy is sufficient to settle the deuterium production question. With respect to errors in the relativistic corrections to the bremsstrahlung rate, we note

that the use of Gould's (1974) quadrapole e-e bremsstrahlung rates instead of those given by Maxon (1972) typically makes only $\sim$ 2% difference in the calculated shock structures.

Navier-Stokes Treatment of Dissipation

Since radiation-dominated shocks typically extend over several Compton lengths, sources of dissipation that are non-linear in the gradients of the physical parameters are unlikely to become important, and so a kinetic or Monte-Carlo treatment of the shock structure does not appear necessary. It is interesting to note, however, that strong hot-ion viscous shocks occurring over 1-2 ion-ion mean-free-paths can show several interesting nonhydrodynamic effects. In particular, two dimensional Monte-Carlo calculations of shocks made up of hard spheres (Bird 1967) show that such shocks are a factor of 1.5-2 broader than predicted by the Navier-Stokes relations, have higher longitudinal than lateral temperatures, and show a secondary peak in the high energy tail of the longitudinal velocity distribution corresponding to particles that have been back-scattered against the general flow while approximately retaining the absolute magnitude of the flow velocity. This last effect, though probably diminished in a realistic plasma due to the usual (i.e. non-nuclear) predominance of low-angle scatters, may have interesting implications for nucleosynthesis if circumstances are found in which hot-ion shocks can occur.

Hot-Ion Shock Nucleosynthesis

Calculations of shock-wave nucleosynthesis (Epstein, Arnett, and Schramm(1974)) based on the hot-ion shock model of Colgate (1974) show overproduction of Li, Be, and B relative to deuterium. While the details of these results depend on the initial composition, and the revised hot-ion shock structures recently proposed by Colgate (1975) may reduce some of the abundance discrepancies, no natural resolution has yet emerged.

Such problems with hot-ion shock nucleosynthesis are, of course, completely consistent with the cool, radiation-dominated shocks found in the present study.

Conclusion

The conclusion thus seems reasonably forced that the production of a cosmologically significant amount of deuterium does not occur in supernova shock waves. The only currently viable and "non-exotic" means for the production of the presently existing deuterium appears to be its formation via the $p+n \rightarrow D+\gamma$ reaction in the primordial Big Bang (Gott et al. 1974). As is well known, such a process requires a low density and thus open universe if subsequent deuterium burn up is to be avoided.

B. Other Astrophysical Applications

While the shock structures in this study were calculated principally to evaluate the prospects for supernova deuterium synthesis, the concepts and results can also be applied to other astrophysical situations involving strong shocks.

Supernova Cosmic Ray Production

Colgate and Johnson (1960) have postulated that cosmic rays are produced as the shock formed in the envelope of a Type I supernova explosion is accelerated to extreme relativistic energies as it transverses the steep density gradient near the surface of the compact star ($\lesssim 10^9$ cm in radius) thought to be involved in such an explosion. The composition of these cosmic rays is clearly critically dependent on the temperatures reached in such relativistic shocks. The initial calculations were made under the assumption of complete radiative equilibrium and resulted in temperatures $\leq$ 500 keV.

It was in this context that the original suggestion was made that sufficiently strong shocks would very probably exhibit a high temperature "precursor", either in the form of a hot-ion viscous shock, or more probably a non-equilibrium radiation-dominated shock, (cf. Weaver et al 1974). While a detailed treatment of the relativistic shock structure is beyond the scope of the present study, naive extension of our non-relativistic results leads to temperatures greatly in excess of 1 MeV. Indeed a preliminary pair-dominated shock model yields a peak temperature of $\gtrsim$ 100 MeV for a shock with a relativistic γ of 15, despite the bootstrap operating between pair-production via the $\gamma\gamma \rightarrow e^+e^-$ reaction and

radiative Compton scattering. (Multiple radiative Compton scattering and multiple bremsstrahlung, however, were not included and may served to limit these temperatures.) Even if the peak radiation temperatures remain $\sim$ 1 MeV, both pair and radiation-dominated models predict that the ions will stream though the radiation/pair field so that a typical photon will appear to have an energy of $\sim 3\gamma$ MeV. Thus, the survival of high-Z nuclei in at all relativistic cosmic rays appears doubtful. More detailed calculations are clearly needed to confirm this conclusion, however, and will be the subject of a later paper.

In such calculations, time dependent effects related to the breakout of the radiation field and the shock thickness becoming of the order of an atmospheric scale height are likely to become important. One interesting point in this respect is that the presence of pairs in the high temperature "precursor" will serve to "dam in" the post-shock radiation, and thus allow the shock to propagate to a lower optical depth than would otherwise have been the case. The magnitude of this effect is uncertain, and indeed it is possible that Rayleigh-Taylor instabilities will ensue.

Accretion onto Neutron Stars

The deceleration of material accreting onto a neutron star at energies $\sim$ 50-100 MeV/nucleon has been studied by several authors (Zel'dovich and Shakura 1969; Alme and Wilson 1973; Shapiro and Salpeter 1974), and is proposed to involve either electron-ion coulomb friction or strong plasma instabilities. A key question in such a process is whether or not a standing

accretion shock forms in the infalling material above the surface of the neutron star, following which the post-shock material is adiabatically compressed up to its final surface density. The results of this study, suggests that a radiation-dominated shock of this type could be formed fairly readily, especially if accretion is occuring at near the Eddington limit. Indeed, if the accretion shock lies $\gtrsim$ 30 Compton lengths deep in the accreting material, the shock structures calculated in this study should be directly applicable. In the more likely case of a less optically thick shock, a multigroup treatment of the radiation field in terms of flux-limited diffusion (see Section III.C) and allowing for higher radiative moments such as momentum transport is required, and is currently being pursued. In such a shock, radiation loss will compete with reduced inverse Compton cooling to determine the shock temperature and thus the characteristics of the emitted radiation spectrum.

Formation of Proto-Galaxies

Shock compression arising from collisions between perturbations in the early universe is thought to be important in the formation of regions sufficiently dense to resist being dispersed by the general expansion of the universe, and thus become proto-galaxies (Silk 1974). If the perturbations involved are optically thin, the radiation loss rate and thus the structure of the shock will be important in determining the velocity and extent of its propagation. The shock structure treatment being developed for neutron star accretion shocks appears applicable to such cases. If the shock energies and resulting temperatures are sufficiently

high, the possibility of nuclear processing, including light element formation, should not be overlooked.

REFERENCES

Abramowitz, M., and Stegun, I. A., ed., 1964, Handbook of Mathematical Functions (Washington: U.S. Government).

Alme, M. L. and Wilson, J. R, 1974, Ap.J., 186, 1015.

Becker, R. 1922, Z. Physik, 8, 321.

Belokon', V. A. 1959, Soviet Phys. - JETP, 9, 235.

Bird, G. A., 1967, J. Fluid Mech., 30, 479.

Bond, J. W., Watson, K. M., and Welch, J. A. 1965, Atomic Theory of Gas Dynamics (Reading, Mass.: Addison-Wesley).

Burgers, J. M. 1960, in Plasma Dynamics, F. H. Clauser, ed. (Reading, Mass.: Addison-Wesley), pp. 119-186.

Chapline, G. F., and Stevens, J. 1973, Ap.J., 184, 1041.

Chiu, H-Y. 1968, Stellar Physics (Waltham, Mass.: Blaisdell).

Clayton, D. D. 1968, Principles of Stellar Evolution and Nucleosynthesis (New York: McGraw-Hill).

Colgate, S. A. 1969, Proc. 11th International Conference on Cosmic Rays, (Budapest).

_____. 1973, Ap.J. (Letters), 181, L53.

_____. 1974, Ap.J., 187, 321.

_____. 1975, Ap.J., 195, 493.

Colgate, S. A., and Johnson, M. H. 1960, Phys. Rev. Letters, 5, 235.

Cooper G. 1971, Phys. Rev. D, 3, 2312.

_____. 1974, J. Quant. Spectrosc. Radiat. Transfer, 14, 887.

Drummond, J. E., 1961, Plasma Physics (New York: McGraw-Hill), p. 319.

Epstein, R.I., Arnett, W. D., and Schramm, D. N. 1974, Ap.J. (Letters), 190, L13.

Fediushin, B. K. 1952, Zh. Eksp. Teor. Fiz, 22, 140.

Fowler, W. A., Caughlan, G. R., and Zimmerman, B. A. 1974, preprint.

Gould, R. J., 1974, preprints.

Hoyle, F., and Fowler, W. A. 1973, Nature, 241 384.

Iben, I., 1973, in Explosive Nucleosynthesis, Schramm, D. N. and Arnett, W. D., ed., p. 115 (Austin: University of Texas Press).

Jackson, J. D. 1962, Classical Electrodynamics (New York: Wiley).

Jaffrin, M. Y., and Probstein, R. F. 1964, Phys. Fluids, 7, 1658.

Jauch, J. M., and Rohrlich, F. 1955, Theory of Photons and Electrons, (Cambridge: Addison-Wesley).

Johnson, M. H., and McKee, C. F. 1971, Phys. Rev. D, 3, 858.

Landau, L. D., and Lifschitz, E. M. 1959, Fluid Mechanics, (London: Pergamon Press).

Mandl, F., and Skyrme, T. H. R. 1952, Proc. Roy. Soc. Ser. A, 215, 497.

Maxon, S. 1972, Phys. Rev, A5, 1630.

McKee, C. F. 1970, Ph.D. Thesis, University of Calif., Berkeley.

Minorsky, N. 1947, Introduction to Non-Linear Mechanics (Ann Arbor, Mich.: Edwards Brothers), pp. 9-23.

Quigg, C. 1968, Phys. Fluids, 11, 461.

Ram, M., and Wang, P. Y. 1971, Phys. Rev. Letters, 26, 476.

Reeves, H., 1974, Ann. Rev. Astron. Ap., 12, 437.

Shapiro, S. L. and Salpeter, E. E., 1974, preprint.

Shklovsky, I. S. 1968, Supernovae (New York: Interscience).

Silk, J. I. 1974, in Confrontation of Cosmological Theories with Observational Data, M. S. Longair, ed., p. 175 (New York: Reidel).

Spitzer, L. 1962, Physics of Fully Ionized Gases (New York: Interscience).

Stone, S. 1971, "Compton Scattering at High Material Temperatures", UCRL-73424, Lawrence Livermore Laboratory.

_____. 1973, "Compton Scattering from Isotropic Electrons of a Single Energy", UCRL-75101, Lawrence Livermore Laboratory.

Stone, S., and Nelson, R. G. 1966, "Compton Scattering from Relativistic Electrons", UCRL-14918-T, Lawrence Livermore Laboratory.

Stringer, T. E. 1964, Plasma Phys., 6, 267.

Weaver, T. A. and Chapline, G. F. 1974, Ap.J. (Letters), 192, L57.

Weaver, T. A., Chapline, G. F., Wood, L. L., and Silk, J. I. 1974, Bull. APS 6, 274.

Weynmann, R. 1965, Phys. Fluids, 8, 2112.

Zel'dovich, Ya. B., and Raizer, Yu.P. 1966, Physics of Shock Waves and High-Temperature Hydrodynamic Phenomena (New York: Academic).

Zel'dovich, Ya. B., and Shakura, N. I. 1969, Soviet Astron. - AJ, 13, 175.

APPENDIX A

Relativistic Distribution-Averaged Reaction Rates

We wish to find the Lorentz invariant rate per unit volume, R_{12}, at which particles of type 1 and type 2 interact to make particles of type 3. In any given observer frame, the reactants are assumed to have a distribution of the form $n_i f_i(\vec{p}_i)$ where n_i is the total number density of particles of type i and $f_i(\vec{p}_i)$ is probability that a given particle will have momentum $\vec{p}_i$. For convenience and clarity we will treat first the case where the masses of the interacting particles, m_1 and m_2, are non-zero, and later relax this restriction.

Particle-Particle Reactions:

In the specific case when the type 1 particles are all at rest and the type 2 particles are all moving in a beam at relative velocity, v_R, the reaction rate can be given directly in the familiar form:

$$R_{12} \equiv n_1 n_2 \, v_R \, \sigma(v_R) \tag{A1}$$

where this relation serves to define the laboratory cross section, $\sigma(v_R)$.

To find R_{12} for more general distributions, we consider the specific momentum groups, $n_1 f_1(\vec{p}_1)\, d\vec{p}_1$ and $n_2 f_2(\vec{p}_2) d\vec{p}_2$, in the observer frame; transform to the rest frame of the 1-group

to calculate their contribution to the reaction rate; use the R_{12} invariance to transform back to the observer frame; and then integrate over $\vec{p}_1$ and $\vec{p}_2$ to find the total reaction rate:

$$R_{12} = \frac{1}{1+\delta_{12}} \iint \{n_1 n_2 \sigma(v_R) v_R\}_{\vec{p}_i \text{ frame}} f_1(\vec{p}_1) f_2(\vec{p}_2) d\vec{p}_1 d\vec{p}_2 \qquad \text{(A2)}$$

where δ_{12} is the Kronecker delta which has been introduced to compensate for the fact that interacting pairs have been counted twice when particles of type 1 and 2 are identical. To evaluate $\{n_1 n_2\}_{\vec{p}_1}$ consider the invariant scaler product of the 4-vector currents, $j_1 = (n_1, n_1\vec{\beta}_1)$ and $j_2 = (n_2, n_2\vec{\beta}_2)$:

$$j_1 \cdot j_2 = n_1 n_2 (1 - \vec{\beta}_1 \cdot \vec{\beta}_2) = \{n_1 n_2\}_{\vec{p}_1 \text{ or } \vec{p}_2 \text{ frame}} \qquad \text{(A3)}$$

Here, $\vec{\beta}_i = \frac{\vec{v}_i}{c}$ where as usual $\vec{v}_i$ is the velocity of particle i and c is the speed of light. In a similar fashion the scaler product of the 4-vector velocities, $(\gamma_i, \gamma_i\vec{\beta}_i)$ gives the relation:

$$\gamma_1 \gamma_2 (1 - \vec{\beta}_1 \cdot \vec{\beta}_2) = \gamma_R \qquad \text{invariant} \qquad \text{(A4)}$$

where $\gamma_i = \{1 - \beta_i^2\}^{-1/2}$ and γ_R and β_R are now specifically understood to be measured in the rest frame of the 1-type particle group.

The expression for R_{12} thus becomes:

$$R_{12} = \frac{(n_1 n_2)_{obs} c}{1 + \delta_{12}} \iint f_1(\vec{p}_1) f_2(\vec{p}_2) \frac{\gamma_R \beta_R}{\gamma_1 \gamma_2} \sigma(\beta_R)\, d\vec{p}_1 d\vec{p}_2 \qquad (A5)$$

If we now restrict our attention to distributions that are isotropic in the observer frame and consider any specified $\vec{p}_1$ to be fixed along the z-axis, (A5) reduces to:

$$R_{12} = \frac{c(n_1 n_2)_{obs}}{2(1 + \delta_{12})} \int_0^\infty \int_0^\infty \int_{-1}^{1} f_1(p_1) f_2(p_2) \frac{\gamma_R \beta_R}{\gamma_1 \gamma_2} \sigma(\beta_R)\, du dp_1 dp_2 \qquad (A6)$$

where $u = \cos\theta = \dfrac{\vec{\beta}_1 \cdot \vec{\beta}_2}{\beta_1 \beta_2}$ and $f_i(p_i) = 4\pi p_i^2 f_i(\vec{p}_i)$

so that $\int_0^\infty f_i(p_i) dp_i = 1$.

Utilizing relation (A4) to eliminate u in favor of $p_R = \gamma_R \beta_R m_2 c$ we obtain R_{12} in the convenient form:

$$R_{12} = \frac{(n_1 n_2)_{obs}}{(1+\delta_{12})} \int_0^\infty \beta_R c \sigma(\beta_R) F(p_R) dp_R \qquad (A7)$$

where:

$$F(p_R) = \frac{\gamma_R \beta_R}{2 m_2 c} \int_0^\infty \frac{f_1(p_1)}{\beta_1 \gamma_1^2} \left\{ \int_{\gamma_1\gamma_R|\beta_1 - \beta_R| m_2 c}^{\gamma_1\gamma_R(\beta_1+\beta_R) m_2 c} \frac{f_2(p_2)}{\beta_2 \gamma_2^2} dp_2 \right\} dp_1 \qquad (A8)$$

To further simplify the expression for $F(p_R)$, it is necessary to know the forms of $f_2(p_2)$ and/or $f_1(p_1)$. We treat first the case where $f_1(p_1)$ is arbitrary, while $f_2(p_2)$ is a

relativistic Maxwell-Boltzmann distribution (RMB) given by:

$$f_2(p_2) = \frac{p_2^2 \, e^{-[p_2^2c^2+m_2^2c^4]^{1/2}/kT_2}}{m_2^2 c \; kT_2 K_2(\frac{m_2c^2}{kT_2})} \tag{A9}$$

where T_2 is the temperature of the 2-type particles, K_2 is the second order modified Bessel function of the second kind, and k is Boltzmann's constant. We then find:

$$F(p_R)\Big|_{\substack{f_1 \text{ arb.} \\ f_2 \text{ RMB}}} = \frac{\gamma_R\beta_R}{2m_2cK_2(\frac{m_2c^2}{kT_2})} \int_0^\infty \frac{f_1(p_1)}{\beta_1\gamma_1^2} \cdot$$

$$\cdot\left\{\exp\left[-[\gamma_1^2\gamma_R^2(\beta_1-\beta_R)^2+1]^{1/2}\frac{m_2c^2}{kT_2}\right] - \exp\left[-[\gamma_1^2\gamma_R^2(\beta_1+\beta_R)^2+1)]^{1/2}\frac{m_2c^2}{kT_2}\right]\right\} dp_1 \tag{A10}$$

In the case where $f_1(p_1)$ is also an RMB, use of symmetry and hyperbolic substitutions allow the integral to be done, resulting in the relatively simple forms:

$$F(p_R)\Big|_{\substack{f_1\text{RMB} \\ f_2\text{RMB}}} = \frac{\gamma_R^2\beta_R^2}{m_2c} \; \frac{(m_1c^2/kT_1)}{K_2(\frac{m_1c^2}{kT_1})K_2(\frac{m_2c^2}{kT_2})} \cdot$$

$$\cdot \frac{K_1[\frac{m_2c^2}{kT_2}(\alpha^2 + 2\alpha\gamma_R + 1)^{1/2}]}{(\alpha^2 + 2\alpha\gamma_R + 1)^{1/2}} \qquad \text{(A11a)}$$

and

$$R_{12}\Big|_{f_2\ \text{RMB}}^{f_1\ \text{RMB}} = \frac{(n_1n_2)_{obs}}{m_2(1+\delta_{12})} \frac{(m_1c^2/kT_1)}{K_2(\frac{m_1c^2}{kT_1})K_2(\frac{m_2c^2}{kT_2})}$$

$$\cdot \int_0^\infty \frac{\gamma_R^2\beta_R^3\sigma(\beta_R)K_1[\frac{m_2c^2}{kT_2}(\alpha^2 + 2\alpha\gamma_R + 1)^{1/2}]}{(\alpha^2 + 2\alpha\gamma_R + 1)^{1/2}} dp_R \qquad \text{(A11b)}$$

where $\alpha = \frac{m_1T_2}{m_2T_1}$ and K_1 is the first order modified Bessel function of the second kind. This last result can be symmeterized into the relatively simple form:

$$R_{12}\Big|_{f_2\ \text{RMB}}^{f_1\ \text{RMB}} = \frac{(n_1n_2)_{obs}}{1+\delta_{12}} \frac{c\phi_1\phi_2}{K_2(\phi_1)K_2(\phi_2)} \int_0^\infty \frac{\sigma(\chi)\chi^3K_1(\Psi)}{(\chi^2+1)^{1/2}\Psi} d\chi \qquad \text{(A11c)}$$

where:

$$\phi_i = \frac{m_ic^2}{kT_i} \qquad \chi = \gamma_R\beta_R$$

and $\Psi = (\phi_1^2 + 2\phi_1\phi_2\ (\chi^2+1)^{1/2} + \phi_2^2)^{1/2}$

In the case when $T_1 = T_2 = T$, we note $kT\Psi$ is just the center of mass energy of the two interacting particles. In the limit when all energies and temperatures of interest are non-relativistic, (11b) reduces to the familiar form (cf. Clayton 1968):

$$R_{12}\Big|_{\substack{f_1\ \mathrm{NRMB}\\ f_2\ \mathrm{NRMB}}} = \frac{n_1 n_2}{1+\delta_{12}}\, 4\pi \left[\frac{m_1 m_2}{2\pi k(m_1 T_2 + m_2 T_1)}\right]^{3/2} \cdot \int_0^\infty e^{-\frac{m_1 m_2 v_R^2}{2k(m_1 T_2 + m_2 T_1)}}\, \sigma(v_R) v_R^3 dv_R \qquad \text{(A12)}$$

Particle-photon Interactions:

The assumption of massive reactants made in the previous section can easily be relaxed in the case when $m_2 = 0$. (For notational convenience in considering this case, we shall discuss photons (i.e. $2 \to \gamma$) though no loss of generality is implied.) The analogous expression to (A4) is then:

$$p_\gamma \gamma_1 (1 - \beta_1 \cos\theta) = p_\gamma^* \quad \text{invariant} \qquad \text{(A13)}$$

where p_γ^* is the momentum of the photon in the rest frame of particle 1, and $\cos\theta = \frac{\vec{\beta}_1 \cdot \vec{\beta}_\gamma}{\beta_1 \beta_\gamma} = u$ where $\vec{\beta}_1$ and $\vec{\beta}_\gamma$ are measured in the observer frame. Expressions (A1), (A2), (A3) are changed only in that $2 \to \gamma$, $v_R \to c$, $\sigma(v_R) \to \sigma(p_\gamma^*)$, and $\delta_{12} = 0$, and so for general distributions, we find:

$$R_{1\gamma} = (n_1 n_\gamma)_{obs} c \iint f_1(\vec{p}_1) f_\gamma(\vec{p}_\gamma) \frac{p'_\gamma}{\gamma_1 p_\gamma} \sigma(p'_\gamma) d\vec{p}_1 d\vec{p}_\gamma \qquad (A14)$$

and for isotropic distributions, we find:

$$R_{1\gamma} = \frac{(n_1 n_\gamma)_{obs} c}{2} \int_0^\infty \int_0^\infty \int_{-1}^{1} f_1(p_1) f_\gamma(p_\gamma) \frac{p'_\gamma}{\gamma_1 p_\gamma} \sigma(p'_\gamma) du dp_1 dp_\gamma \qquad (A15)$$

or

$$R_{1\gamma} = (n_1 n_\gamma)_{obs} \int_0^\infty c\sigma(p'_\gamma) F_\gamma(p'_\gamma) dp'_\gamma \qquad (A16)$$

where

$$F_\gamma(p'_\gamma) = \frac{p'_\gamma}{2} \int_0^\infty \frac{f_1(p_1)}{\beta_1 \gamma_1^2} \left\{ \int_{\gamma_1 p'_\gamma(1-\beta_1)}^{\gamma_1 p'_\gamma(1+\beta_1)} \frac{f_\gamma(p_\gamma)}{p_\gamma^2} dp_\gamma \right\} dp_1 \qquad (A17)$$

$$= \frac{p'_\gamma}{2} \int_0^\infty \frac{f_\gamma(p_\gamma)}{p_\gamma^2} \left\{ \int_{\frac{1}{2}\left|\frac{p'_\gamma}{p_\gamma} - \frac{p_\gamma}{p'_\gamma}\right| m_1 c}^{\infty} \frac{f_1(p_1)}{\beta_1 \gamma_1^2} dp_1 \right\} dp_\gamma$$

We now take $f_\gamma(p_\gamma)$ to be a relativistic Bose-Einstein distribution (RBE) given by:

$$f_\gamma(p_\gamma) = \frac{8\pi}{h^3 n_\gamma} \frac{p_\gamma^2}{Ce^{p_\gamma c/kT_\gamma} - 1} \qquad (A18)$$

where h is Planck's constant, T_γ is the photon temperature and C is a dimensionless degeneracy parameter which is equal to 1 for a blackbody distribution and goes to infinity in the non-degenerate limit. n_γ and C are related by:

$$n_\gamma = \frac{16\pi(kT_\gamma)^3}{c^3h^3} \sum_{n=1}^{\infty} \frac{1}{n^3C^n} = \begin{cases} \zeta(3)n_\gamma^0 & C=1 \\ n_\gamma^0/C & C\to\infty \end{cases} \qquad \text{(A19)}$$

where $\zeta(3) = \sum_{n=1}^{\infty} \frac{1}{n^3} = 1.2021....$; and $n_\gamma^0 = \frac{16\pi(kT)_\gamma^3}{c^3h^3}$.

For this case, we find:

$$F_\gamma(p_\gamma')\Big|_{\substack{f_1 \text{ arb} \\ f_\gamma \text{ RBE}}} = \frac{n_\gamma^0}{2n_\gamma} \frac{p_\gamma' c^2}{(kT_\gamma)^2} \sum_{n=1}^{\infty} \frac{1}{nC^n} \int_0^\infty \frac{f_1(p_1)}{\beta_1\gamma_1^2} \cdot$$

$$\cdot\, e^{-\gamma_1 p_\gamma' nc/kT_\gamma} \sinh(\gamma_1 p_\gamma' \beta_1 nc/kT_\gamma)dp_1 \qquad \text{(A20)}$$

For the case when f_1 is an RMB, while f_γ is an arbitrary isotropic distribution, we find:

$$F_\gamma(p_\gamma')\Big|_{\substack{f_1 \text{ RMB} \\ f_\gamma \text{ arb}}} = \frac{p_\gamma'}{2K_2(\frac{m_1c^2}{kT_1})} \int_0^\infty \frac{f(p_\gamma)}{p_\gamma^2} e^{-\frac{1}{2}(\frac{p_\gamma}{p_\gamma'} + \frac{p_\gamma'}{p_\gamma})\frac{m_1c^2}{kT_1}} dp_\gamma \qquad \text{(A21)}$$

Finally, when f_1 is an RMB and f_γ is an RBE, we find $R_{1\gamma}$ to be:

$$R_{1\gamma}\Big|_{\substack{f_1 \text{ RMB} \\ f_\gamma \text{ RBE}}} = \frac{(n_1n_\gamma^0)_{obs}\, c^4}{2(kT_\gamma)^3K_2(\frac{m_1c^2}{kT_1})} \sum_{n=1}^{\infty} \frac{1}{C^n} .$$

$$\cdot \int_0^\infty \frac{p_\gamma'^2 \sigma(p_\gamma') \; K_1\left(\frac{m_1c^2}{kT_1}[1+2n\,\frac{p_\gamma'}{m_1c}\,\frac{T_1}{T_\gamma}]^{1/2}\right)}{[1+2n\,\frac{p_\gamma'}{m_1c}\,\frac{T_1}{T_\gamma}]^{1/2}}\, dp_\gamma' \qquad \text{(A22a)}$$

or in more convenient notation:

$$R_{1\gamma}\Big|_{\substack{f_1 \text{ RMB} \\ f_\gamma \text{ RBE}}} = \frac{(n_1 n_\gamma^o)_{obs}}{2}\; \frac{c\phi_1}{K_2(\phi_1)} \sum_{n=1}^{\infty} \frac{1}{c^n} \int_0^\infty \frac{\zeta^2 \sigma(\zeta) K_1(\psi_n')}{\psi_n'}\, d\zeta \qquad \text{(A22b)}$$

where:

$$\zeta = \frac{p_\gamma' c}{kT_\gamma} \quad \text{and} \quad \psi_n' = (\phi_1^2 + 2n\phi_1\zeta)^{1/2} \; .$$

The sum involved here is rapidly convergent, and vanishes in the non-degenerate limit.

In the limit when the energies and temperatures of interest are nonrelativistic (except in the the case of the inherently relativistic photon where we require $p_\gamma' << m_1 c$), (A22b) reduces as required to:

$$R_{1\gamma}\Big|_{\substack{f_1 \text{ NRMB} \\ f_\gamma \text{ "NR"BE}}} = n_1 c\, \frac{8\pi}{h^3} \int_0^\infty \frac{p_\gamma'^2\, \sigma(p_\gamma') dp_\gamma'}{C\, e^{p_\gamma' c/kT_\gamma} - 1} \qquad \text{(A23)}$$

In the non-degenerate case, expressions (A13)-(A23) can also be obtained as the limits of the equivalent massive particle forms when $\gamma_R \to p_\gamma' c/m_2 c^2$ and $m_2 \to 0$.

Photon-Photon Reactions

The above formalism is still not in a suitable form to treat reactions between massless particles, since it is impossible to transform to a massless particle's rest frame. It is therefore necessary to generalize the definition of the cross-section. This could be done by directly assuming that the definition in (A1) holds in a general reference frame (Stone and Nelson 1966), but this results in a generalized cross-section that is not Lorentz invariant. It is more conventional (Jauch and Rohrlich 1955) to define the cross-section by the invariant relation:

$$R \equiv \frac{n_1 n_2 (1-\vec{\beta}_1\cdot\vec{\beta}_2)\,[\,(P_{1\mu}\cdot P_2^{\mu})^2 - m_1^2 m_2^2 c^4]^{1/2}}{P_{1\mu}\cdot P_2^{\mu}}\, c\sigma \qquad \text{(A24a)}$$

$$= n_1 n_2\,[(1-\vec{\beta}_1\cdot\vec{\beta}_2)^2 - \frac{m_1^2 m_2^2 c^8}{E_1^2 E_2^2}\,]^{1/2}\, c\sigma \qquad \text{(A24b)}$$

$$= \begin{cases} n_1 n_2 (1-\vec{\beta}_1\cdot\vec{\beta}_2)\beta_R c\sigma & \text{for } m_1, m_2 = 0 \qquad \text{(A24c)} \\ n_1 n_2 (1-\vec{\beta}_1\cdot\vec{\beta}_2) c\sigma & \text{for } m_1 \text{ or } m_2 = 0 \qquad \text{(A24d)} \end{cases}$$

where $P_{1\mu}\cdot P_2^{\mu}$ is the scaler product of the 4-momenta of particles of type 1 and 2 (assumed to be in beams) and E_i is the total energy of particle i. Equation (A24c) can be interpreted as defining the cross-section as the ratio of the reaction rate to the proper particle flux, and reduces to (A1) in the rest frame

of one of the particles; while (A24d) reduces to the natural result, $R = n_1 n_2 2c\sigma$, in the center of momentum frame for two massless particles.

The case of reactions between distributions of massless particles can now be treated in a fashion analogous to the massive particle case, except that a transformation to the center of momentum frame is used. The invariants analogous to (A3) and (A4) are then:

$$n_{\gamma 1} n_{\gamma 2}(1-\cos\theta) = 2n^*_{\gamma 1} n^*_{\gamma 2} \tag{A25}$$

and

$$p_{\gamma 1} p_{\gamma 2}(1-\cos\theta) = 2p^{*2}_{\gamma 1} = 2p^{*2}_{\gamma 2} \equiv 2p^{*2}_{\gamma} \tag{A26}$$

where $p_{\gamma 1}$ and $p_{\gamma 2}$ are the magnitudes of the momenta of two specific photon groups and θ is the angle between them, while $n_{\gamma i}$ is the photon number density of group i. The superscript "*" denotes measurement in the center of momentum frame. Here again the trivial but convenient specialization to the photon case has been made.

The reaction rate for general distributions can then be written:

$$R_{\gamma\gamma} = (n_{\gamma}^2)_{obs} c \iint f(\vec{p}_{\gamma 1}) f(\vec{p}_{\gamma 2}) \frac{p^{*2}_{\gamma}}{p_{\gamma 1} p_{\gamma 2}} \sigma(p^*_{\gamma}) d\vec{p}_{\gamma 1} d\vec{p}_{\gamma 2} \tag{A27}$$

and for isotropic distributions, we find:

$$R_{\gamma\gamma} = (n_{\gamma}^2)_{obs} c \int_0^{\infty} \sigma(p^*_{\gamma}) F^*_{\gamma}(p^*_{\gamma}) dp^*_{\gamma} \tag{A28}$$

Where:

$$F^*_\gamma(p^*_\gamma) = 2p^{*3}_\gamma \int_0^\infty \frac{f(p_{\gamma 1})}{p^2_{\gamma 1}} \left\{ \int_{p^{*2}_\gamma/p_{\gamma 1}}^\infty \frac{f(p_{\gamma 2})}{p^2_{\gamma 2}}\, dp_{\gamma 2} \right\} dp_{\gamma 1} \qquad (A29)$$

Specializing to a relativistic Bose-Einstein photon distribution, we find:

$$R_{\gamma\gamma}\Big|_{RBE} = \frac{(n^0_\gamma)^2 c^6}{(kT_\gamma)^5} \sum_{n=1}^\infty \sum_{\ell=1}^\infty \frac{1}{\sqrt{n\ell}\; c^{n+\ell}} \int_0^\infty \sigma(p^*_\gamma) p^{*4}_\gamma \cdot$$

$$\cdot\, K_1\left[\frac{2p^*_\gamma c}{kT_\gamma}\sqrt{n\ell}\right] dp^*_\gamma \qquad (A30)$$

or:

$$R_{\gamma\gamma}\Big|_{RBE} = (n^0_\gamma)^2 c \sum_{n=1}^\infty \sum_{\ell=1}^\infty \frac{1}{\sqrt{n\ell}\; c^{n+\ell}} \cdot$$

$$\cdot \int_0^\infty \sigma(\xi)\xi^4 K_1(2\sqrt{n\ell}\,\xi)\, d\xi \qquad (A31)$$

where $\xi = p^*_\gamma c/kT_\gamma$ and , as before, the sums are generally rapidly convergent.

In this case also, the non-degenerate form of (A30) can be obtained as the limit of (A11b) if a transform from lab to center of momentum coordinates is made and the invariance of the cross-section is used.

APPENDIX B

Numerical Solution Methods: Radiation-Dominated Shock Model

The photon continuity equation (5.3) can be written in the form:

$$D_1 \frac{d^2 n_\gamma}{dx^2} + D_2 \frac{dn_\gamma}{dx} + D_3 n_\gamma = -Q\left(1 - \frac{n_\gamma}{n_{eq}}\right) \tag{B1}$$

where:

$$D_1 = \frac{cv}{3n_o v_o \bar{\sigma} c} \qquad D_2 = \frac{v^2 - 8v_o v + v_o^2}{6v}$$

$$D_3 = \frac{(7v - v_o)(v_o - v)}{2vc} n_o v_o \bar{\sigma} c \tag{B2}$$

$$n_{eq} \equiv bT_e^3 \qquad Q \equiv \frac{Q_\gamma^{eff}}{1 - n_\gamma / n_{eq}} \tag{B3}$$

Utilizing a three point difference scheme on an unequally spaced mesh of points x^i $(i = 1,N)$, (B1) can be differenced in the form:

$$\frac{2D_1^i}{\Delta^i}\left[\Delta x^{i-1/2}\left(n_j^{i+1} - n_j^i\right) - \Delta x^{i+1/2}\left(n_j^i - n_j^{i-1}\right)\right]$$

$$+ \frac{D_2^i}{\Delta^i}\left[\left(\Delta x^{i-1/2}\right)^2\left(n_j^{i+1} - n_j^i\right) + \left(\Delta x^{i+1/2}\right)^2\left(n_j^i - n_j^{i-1}\right)\right]$$

$$+ D_3 n_j^i = -Q_{j-1}^i\left(1 + \frac{3n_{j-1}^i}{n_{eq_{j-1}}^i} - \frac{4n_j^i}{n_{eq_{j-1}}^i}\right) \tag{B4}$$

where "i" superscripts denote evaluation at point x^i and "j" subscripts, evaluation at the j^{th} iteration; and where:

$$\Delta x^{i-1/2} = x^i - x^{i-1} \qquad \Delta x^{i+1/2} = x^{i+1} - x^i \tag{B5}$$

$$\Delta^i = \Delta x^{i+1/2} (\Delta x^{i-1/2})^2 + \Delta x^{i-1/2} (\Delta x^{i+1/2})^2 \tag{B6}$$

The form of the factor multiplying Q^i_{j-1} was derived by linearizing

$$\left(\frac{n_\gamma}{n_{eq}}\right)^i_j \quad \text{about} \quad \left(\frac{n_\gamma}{n_{eq}}\right)^i_{j-1} \text{ making use of (5.1).}$$

Solving (B4) and n^i_j we find:

$$n^i_j = \frac{n^{i+1}_j\left[\frac{2D^i_1\Delta x^{i-1/2}+D^i_2(\Delta x^{i-1/2})^2}{\Delta^i}\right] + n^{i-1}_j\left[\frac{2D^i_1\Delta x^{i+1/2}-D^i_2(\Delta x^{i+1/2})^2}{\Delta^i}\right]}{2D^i_1(\Delta x^{i+1/2}+\Delta x^{i-1/2})/\Delta^i + D^i_2[(\Delta x^{i-1/2})^2 - (\Delta x^{i+1/2})^2]/\Delta^i - D^i_3}$$

$$\cdots \frac{+ Q^i_{j-1}\,(1 + 3n^i_{j-1}/n^i_{eq_{j-1}})}{+ 4Q^i_{j-1}/n^i_{eq_{j-1}}} \tag{B7}$$

and define for convenience the coefficients P^i_1, P^i_o, and C^i, so that

$$n^i_j \equiv P^i_1 n^{i+1}_j + P^i_o n^{i-1}_j + C^i \tag{B8}$$

Now let:

$$n^i_j = \alpha^i_j n^{i+1}_j + \beta^i_j \tag{B9}$$

$$n_j^{i-1} = \alpha_j^{i-1} n_j^i + \beta_j^{i-1} \tag{B10}$$

Here the α_j^i and β_j^i are termed back-substitution coefficients and can be found recursively by substituting (B9) and (B10) into (B8) in the form:

$$\alpha_j^i = \frac{P_1^i}{(1-P_o^i \alpha_j^{i-1})} \qquad \beta_j^i = \frac{P_o^i \beta^{i-1} + C^i}{(1-P_o^i \alpha_j^{i-1})} \tag{B11}$$

with the boundary conditions that:

$$\alpha^{(2)} = P_1^{(2)} \qquad \beta^{(2)} = P_o^{(2)} n^{(1)} + C^{(2)} \tag{B12}$$

where we have assumed all quantities are known at $x^{(1)}$.

Having found all the back substitution coefficients for i=2, N-i, we can then use (B10) together with the assumed known value of $n^{(N)}$ to recursively solve for the unknown n_j^i. Since Q_{j-1}^i and $n_{eq_{j-1}}^i$ rely on previous knowledge of n_{j-1}^i, we must begin our calculation by assuming initial values for the photon density distribution ($n_{(1)}^i$), and then iterating the back substitution procedure described above until the results converge. Typically 400 mesh points and 20 iterations are sufficient to achieve an accurate, converged solution.

The ion-heating equation (5.5) can be rewritten in the form:

$$\frac{d\theta_i}{dx} = H_{comp}\theta_i + H_{visc}\theta_i^{5/2} + H_{ei}(\theta_e - \theta_i) \tag{B13}$$

where:

$$H_{comp} = -\frac{2}{3}\frac{1}{v}\frac{dv}{dx} \qquad H_{visc} = \frac{2}{3}\frac{A_2}{n_o v_o}\left(\frac{dv}{dx}\right)^2$$

$$H_{ei} = 2\frac{n_o v_o}{v^2}\frac{A_1}{\theta_e^{3/2}} \tag{B14}$$

with $\frac{dv}{dx}$ following analytically from (5.6), and θ_e from the solution of the photon continuity equation. Explicitly differencing (B13) and linearizing the $\theta_i^{5/2}$ term gives the difference equation:

$$\frac{\theta_i^{i+1} - \theta_i^i}{\Delta x^{i+1/2}} = (\theta_i^i)^{3/2} H_{visc}^{i+1/2}\left(\frac{5}{4}\theta_i^{i+1} - \frac{1}{4}\theta_i^i\right) + H_{comp}^{i+1/2}\left(-\frac{\theta_i^{i+1}+\theta_i^i}{2}\right)$$

$$+ H_{ei}^{i+1/2}\left(\theta_e^{i+1/2} - \frac{1}{2}\theta_i^{i+1} - \frac{1}{2}\theta_i^i\right) \tag{B15}$$

where $\theta_e^{i+1/2} = \frac{1}{2}(\theta_e^{i+1} + \theta_e^i)$. This can be solved directly for θ_i^{i+1}, yielding:

$$\theta_i^{i+1} = \frac{\theta_i^i + \Delta x^{i+1/2}\left[\frac{1}{4}H_{visc}^{i+1/2}(\theta_i^i)^{5/2} + \frac{1}{2}H_{comp}^{i+1/2}\theta_i^i + H_{ei}^{i+1/2}(\theta_e^{i+1/2} - \frac{1}{2}\theta_i^i)\right]}{1 - \Delta x^{i+1/2}\left[\frac{5}{4}H_{visc}^{i+1/2}(\theta_i^i)^{3/2} + \frac{1}{2}H_{comp}^{i+1/2} - \frac{1}{2}H_{ei}^{i+1/2}\right]} \tag{B16}$$

Given $\theta_i^{(1)}$, (B16) then yields the remaining θ_i^i. The integration is stable provided $\theta_i^{(1)}$ is taken at the upstream boundary of the shock ($x=x_o$).

Appendix C

Numerical Solution Methods: Simple Viscous Shock Models

Equations (7.1) - (7.2) are differenced in the form:

$$n_o v_o k \frac{T^i+T^{i+1}}{2} - \mu v^i \frac{v^{i+1}-v^i}{\Delta x^{i+1/2}} = \dot{m} n_o v_o \cdot$$

$$\cdot\left[(v_o-2v^i)\frac{v^{i+1}}{2} + \frac{v_o v^i}{2}\right] + P_o\left(\frac{v^i+v^{i+1}}{2}\right) \qquad (C1)$$

$$\alpha n_o v_o k \frac{T^i+T^{i+1}}{2} - \kappa \frac{T^{i+1}-T^i}{\Delta x^{i+1/2}} = \frac{1}{2}\dot{m} n_o v_o \cdot$$

$$\cdot\left[(v^i-v_o)v^{i+1} + v_o(v_o-v^i)\right] + \alpha_o P_o v_o$$

$$+ \frac{1}{2}\dot{m} n_o v_o^2 \varepsilon_o \left[2v_o - v^i - v^{i+1}\right] \qquad (C2)$$

where the notation of Appendix B has been adopted. T^{i+1} and v^{i+1} are then readily found provided T^i and v^i are known. The integration is started by means of the asymptotic solution derived in § VII.A, and must proceed from downstream to upstream to be stable.

By multiplying (7.23) by $\alpha \equiv (\frac{3}{2} + 3\chi\eta)/(1 + \chi\eta)$, and substracting the result from (7.23), we derive an equation for the required shock dissipation in the form:

$$\alpha\mu v \frac{dv}{dx} - \lambda_0 vkTn_0 \frac{d\chi}{dx} - \kappa' \frac{dT}{dx} = \frac{1}{2}mn_0 v_0 \cdot$$

$$\cdot [v_0 - v(1+2\alpha) + 2(1+\alpha)\varepsilon_0 v_0][v_0 - v]$$

$$+ \varepsilon_0 (\alpha_0 - \alpha) mn_0 v_0^3 \qquad \text{(C3)}$$

Equations (7.23) and (C3) are then differenced as:

$$\left[2 + \frac{\chi^{i+1/2}(v^{i+1}+v^i)}{v_0}\right] n_0 v_0 kT^i - 2\mu v^i \frac{(v^{i+1}-v^i)}{\Delta x^{i+1/2}}$$

$$= mn_0 v_0 [v^i v_0 + v^{i+1} v_0 - 2v^i v^{i+1} + 2v^i v_0 \varepsilon_0] \qquad \text{(C4)}$$

$$2\alpha^i \mu v^i \frac{v^{i+1}-v^i}{\Delta x^{i+1/2}} - \lambda_0 n_0 v^i k(T^{i+1}+T^i)\left(\frac{d\chi}{dx}\right)^{i+1/2}$$

$$- 2(\kappa')^i \frac{(T^{i+1}-T^i)}{\Delta x^{i+1/2}} = mn_0 n_0 [v_0 - v^{i+1}(1+2\alpha^i)$$

$$+ 2(1+\alpha^i)\varepsilon_0 v_0][v_0 - v^i] + 2\varepsilon(\alpha_0 - \alpha^i) mn_0 v_0^3 \qquad \text{(C5)}$$

Since χ^i is known at all points, these equations can be readily integrated starting from the downstream asymptotic solutions derived in § VII.B.

Appendix D

Numerical Solution Methods: Effective Photon Shock Model

The difference equations used to solve equations (8.1) - (8.2) are given by:

$$\left(1 + \tau_R^i + \chi^{i+1/2}\,\frac{(v^{i+1}+v^i)}{2v_o}\right) n_o v_o k T^i$$

$$- \mu^i v^i\,\frac{(v^{i+1}-v^i)}{\Delta x^{i+1/2}} = mn_o v_o\left(v_o\,\frac{(v^{i+1}+v^i)}{2} - v^i v^{i+1}\right)$$

$$+ P_o v^i \qquad \text{(D1)}$$

$$2\alpha^i \mu^i v^i\,\frac{v^{i+1}-v^i}{\Delta x^{i+1/2}} - \lambda_o n_o v k (T^{i+1}+T^i)\left(\frac{dx}{dx}\right)^{i+1/2}$$

$$- 2(\kappa')^i\,\frac{(T^{i+1}-T^i)}{\Delta x^{i+1/2}} = mn_o v_o\left[v_o - v^{i+1}(1+2\alpha^i)\right.$$

$$\left. + 2\,(1+\alpha^i)\,\epsilon_o v_o\right]\left[v_o - v^i\right] + 2\epsilon_o(a_o - \alpha^i)\,mn_o v_o^3 \qquad \text{(D2)}$$

where $$\frac{1}{\alpha} \equiv \frac{1 + \tau_R + \chi\eta}{\alpha_e + \frac{3}{2}\tau_R + 3\chi\eta} \qquad \text{(D3)}$$

As in Appendix C, we have first transformed the energy conservation equation (8.2) into an expression for the required shock dissipation before differencing. These equations are then

integrated upstream by the method described in Section VIII.

The photon continuity equation (8.3) is solved in the manner described in Appendix B, except that the D_i coefficients in equation (B1) are defined in more general form:

$$D_1^i = \frac{\lambda_e}{3} v^i \qquad D_2^i = -v^i + \frac{\lambda_e}{3}\left(\frac{dv}{dx}\right)^i \qquad D_3^i = -\left(\frac{dv}{dx}\right)^i \tag{D4}$$

The ion-heating equation, (8.4), is differenced as:

$$\frac{3}{2} n_0 v_0 k T^{i+1/2} \frac{\left(\tau_R^{i+1} - \tau_R^i\right)}{\Delta x^{i+1/2}} + \frac{3}{2} n_0 v_0 k \left(\frac{dT}{dx}\right)^{i+1/2} \cdot \left(\frac{\tau_R^{i+1} + \tau_R^i}{2}\right) = -\frac{n_0 v_0}{v^{i+1/2}} k T^{i+1/2} \left(\frac{dv}{dx}\right)^{i+1/2} \left(\frac{\tau_R^{i+1} + \tau_R^i}{2}\right)$$

$$+ A_2^i \left(k T^{i+1/2}\right)^{5/2} \left[\left(\frac{dv}{dx}\right)^{i+1/2}\right]^2 \left(\tau_R^i\right)^{5/2}$$

$$+ \left(\frac{n_0 v_0}{v^{i+1/2}}\right)^2 \frac{3 A_1^i}{\left(k T^{i+1/2}\right)^{1/2}} \left[1 - \frac{\left(\tau_R^{i+1} + \tau_R^i\right)}{2}\right]$$

$$+ \left(\tau_R^{-3/2} H_{ap}\right)^{i+1/2} \left(\tau_R^i\right)^{3/2} \tag{D5}$$

and integrated from the upstream to the downstream limit with the boundary condition that $\tau_R = 1$ at the upstream boundary.

The iterative solution of these equations requires that the zoning be sufficiently fine that only a small change in the variables takes place across a zone. It is thus sometimes convenient, though not necessary, to limit the ratio of λ_μ/λ_0 (typically to $\gtrsim 10^{-3}$) in

order to reduce the number of zones required.

APPENDIX E

List of Symbols

The principal symbols and subscripts employed in this study are listed below with their units and defining equation where applicable. *Notation* peculiar to the Appendices or figure captions, as well as briefly used notation, is not included.

Symbols

A - Ratio of radiative to matter heat conduction lengths ($\equiv \lambda_0/\lambda_\kappa$)

A_i - Mass of species i in proton mass units

A^* - $\equiv \lambda_0/\lambda_X$

A_1 - ($erg^{3/2}\ cm^3\ sec^{-1}$) - Electron-ion coupling parameter (3.45)

A_2 - ($erg^{-3/2}\ cm^{-3}\ sec$) - Viscosity parameter ($\equiv \mu_i (kT_i)^{-5/2}$)

b - ($20.3\ cm^{-3}\ {}^\circ K^{-3}$) - Radiation equilibrium number density constant

C - Radiation field degeneracy parameter (see (A19))

c - (cm/sec) - Velocity of light

c_κ - see (7.32)

c_κ^* - see (8.17)

c_s^0 - (cm/sec) - Pre-shock sound speed

$D_\gamma(\epsilon_\gamma)$ - ($cm^2\ sec^{-1}$) - Radiation diffusion coefficient

E_x^i - ($erg\ cm^{-2}\ sec^{-1}$) - x energy component of stress-energy tensor

E_0 - (Mev) - Initial shock energy ($\equiv m_H v_0^2/2$)

E_1 - First order exponential integral function

E_γ - ($erg\ cm^{-3}$) - Total radiation energy density

E^{ij} - (erg cm^{-3} sec^{-1}) - Energy transfer rate from species j to i

E_{ei}^{*} - (erg cm^{-3} sec^{-1}) - Non-electrical energy transfer rate from ions to electrons

e - (erg$^{1/2}$ $cm^{1/2}$) - Protonic charge

f_E - Equilibrium parameter (3.10)

f_{ei} - Electron-ion coupling relativistic correction factor (3.46)

g_1 - Bremsstrahlung Gaunt factor defined by (3.3)

g_2 - Combined bremsstrahlung Gaunt factor ($g_2(\lambda) \equiv g_1(\lambda)\, E_1(\lambda)$)

$H_{\alpha p}$ - (erg sec^{-1})-Coulomb friction heating between protons and alphas

$\hbar$ - (erg sec) - Planck's constant/2π

J_{ei}^{NR} - (cm^{-3} sec^{-1} erg^{-1}) - Non-relativistic bremsstrahlung emission spectrum

J_o - ($\equiv 5.692 \times 10^{-12}$ $^oK^{1/2}$ cm^3 sec^{-1}) - Bremsstrahlung emission coefficient (see (3.2))

$J_\pm$ - (erg$^{1/2}$ $cm^{-3/2}$ sec^{-1}) - Net current density in the pair fluid ($\equiv en_+(v_e - v_+)$)

j_e - (erg$^{1/2}$ $cm^{-3/2}$ sec^{-1}) - Current density due to the electron-positron fluid

K_i - Modified Bessel functions of the second kind of order i

k - (erg $^oK^{-1}$) - Boltzmann's constant

ℓ_c - (cm) - Compton length ($\equiv 1/\sigma_c n_e$)

ℓ_{ei} - (cm) - Stopping length for ions in an electron gas

ℓ_T - (cm) - Thompson length ($\equiv 1/\sigma_T n_c$)

$\ell n\Lambda$ - Coulomb logarithm (3.30)

M - Mach number - see (7.16)

$M_\odot$ - (g) - Solar mass

m - (g) - Mass of shocked particle species, usually m_H

m_e, m_H, m_i, m_p, m_α - (g)-Electron, hydrogen, ion, proton, helium mass

n - (cm^{-3}) - Common electron, proton number density

n^i - (cm^{-3}) - Number density of component i

n_e, n_i, n_p, n_α, n_+, n_{e^-}, $n^\pm$ - (cm^{-3}) - Number density of electrons, ions, protons, alphas, positrons, negatrons, and pairs.

n_o - (cm^{-3}) - Pre-shock number density

n_{20}^o - $n_o/10^{20}$ cm^{-3}

$n_\gamma(\epsilon_\gamma)$ - (cm^{-3} erg^{-1}) - Number density of photons with energy ϵ_γ per unit energy

n_γ^{eq} - (cm^{-3}) - Equilibrium photon number density (5.21)

n_γ^s - (cm^{-3}) - Upstream starting photon density

$n\tau$ - (cm^{-3} sec) - Number density - confinement time product

p_m - (erg cm^{-3}) - Matter pressure

p_{xx}^i - (erg cm^{-3}) - xx pressure component of the stress-energy tensor

P_o - (erg cm^{-3}) - Pre-shock pressure

P_γ - (erg cm^{-3}) - Radiation pressure

p^{ij} - (dyne cm^{-3}) - Momentum transfer rate from species j to i

p_{ei}^* - (dyne cm^{-3}) - Non-electrical momentum transfer rate from ions to electrons

$Q_\gamma(\epsilon_\gamma)$-($cm^{-3}$ sec^{-1} erg^{-1}) - Photon emission rate at ϵ_γ per unit energy

$Q(\epsilon_c,\theta_e)$ - (cm^{-3} sec^{-1}) - Total photon emission rate down to an $\epsilon_\gamma = \epsilon_c$ cutoff

Q_γ^{eff} - (cm^{-3} sec^{-1}) - Effective photon emission rate

Q_{ei}^{NR}, Q_{RCB}, Q_{RC} - (cm^{-3} sec^{-1}) - Effective photon emission rates due to non-relativistic bremsstrahlung, relativistic corrections to bremsstrahlung, and radiative Compton scattering.

$Q_{\gamma\gamma}^{\pm}$ - (cm^{-3} sec^{-1}) - Pair production rate due to the $\gamma\gamma \rightarrow e^+e^-$ reaction

$Q_\pm$ - (cm^{-3} sec^{-1}) - Total pair production rate

r_o - (cm) - Classical electron radius

S_o - (erg cm^{-2} sec^{-1}) - Pre-shock internal energy flux

S_γ - (erg cm^{-2} sec^{-1}) - Total radiative energy flux relative to the electrons

$S_\gamma(\epsilon_\gamma)$ - (cm^{-2} sec^{-1}) - Radiative energy flux relative to the electrons per unit photon energy at ϵ_γ

T - (°K) - Common radiation and electron temperature

T_e, T_i, T_γ, $\bar{T}_m$(°K) - Electron, ion, radiation, and mean matter temperatures

T_S, T_o, T_{eq} - (°K) - Upstream starting, initial and final equilibrium (5.20) temperatures

T_ν, $T_\pm$ - Critical temperatures for the onset of viscous and pair effects

t_{sjk} - (sec) - Transport collision period (3.27)

v - (cm/sec) - Common electron and ion velocity

v^i - (cm/sec) - Velocity of species i

v_e, v_i, v_+, v_γ - (cm/sec) - Electron, ion, positron, and effective photon velocities

v_{drift} - Relative velocity between α's and protons

v_j^{th} - (cm/sec) - Thermal velocity of species j (3.25)

v_s - (cm/sec) - Starting velocity for shock integration

v_0 - (cm/sec) - Pre-shock fluid velocity in the shock frame

W_{ei}^{NR}, W_{ei}^{RC}, W_{ee} - (erg cm^{-3} sec^{-1}) - Energy loss rates due to non-relativistic bremsstrahlung, relativistic e-i bremsstrahlung corrections, and electron-electron bremsstrahlung

w - (cm/sec) - Velocity of a particle

x - (cm) - Spatial coordinate

x_s - (cm) - Starting value of x for shock integration

x_0, x_1 - (cm) - Upstream and downstream boundary points

Y - Helium mass fraction

Z_i - Number of protonic charges contained in particle i

α - Ratio of energy density to pressure; fine structure constant

α_0 - Pre-shock value of α

α_e, α_j - Ratio of energy density to pressure for electrons and species j

γ - Relativistic $\gamma \equiv (1-v^2/c^2)^{-1/2}$

Δ - Characteristic radiation-dominated shock width ($\equiv c\ell_c/3v_0$)

$\Delta_\pm$ - Characteristic pair-dominated shock width (6.9)

δ - Ratio of viscous to matter heat conduction lengths (7.7)

δ' - $\equiv \lambda_\mu/\lambda_\chi$

δ_κ - $\equiv \lambda_\kappa/\lambda_\chi$

ε - Dimensionless velocity difference ($\equiv \eta-\eta_1$)

ε_c - (erg) - Low energy cutoff for effective photon emission

ε_B, ε_{sc}, ε_d - (erg) - Radiation emission cutoff energies due to inverse bremsstrahlung, screening, and dynamical considerations

ε_s - Starting value of ε

ε_0 - Dimensionless pre-shock pressure ($\equiv P_0/mn_0v_0^2$)

ε_τ, ε_π - Dimensionless pressure differences ($\varepsilon_\tau \equiv \tau_1-\tau$, $\varepsilon_\pi \equiv \pi_1-\pi$)

ε_γ - (erg) - Photon energy

ζ - Dimensionless distance ($\equiv x/\lambda_\kappa$)

ζ' - Dimensionless distance ($\equiv x/\lambda_\chi$)

η - Dimensionless velocity ($\equiv v/v_0$)

θ_e, θ_i - (erg) - $\equiv kT_e$, kT_i

θ_γ - (erg) - $\equiv 0.9\ kT_\gamma$

κ - (erg cm^{-1} sec^{-1} $^oK^{-1}$) - Heat conduction coefficient

κ' - (erg cm^{-1} sec^{-1} $^oK^{-1}$) - Heat conduction coefficient including radiative processes (7.25)

κ_e, κ_i - (erg cm^{-1} sec^{-1} $^oK^{-1}$) - Electron and ion heat conduction coefficients

λ - Low energy radiative cutoff parameter ($\equiv \varepsilon_c/\theta_e$)

λ_D - (cm) - Debye length ($\equiv (\theta_e/4\pi n_e e^2)^{1/2}$)

λ_j - (cm) - Transport mean-free-path for species j - see (3.26)

λ_{jk} - (cm) - Transport mean-free-path for species j with respect to species k

λ_{max} - Maximum cutoff parameter (4.11)

λ_χ - (cm) - Convenient scale length

λ_0 - (cm) - Radiation diffusion scale length (7.25)

λ_κ - (cm) - Matter heat conduction scale length ($\equiv \kappa/kn_0v_0$)

λ_μ - (cm) - Viscous scale length ($\equiv \mu/mn_0v_0$)

μ - (erg cm^{-3} sec) - Viscosity coefficient

μ_e, μ_i - (erg cm^{-3} sec) - Electron and ion viscosity coefficients

μ_j - (erg) - Chemical potential of species j

μ_1 - see (7.32)

μ' - see (8.15)

ξ - Ratio of radiation to matter pressure

π - Dimensionless pressure ($\equiv (1+\chi\eta)\tau$)

ρ - (erg$^{1/2}$ cm$^{-5/2}$) - Net charge density

ρ_e - (erg$^{1/2}$ cm$^{-5/2}$) - Charge density of the electron - positron fluid

Σ_x - (erg$^{1/2}$ cm$^{-3/2}$) - x component of electric field

Σ_{max} - (erg$^{1/2}$ cm$^{-3/2}$) - Maximum shock electric field ($\equiv E_0/(e\Delta)$)

σ - (cm^2) - Reaction or scattering cross-section

$\sigma_c(\epsilon_\gamma)$ - (cm^2) - Compton transport cross-section at photon energy ϵ_γ

$\bar{\sigma}_c$ - (cm^2) - Mean Compton transport cross-section

σ_T - (cm^2) - Thompson cross-section ($8\pi r_0^2/3$)

$\langle\sigma v\rangle$ - (cm^3 sec^{-1}) - Density normalized reaction rate

τ - Dimensionless temperature (7.7); also $\tau \equiv \theta_e/m_ec^2$ in § III

τ_d - (sec) - Dynamical time scale

τ_R - Ion-electron temperature ratio ($\equiv T_i/T$)

ϕ - $\equiv m_ec^2/kT$

χ - Dimensionless radiation number density ($\equiv 0.9\, n_\gamma/n_0$)

x_{He} - Helium - hydrogen number density ratio

Subscripts and Superscripts:

0 - Pre-shock value

1 - Post-shock or pseudo-downstream value

ER - Extreme relativistic

e - Electron value

f - Final post-shock value

i,p - Ion or proton value

NR - Non-relativistic

γ - Photon value